学位申請論文

岡田邦英

主論文

A STUDY OF HYPERFINE FIELD AT Co NUCLEUS IN AN ANTIFERROMAGNETIC CoO

By

Kunihide OKADA

1975

ABSTRACTS

By using a He^3-He^4 dilution refrigerator, some Mössbauer experiments at very low temperatures were performed.

The magnetic hyperfine field at parent nuclei, Co^{57}, in an antiferromagnetic CoO was measured by Mössbauer experiments at very low temperatures. The sample was cooled down to 0.08 K by the He^3-He^4 dilution refrigerator. Then the nuclear polarization of the parent nuclei, Co^{57}, occured and the Fe^{57} Mössbauer emission spectrum became to be asymmetric. From the intensity ratio of the outermost peaks of the emission spectrum of Fe^{2+} ions, it was derived that the sign of the hyperfine field at Co^{57} nucleus in CoO was plus and its magnitude was 590 ± 40 kOe. A considerable amount of Fe^{3+} ions were also existed in addition to th Fe^{2+} ions. The origen of the co-existensy of both ions has not been understood yet theoretically. The hyperfine field at the parent nucleus, Co^{57}, estimated from the Fe^{3+} spectrum was $+603\pm80$ kOe, which agreed with the value estimated from the Fe^{2+} spectrum.

With the help of the information mentioned above, an investigation of Co^{59} NMR in CoO single crystal was performed in the antiferromagnetic state. The value of the hyperfine field at Co^{59} nucleus was found to be 495.5 ± 0.5 kOe at 4.2 K in zero external magnetic field which was smaller than the

value of 590 kOe estimated by Mössbauer experiments. A main cause for the error in the estimation from the Mössbauer spectrum may be an overestimation of the absolute temperature of sample. The value of the observed hyperfine field agreed with that of 511 kOe calculated theoretically. The rotational spectra of Co^{59} NMR in CoO single crystal with the small external magnetic field were measured, from which the tilt angle of the axis of the hyperfine field from the c-axis was obtained.

ACKNOWLEDGEMENTS

During the course of this reserch, many people have contributed their times and advices, which have been greatly appreciated. It is a pleasure to acknowledge them here. The author would like to express his sincere gratitude to Prof. A. Hirai and Dr. T. Shinjo for their valuable advices, guidances and encouragements. His thanks are also due to Prof. T. Takada for his continual encouragements. He is indepted to Prof. K. Motizuki, Osaka University, and Dr. H. Yasuoka for informative discussions. He expressed his thanks to Mr. T. Matsuzawa for helpful advices about a computer programing and also members of Hirai unit for their discussions and assistances throughout this work. Finally, he wishes to acknowledge to Prof. T. Hashi for his encouragements and advices.

TABLE OF CONTENTS

ABSTRACT i

ACKNOWLEDGEMENTS ii

TABLE OF CONTENTS iii

LIST OF TABLES vi

LIST OF FIGURES vi

CHAPTER I GENERAL INTRODUCTION 1

CHAPTER II He^3-He^4 DILUTION REFRIGERATOR. 4

§ 2.1 Introduction to He^3-He^4 Dilution Refrigerator. 5

§ 2.2 Basic He^3-He^4 Properties 8

§ 2.3 Cooling Power of Refrigerator. 15

§ 2.3.a In the Case of He^3 Refrigerator. 15

§ 2.3.b In the Case of He^3-He^4 Dilution Refrigerator 20

§ 2.3.c Comparison of He^3 Refrigerator and Dilution Refrigerator 27

§ 2.4 Continuous Dilution Refrigerator 31

§ 2.4.a Dilution Refrigerator based on the Circulation of Helium-4. 32

§ 2.4.b Dilution Refrigerator based on the Circulation of Helium-3. 34

§ 2.5 Construction of Dilution Refrigerator. 36

§ 2.5.a Mixing Chamber and Ultimate Temperature. . 36

$ 2.5.b Heat Exchanger. 47
$ 2.5.c Still 56
$ 2.6 Experimental Apparatus. 58
$ 2.6.a Circulation System of He^3-He^4 Dilution Refrigerator. 58
$ 2.6.b Main parts and Operating Characteristic of the Dilution Refrigerator 62
CHAPTER III NUCLEAR POLARIZATION AND THE EFFECT ON THE MÖSSBAUER SPECTRUM AT THE VERY LOW TEMPERATURE. 70
$ 3.1 Introduction. 71
$ 3.2 Review of Mössbauer Effect. 72
$ 3.2.a Emission from Bounded Atoms and Recoilless fraction. 73
$ 3.2.b Width of Gamma-Ray Spectrum and Why the Mössbauer effect is valuable. 82
$ 3.2.c Study of Hyperfine Structure. 90
$ 3.3 Nuclear Polarization and the Effect on the Mössbauer Spectrum. 94
$ 3.4 Mössbauer Thermometer 99
$ 3.5 Matrix Element of the β-Transition. 113
CHAPTER IV THE MAGNETIC HYPERFINE FIELD AT Co^{57} IN ANTIFERROMAGNETIC CoO. 137

§ 4.1 Introduction. 138
§ 4.2 Crystalographic and Magnetic Structure of Antiferromagnetic CoO 141
§ 4.2.a Crystalographic structure 141
§ 4.2.b Magnetic structure. 144
§ 4.3 Mössbauer experiments on CoO. 150
§ 4.4 Experimental 157
§ 4.5 Experimental result 160
§ 4.6 Analysis and Discussion 175
§ 4.6.a The Fe^{2+} spectrum 175
§ 4.6.b The Fe^{3+} spectrum 183
CHAPTER V NMR STUDY OF Co^{59} NUCLEUS IN ANTIFERROMAGNETIC CoO 193
§ 5.1 Introduction to Co^{59} NMR. 194
§ 5.2 Experimental Methods. 197
§ 5.3 Experimental Results in Zero External Magnetic Field 200
§ 5.4 Analysis and Discussions about Zero Field Spectrum. 204
§ 5.5 Experimental Results about Spin Echo Pattern in External Magnetic Field 211
§ 5.6 Analysis and Discussions about Spin Echo Pattern 214
REFERENCES. 225

LIST OF TABLES

TABLE NO.

2.1 Equilibrium properties of He^3-He^4 dilution refrigerator. 69

3.1 The specific heat and the recoil-free fraction of a Einstein model solid and a Debye model solid . 81

3.2 Properties of Fe^{57}. 89

3.3 The intensity ratio of Mössbauer thermometer (Co^{57} in Fe metal) as a function of temperature . .104

3.4 Clebsch-Gordon Coefficient. 121

3.5 The intensity ratio versus H/T 127

4.1 Comparison of the Néel temperature of CoO obtained by different methods 143

4.2 Spin arrangement in CoO 145

4.3 The possible mechanism of Fe^{3+} formation. 155

4.4 The magnetic hyperfine field at the site of Co^{57} nucleus in CoO (from the Mössbauer spectrum for Fe^{2+} ion). 182

4.5 The magnetic hyperfine field at the site of Co^{57} nucleus in CoO (from the Mössbauer spectrum for Fe^{3+} ion). 188

5.1 The obtained results from Co^{59} NMR experiments . . .224

LIST OF FIGURES

FIGURE NO.

2.1 The phase diagram of He^3-He^4 mixtures 11

2.2 Schematic of phase separated He^3-He^4 mixtures at T/0.1 K. 14

2.3 Latent heat of helium-3 versus temperature. . . 17

2.4 Saturated vapor pressure versus temperature for a lquid helium-3 and a liquidhelium-4 . . . 19

2.5 Specific heat of a pure helium-3 at low temperatures. 21

2.6 Molar enthalpies of a pure helium-3 and of the equilibrium He^3-He^4 solution at low temperatures. 24

2.7 The cooling power of a He^3 evaporation refrigerator and of a He^3-He^4 dilution refrigerator as a function of temperature . . . 30

2.8 Schematic diagram of the continuous refrigerator based on the circulation of He^3. . 33

2.9 Schematic diagram of the continuous refrigerator based on the circulation of He^4. . 35

2.10 Schematic diagram ellustrating the thermodynamics of the mixing chamber. 37

2.11 Diagram for viscous heating analysis. 41

2.12 Thermal conductivity coefficient for dilute solutions of He^3 in He^4 44

2,13 differential element of the continuous heat exchanger 49

2.14 Schematic of step heat exchanger. 55

2,15 Circulation system of He^3-He^4 dilution refrigerator. 59

2.16 Cooling curve for the dilution refrigerator. . 63

2.17 Principle parts of the dilution refrigerator . 66

2.18 Heat extraction curve for the dilution refrigerator 68

3.1 Perturbation of 14.4 keV and ground state energy levels of Fe^{57} by isomer shift, quadrupole coupling and magnetic hyperfine field. 71

3.2 The Mössbauer spectrum of Co^{57} in Fe metal . . 84

3.3 The intensity ratio of LINE(6) in Mössbauer thermometer(Co^{57} in Fe metal) versus temperature. 97

3.4 The intensity ratio of LINE(6) versus H/T. . .101

4.1 Antiferromagnetic structure of CoO 142

4.2 Schematic spin sptructure models of CoO. . . .145

4.3 Auger after effect 151

4.4 Delayed coincidence Mössbauer effect 153

4.5 Schematic of sample attachment 158

4.6 The Mössbauer spectrua of Fe^{57} in antiferromagnetic CoO at various temperatures 173

4.7 The Mössbauer spectra for Fe^{2+}state in antiferromagnetic CoO at various temperatures. . .175

4.8 Intensity ratio of the outer peaks of the

Mössbauer spectra for Fe^{2+} state in anti-ferromagnetic CoO as a function of temperature.. 178

4.9 Mössbauer spectra for Fe^{3+} state in antiferro-magnetic CoO (Sample-II) at various temperatures. 185

4.10 Intensity ratio of the outermost lines of the Mössbauer spectra for Fe^{3+} state in antiferro-magnetic CoO as a function of temperature 186

4.11 Atomic ratio of Fe^{3+}/Fe^{2+} versus temperature. . .190

5.1 The schematic of setting the single crustal specimen of CoO in the re-entrant type coaxial cavity. 199

5.2 Spin echo spectra of Co^{59}NMR in CoO at 77 K(-●-) and at 4.2 K(-o-)in zero external field 202

5.3 Echo decay constants of zero field spectra at 77 K (-●-) and at 4.2 K (-o-) 203

5.4 Spin echo intensity as a function of the angle between the external field and c-axis at the operating frequency of 498.010 MHz and 500.011 MHz. 212

5.5 The frequency-field direction pattern. The solid lines are best fit curves of experimental data in correspond to the application of the external field in the a-c plane of CoO single crystal. The broken lines are predicted curves in correspond to the application in the a-b plane. 213

5.6 The schematic of the effective field acting on the Co^{59} nucleus in CoO. Here x, y, and z stand for the a, b, c axis in CoO single crystal and H_{ext} the external field and H_N the hyperfine field And Θ is the angle between the external field and c-axis, and ϕ is the angle between the hyperfine field and c-axis. 215

5.7 The schematic of the relation between H_S, H_l and the angle of spin of Co^{2+} ion etc. Here Θ_{H_N} and Θ_S are the angle of the observed hyperfine field and the reported spin associated with c-axis, respectively. 220

5.8 The schematic of the direction of the spin and the orbital momentum of Co^{2+} ion and the hyperfine field at Co^{59} nucleus in CoO. 222

CHAPTER I

GENERAL INTRODUCTION

Almost Mössbauer experiments at low temperatures published have been performed in cryostats in which liquid helium-4 is the ultimate cooling agent. With a pure helium-3 refrigerator[1-3], Taylor and his colleagues got the temperature down to 0.35 K. So far, Mössbauer studies at very low temperatures below 0.35 K, could be carried out by the following two technique; adiabatic demagnetization technique[4,5] and He^3-He^4 dilution refrigerator technique[6,7].

Adiabatic demagnetization technique, however, is not very suitable for Mössbauer work because a 'one shot' method cannot satisfactorily cope with the rather long

counting times and the relatively large heat leaks normally encountered in these experiments, especially in the presence of the large heat leak one encounters with cooled sources. Thus, the use of a Mössbauer demagnetization cryostat has been limited to absorber experiments with Fe^{57}, where a good spectrum can be obtained within an hour or so and the source is kept outside the cryostat at room temperature.

The recent advent of the He^3-He^4 dilution refrigerator (T.E.Katila et al. group[6,7]) has brought a new and promising method for cooling and has been used successfully for Mössbauer experiments. A cryostat of this type is a continuously operating refrigerator capable of removing large amounts of heat even with modest pumping arrangements. In fact, once the necessary "know how" has been mastered, the operation of dilution machine is very easy and stable. The lowest temperature using a dilution refrigerator has been obtained by Wheatly et al.[8,9], who reached 0.010 K in continuous operation and 0.0045 K in a "one shot" process.

There are many reasons for pursuing Mössbauer experiments to very low temperatures. We should first mention studies of hyperfine interactions as a function of temperature in substances with magnetic transitions well below 1.0 K. Second, experiments which make use of nuclear polarization

can only be conducted at temperatures at which the thermal energy kT is comparable with the hyperfine interaction energy. For most practical cases significant polarization occurs only at the temperatures below 0.3 K. A typical application of this effect is the Mössbauer thermometer. A valuable feature of polarization experiments using the Mössbauer technique is that macroscopic orientation of the nuclei is not necessary. Finally, we should mention relaxation phenomena and localized moments in dilute alloys , in particular the Kondo effect, as possible candidates for Mössbauer studies at very low temperatures.

It further allows that a Mössbauer experiment on oriented nuclei gives information conserning the matrix elements of the β-decay of parent nucleus.[10,11)]

In this theses, the followings will be presented;

A) A He^3-He^4 dilution refrigerator for a Mössbauer study.

B) A Mössbauer study on Fe^{57} and Co^{57} nucleus in antiferromagnetic CoO at very low temperatures, which was done by using the He^3-He^4 dilution refrigerator.

C) A Co^{59} NMR investigation in CoO single crystal in antiferromagnetic state, which was enable to make with the help of the information on the hyperfine field at Co^{57} nucleus on CoO obtained by the Mössbauer experiments at very low temperatures.

CHAPTER II

He^3-He^4 DILUTION REFRIGERATOR

Today, a He^3-He^4 dilution refrigerator become a very powerful tool to study various properties of materials at very low temperatures. In this chapter, the general characteristics of the refrigeration device itself are reviewed and the apparatus operated by auther is described.

$ 2.1 Introduction to He^3-He^4 Dilution Refrigerator

In 1951 H.London suggested a method for using solutions of helium-3 in superfluid helium-4 to produced refrigeration at low temperatures[12]. He noted that if the mixture can be initially cooled to a point where the helium-4 is mostly superfluid and has zero entropy, then the total entropy of the mixture is determined by the concentration of helium-3. In the proposed method the temperature would be reduced by allowing helium-3 system to do work adiabatically at the extense of its kinetis energy. The proposal is based on a conception of the properties of helium-3 dissolved in superfluid helium-4 due to Landau and Pomeranchuk[13]. The helium-3 particles are regarded as impurity with an energy spectrum which might be as simple as the ideal gas like

$$E = -E_{o3} + \frac{p^2}{2m^*} , \qquad (2.1)$$

where E_{o3} is a binding energy, P is helium-3 quasiparticle momentum, and m* is an effective mass. Hence adiabatic dilution, in analogy with adiabatic expansion of a gas, shuld result in a decrease in total entropy and a concurrent decrease in temperature. London predicted that

$$\frac{T_f}{T_i} = \left|\frac{X_f}{X_i}\right|^{\frac{3}{2}}$$

where T_f = final temperature, X_f = final He^3 concentration, T_i = initial temperature, X_i = initial He^3 concetration. Thus by a tenfold dilution starting at 0.3 K, a final temperature of about 0.65 K should be obtained. This process has actually been carried out with limited success by Taconis , Das and de Bruyn Ouboter[14].

Following the discovery by Walters and Fairbank[15] of the phase separation phenomenon in He^3–He^4 mixtures, analogous to the " condensation of the Landau-Pomeranchuk He^3 gas ", London, Clarke and Mendoza[16] proposed a more powful method for producing refrigeration using He^3-He^4 solutions. The He^3-He^4 mixtures separate into a lighter He^3 rich phase and a heavier He^4 rich phase below about 0.8 K. Since the rigime in which phase separation takes place is always at a temperature below the λ-point, or superfluid transition point for the mixture, London, Clarke and Mendoza noticed that a phase separated He^3–He^4 mixture at very low temperatures looks like a quasi-liquid, the He^3 rich phase, in equiliblium with a quasi-vapor, the He^3 poor phase, and a superfluid He^4 vacuum. The system has the odd property that the He^3 rich quasi-liquid is less dense than the He^4 rich quasi-vapor and floats above it. London et. al

realized that the heat of transition from the quasi-liquid to the quasi-vapor could be utilized for refrigeration just as the latent heat of real liquid-vapor system is used.[12] Their measurements showed that the quasi-vapor "pressure" remained quite high at the temperature below 0.1 K and thus refrigeration could be produced at those temperatures. They also noted that if He^3 could be distilled from the quasi-vapor phase and returned to the quasi-liquid phase then continuous refrigeration would result, in analogy with a conventional He^3 refrigerator.

The first really successful dilution refrigerator was built by Hall, Ford and Tompson[17]. Their refrigerator based on the "evaporation" idea and operating continuously reached a temperature of 65 mK(1 mK=10^{-3}K). Working independently, Naganov, Borisov and Liburg[18] constructed a high refrigeration capacity device which operating continuously reached a temperature of 25 mK.

The refrigerator of the author has a simple structure and only 20 minutes were necessary for the cooling from 1.27 K to 0.08 K.

$ 2.2 Basic He^3-He^4 Properties

The fact that liquid He^3-He^4 mixtures would separate into two distinct phases at very low temperatures had been predicted theoretically by Prigogine et al.[19] and by Chester [20] before it was discovered experimentally by Fairbank and Walters[15] in 1956. The basic reason for phase separation into isotropic components is the difference, in the molar volumes of liquid helium-3 and helium-4. The inter-atomic potentials of helium-3 and helium-4 are nearly the same but the zero point energy is inversely propotionaly to the mass. This means that the volume per atom (the molar volume) is larger for helium-3 than helium-4.

The following thermodynamic argument shows that this molar volume difference is likely to lead to isotropic phase separation as the temperature approaches absolute zero. Let us assume we have n_3 moles of He^3 and n_4 moles of He^4 both at a temperature T and a pressure P. The respective molar Gibbs function, g_3 and g_4 are

$$g_3 = u_3 - Ts_3 + Pv_3, \qquad g_4 = u_4 - Ts_4 + Pv_4 , \tag{2.2}$$

where u_i is molar binding energy, s_i is molar entropy

and v_i is molar volume. If we consider our system to be a box containing the two isotope, but with a wall prohibiting thier mixing, the molar Gibbs function g_{3+4} is just

$$g_{3+4} = x_3 g_3 + x_4 g_4, \tag{2.3}$$

where $x_3 = \frac{n_3}{n_3+n_4}$, and $x_4 = \frac{n_3}{n_3+n_4}$.

Now let us remove the restraining wall and allow the two isotopes to mix. The molar Gibbs function of the mixture will be

$$g_m = u_m - Ts_m + Pv_m , \tag{2.4}$$

where
$$u_m = x_3 u_3 + x_4 u_4 + P(v_m - v_4) + P(v_3 - v_m) , \tag{2.4.a}$$
$$s_m = x_3 s_3 + x_4 s_4 + s_{mixing} , \tag{2.4.b}$$
$$v_m = x_3 v_3 + x_4 v_4 . \tag{2.4.C}$$

The last two terms in equation (2.4.a) arises from the fact that during the mixing the He^4 must have its molar volume expanded to the mixing molar volume and, likewise, the He^3 must be compressed. The term s_{mixing} in equation (2.4.b) we get for the difference in molar Gibbs function between the mixed and the unmixed states;

$$g_m - g_{3+4} = P(v_3-v_m) + P(v_m-v_4) - Ts_{mixing} ,$$
$$= P(v_3-v_4) - Ts_{mixing} . \qquad (2.5)$$

Thus, we see that if the temperature is low enough so that the second term on the right hand side of equation (4) is smaller than the first, it is energetically more favorable for the isotopes to remain separated than it is for them to mix.

Of course the above argument does not guarantee that the conditions for phase separation can met. Several authers have done calculations based on microscopic theories of the interactions involved and have shown that the conditions for phase separation are indeed met for liquid solutions of He^3 and He^4 (see for example Cohen and Van Leewen [21]).

The phase separation curve for He^3-He^4 mixtures is shown in Figure 2.1 and has been established experimentally by many workers [22,23]. The region between the horizontal axis and phase separation curve is a non physical region. Any liquid mixture of He^3 and He^4, under its own vapor pressure, at a temperature below the maxmum in the curve will consist of light He^3 rich phase, whose concentration is determined by the left hand portion of the curve.

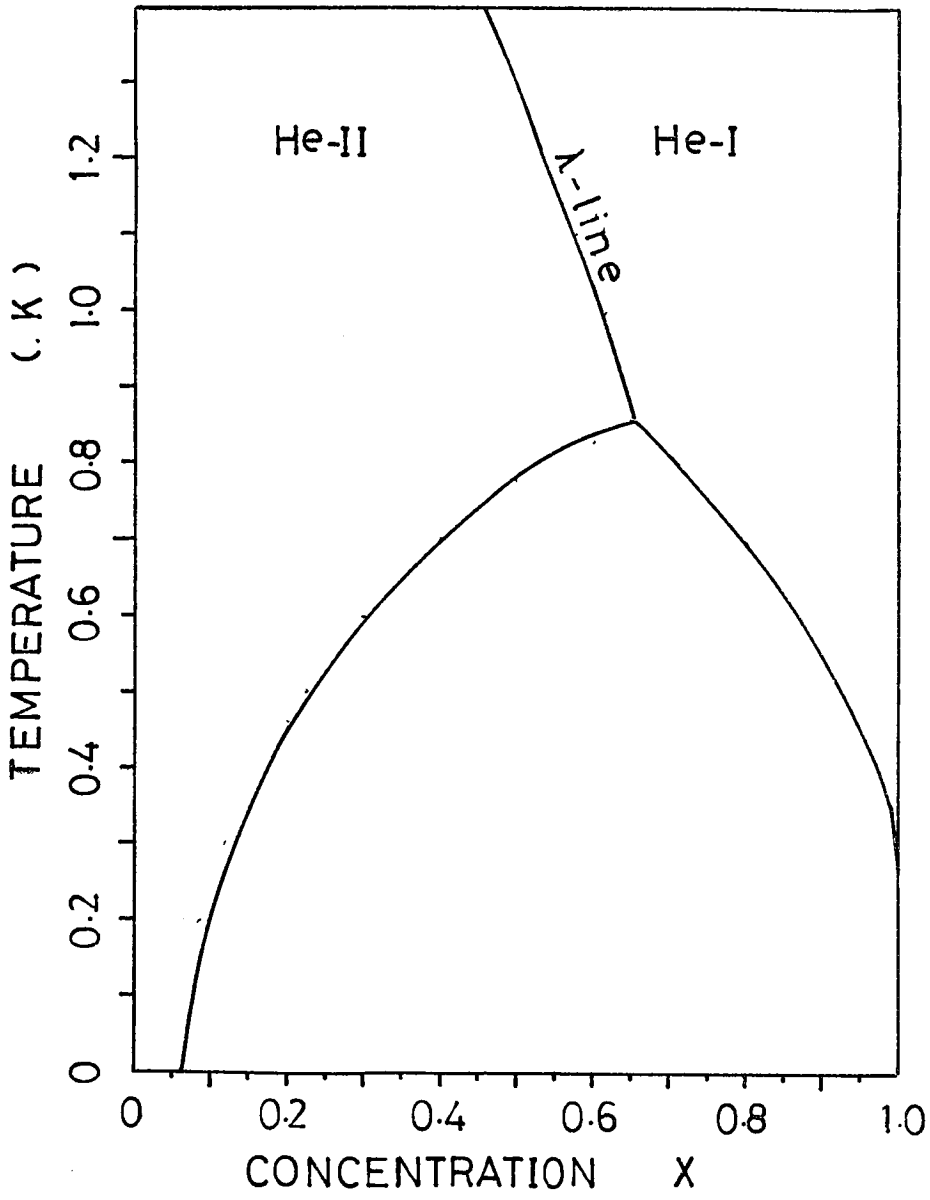

Figure 2.1 Phase diagram of He^3-He^4 mixtures.

X is the concentration of He^3 ($X=n_3/(n_3+n_4)$)

At all temperatures below the λ-line on Figure 2.1 the He^3-He^4 mixtures are superfluid.

Perhaps the two most important features of the phase separation curve relating to the dilution refrigeration are the finite concentrations as T approaches 0.0 K. The upper phase becomes essentially pure helium-3 and the lower phase has a limiting helium-3 concentration of 6.4%. These two features as we shall see below contribute both to the simplicity of the theoretical description of the dilution process and to the effectiveness of the process at very low temperatures.

Looking at figure 2.2 we can easily notice the similarity of this system with a liquid in equilibrium with its own vapor. It turns out that this analogy provides a usefull model for the theoretical treatment of dilution refrigerator. London, Clarke and Mendoza[16] first used this analogy when they noted that the isotherms of osmotic pressure versus helium-3 molar volume for He^3-He^4 mixture at low temperatures are strikingly similar to the pressure-volume isotherms of a condencible gas. The osmotic pressure is a real pressure due to the pressure of helium-3 in a weak He^3-He^4 solution.

The helium-3 in dilute solutions of helium-3 in superfluid helium-4 has been shown both theoretically[12,24] and

experimentally[25,26] to be well described as an ideal non-interacting Fermi-gas in which the effective mass of the heliun-3 atoms is modified by the presence of the superfluid helium-4. The osmotic pressure is just the pressure of this ideal Fermi gas. Since there are no dissipative interactions between the helium-3 atoms and the helium-4 atoms, the analogy extends to hydrodynamics as well as thermodynamics.

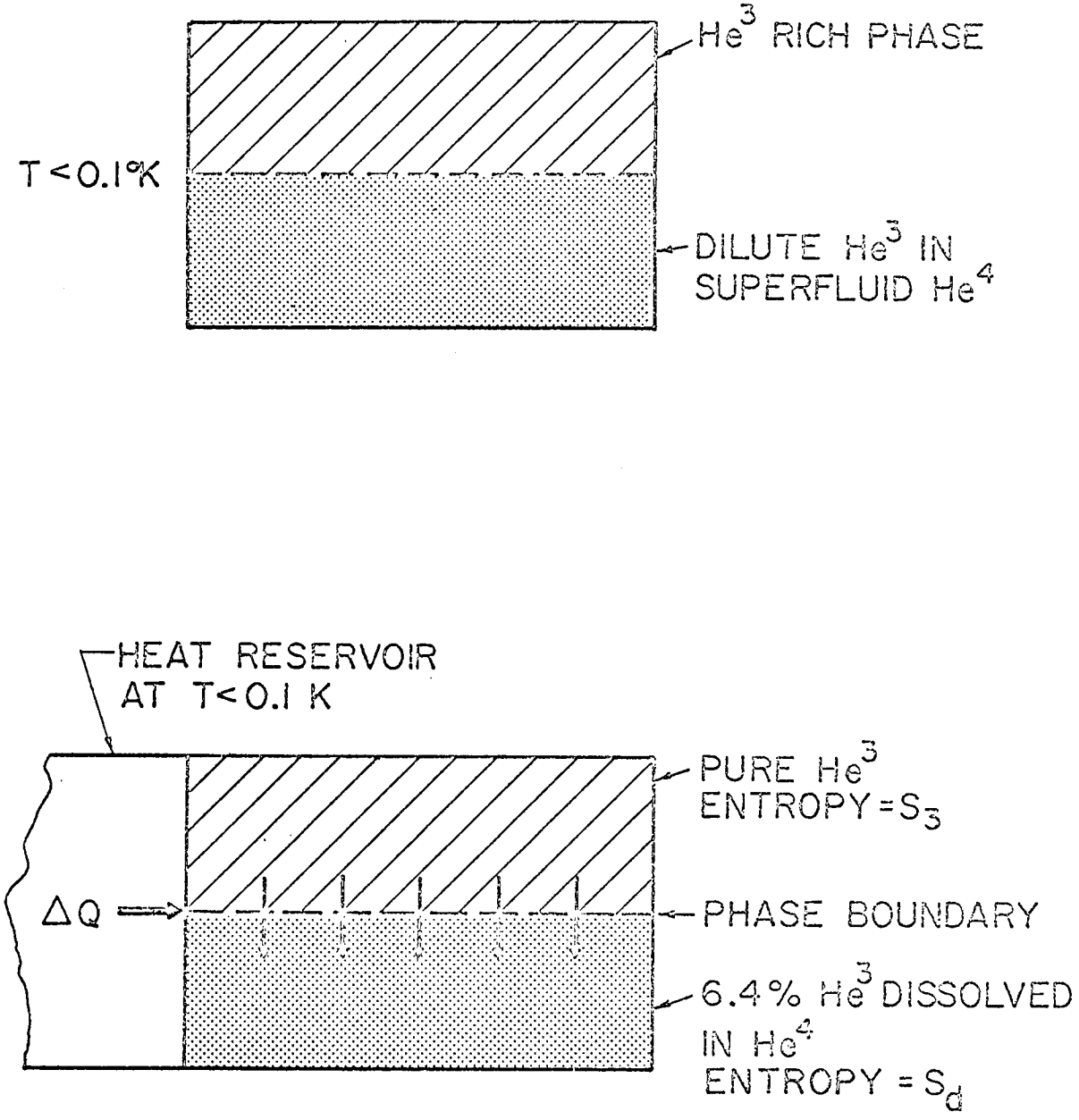

Figure 2.2 Schematic of phase separated He^3-He^4 mixtures at T< 0.1 K.

$ 2.3 Cooling Power of Refrigerator

With the liquid vapor model it will be done to calculate the cooling that takes place which helium-3 is transferred adiabatically across the phase boundary in a phase separated mixture. The correspondeces in the analogy are as follows;

concentrated He^3 (upper) phase . . liquid
dilute He^3 (lower) phase . . . . . vapor
osmotic pressure of He^3 in He^4 . . vapor pressure

It is considered that the cooling process is essentially the same as that which takes place when the vapor is removed from above a liquid.

$ 2.3.a In the Case of He^3 Refrigerator

Consider a vessel containing a pure heliun-3 liquid and a helium-3 gas under the satulated vapor pressure in thermal equilibrium at very low temperatures. Our method will be to calculate the difference in the enthalpy of the

upper phase and the lower phase. Since the lower phase is pure helium-3, the molar enthalpy (h_3) of a liquid helium-3 is

$$h_{liq} = h_{o3} + \int^{T} c^{p}_{liq}\, dT' \qquad (2.5)$$

where h_{o3} is a molar binding energy and c^{p}_{liq} is a molar specific heat under the constant pressure. Since there is a very rare gas in the upper phase, the binding energy is zero Therefore, the molar enthalpy (h_{gas}) is

$$h_{gas} = \int^{T} c^{p}_{gas}\, dT' \qquad (2.6)$$

where c_{gas} is the molar specific heat of a helium-3 gas under the constant pressure. The difference of molar enthalpy is

$$h_{gas} - h_{liq} = h_{o3} + \int^{T} (c^{p}_{gas} - c^{p}_{liq})\, dT' \qquad (2.7)$$

Usually, $L(=h_{gas}-h_{liq})$ is called the latent heat and is the quantity of heat needed to boil off one mole of a liquid. This latent heat is shown in figure 2.3 and is almost constant in the low twmperatures.

For evaporation of helium-3 a pump is used and the pumping speed is assumed to be $\dot{v}$ (cc/sec)

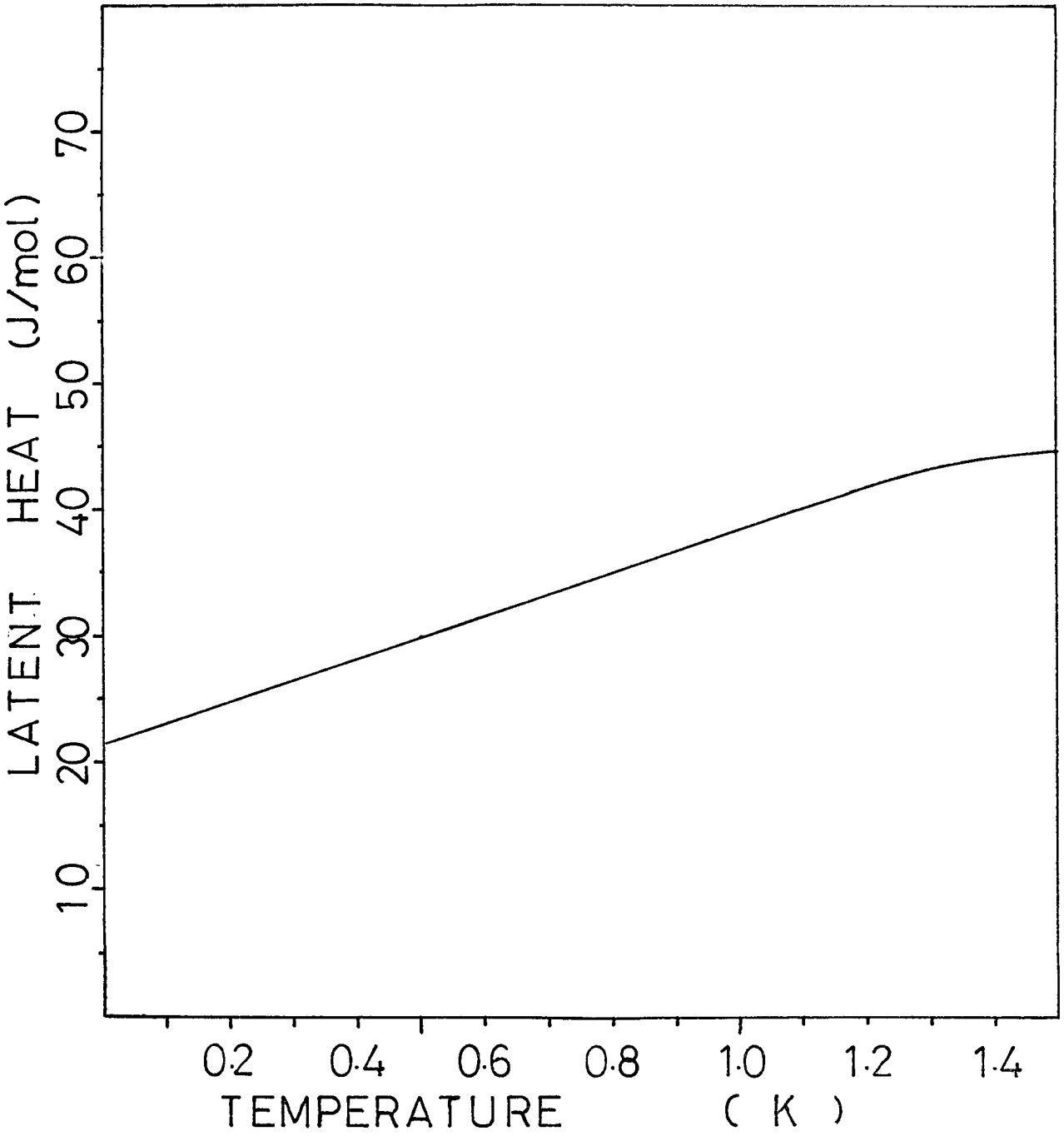

Figure 2.3 Latent heat of helium-3 versus temperature.

If a flow impeadance of helium-3 is neglected, the pressure of gas in a pumping tube is equal to a saturated vapor pressure of helium-3. Therefore, a mole-number of outgoing helium-3 gas ($\dot{n}_3$) is

$$\dot{n}_3 = P_s \dot{v} / RT_{room} \qquad (2.8)$$

where P_s, R and T_{room} are a saturated vapor pressure, a gas constant and a room temperature. Figure 2.4 shows a saturated vapor pressure of helium-3 versus temperature and P_s falls down exponentially below 0.5 K. An analytical form of the saturated vapor pressure between 0.2 and 3.324 K is

$$\begin{aligned} \ln P_s \text{ (mmHg)} = & -2.49174 / T + 2.24846 \ln T + 4.80386 \\ & -0.286001\, T + 0.198608\, T^2 \\ & -0.0502237\, T^3 + 0.00505486\, T^4 , \end{aligned} \qquad (2.9)$$

(see ref. 27). The cooling power of helium-3 evapolation refrigerator is

$$\dot{Q} \text{ (ergs/sec)} = \dot{n}_3 L, \qquad (2.10)$$

where L is a latent heat of helium-3.

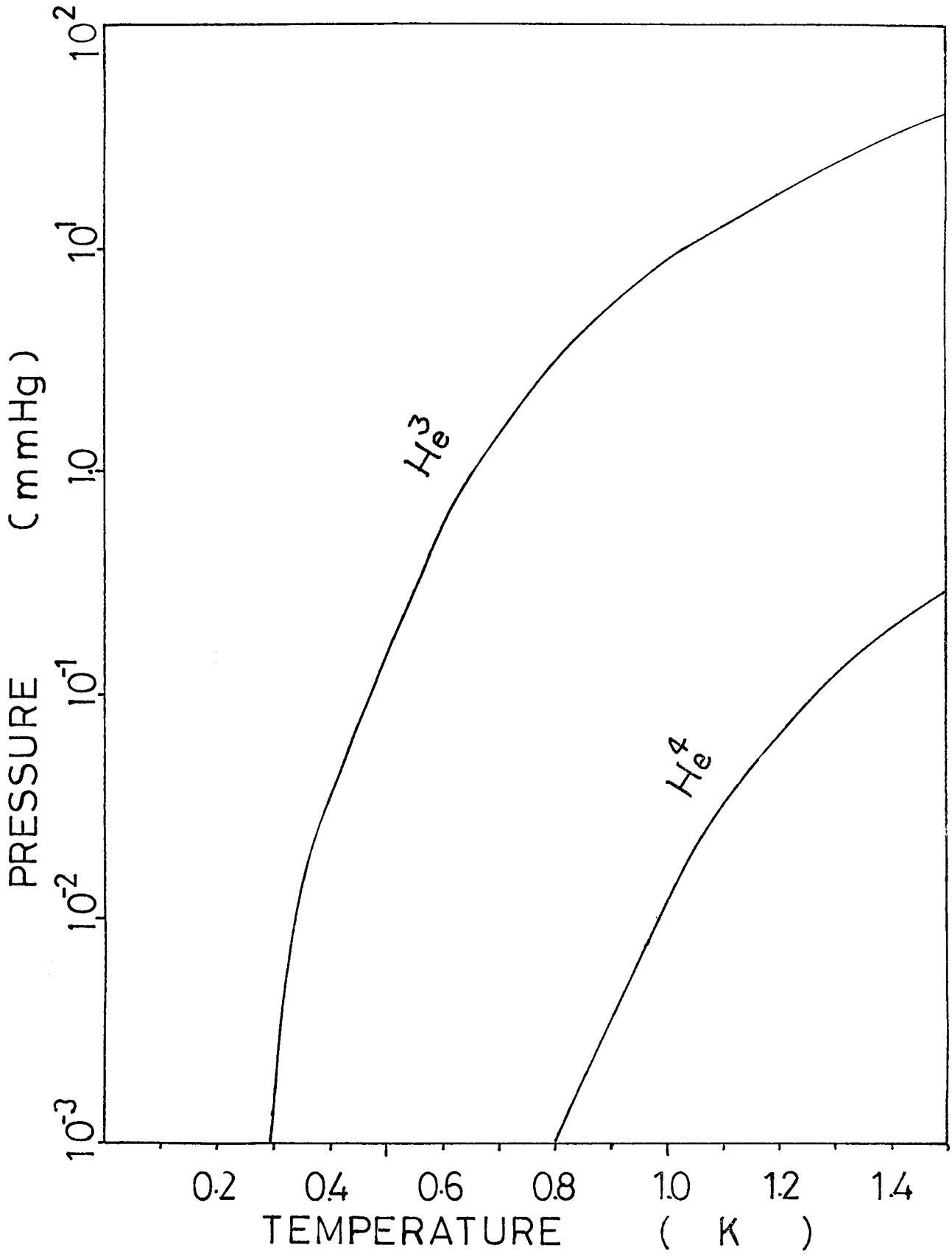

Figure 2.4 Saturated vapor pressure versus temperature for liquid helium-3 and liquid helium-4.

$ 2.3.b In the case of He^3-He^4 Dilution Refrigerator

Now consider a vessel containing a phase separated liquid helium-3 and helium-4 mixture in thermal equilibrium at a temperature below 0.1 K (see figure 2.2). Our method will be to calculate the difference in enthalpy of upper phase, h_3, and that of the lower phase, h_d, where h_3 and h_d are molar enthalpy on each phase. Since the upper phase is essentially pure helium-3, h_3 is equal to h_{liq} (see eq.(2.5)). The specific heat of pure helium-3 at the constant pressure, c_{liq}, was deduced from the data of Brewer, Daunt and Sreedhar[28] and Abel, Anderson, Black and Wheatley[29]. Figure 2.5 shows the specific heat of pure helium-3 at low temperatures. Below 45 mK, $c^p_{liq}=2.7RT$; thus we get

$$h_3 = h_{o3} + 1.35\ RT^2 , \qquad (2.11)$$

where h_{o3} is the zero point enthalpy. Pure liquid helium-3 in this temperature region is well described by Landau theory of Fermi liquids[30,31,32] with the effective mass, m^* , of the quasi-particles equal to about 2.8 m_3 where m_3 is the

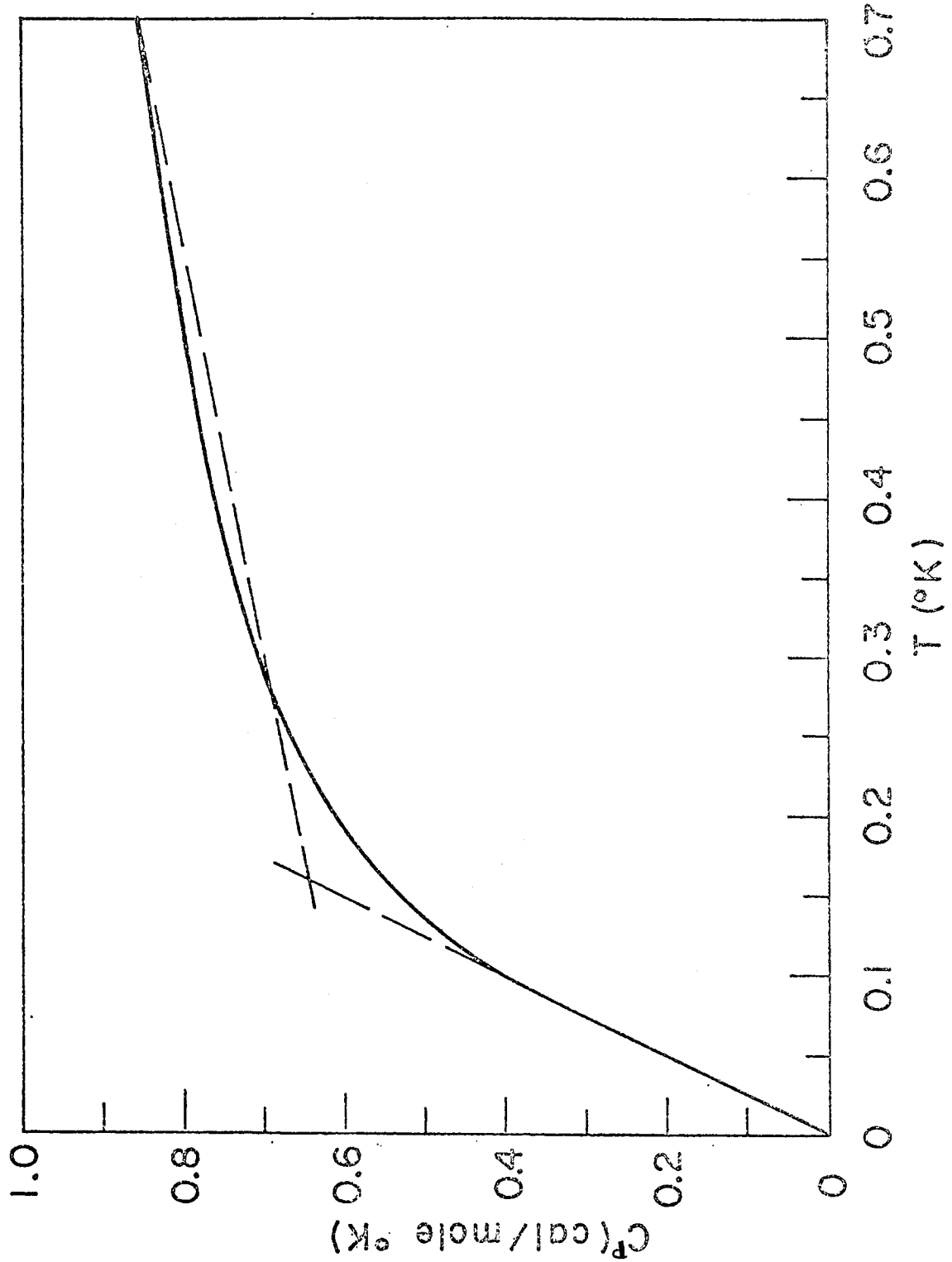

Figure 2.5 Specific heat of pure helium-3 at low temperatures

bare mass of helium-3 atom.

Since the helium-4 in the dilute phase is superfluid, the total entropy of the lower phase is just the entropy of the helium-3 atoms, which is can be well represented as an ideal degenerate Fermi gas. Thus the molar entropy of the dilute phase is(see for example, Landau and Lifshitz ; Statistical Physics)

$$s_d = \frac{\pi^2}{2} R \frac{T}{T_F} , \tag{2.12}$$

where T_F , the Fermi temperature, is given by

$$T_F = \frac{\hbar^2}{2km_e} (3\pi^2 N)^{\frac{2}{3}} , \tag{2.13}$$

with m_e = effective mass of a helium-3 atom in a background superfluid helium-4 = 2.4 m_3 ,

N = number of helium-3 atoms per cm^3.

The enthalpy can, in general, be calculated from the relation

$$dh_d = Tds_d + VdP = T(\frac{ds_d}{dT})dT + VdP \tag{2.14}$$

The most important contribution to P is the osmotic pressure.

Along the coexistence curve (see figure 2.1) the VdP term in equation (2.14) makes a significant contribution; in this case the condition $u_{3c}=u_{3d}$ is valid, that is the chemical potentials of the two phases must be equal. After inserting the proper numerical values,we obtain

$$h_d = h_{d3} + 14.65\ RT \quad (J/mole.K^2) \tag{2.15}$$

This relation is needed for caluculating the cooling that occurs in the mixing chamber by dilution. Equation(2.15) can be obtained more easily by starting from the basic equation along the coexsistence curve; $\mu_{3c}=\mu_{3d}$, that is

$$\mu_{3c}= \mu_{3d}= h_3- Ts_3 = h_d - Ts_d \tag{2.16}$$

$$s_3 = \int_{T'}^{T} \frac{c^p_{liq}}{T'}\ dT' = c^p_{liq} \tag{2.17}$$

Thus it is seen that the molar entalpy difference between the lower end upper phases is given by

$$h_d - h_3 = 10.6\ RT^2 + h_{d3} - h_{o3} \quad (J/mole\ K^2) \tag{2.18}$$

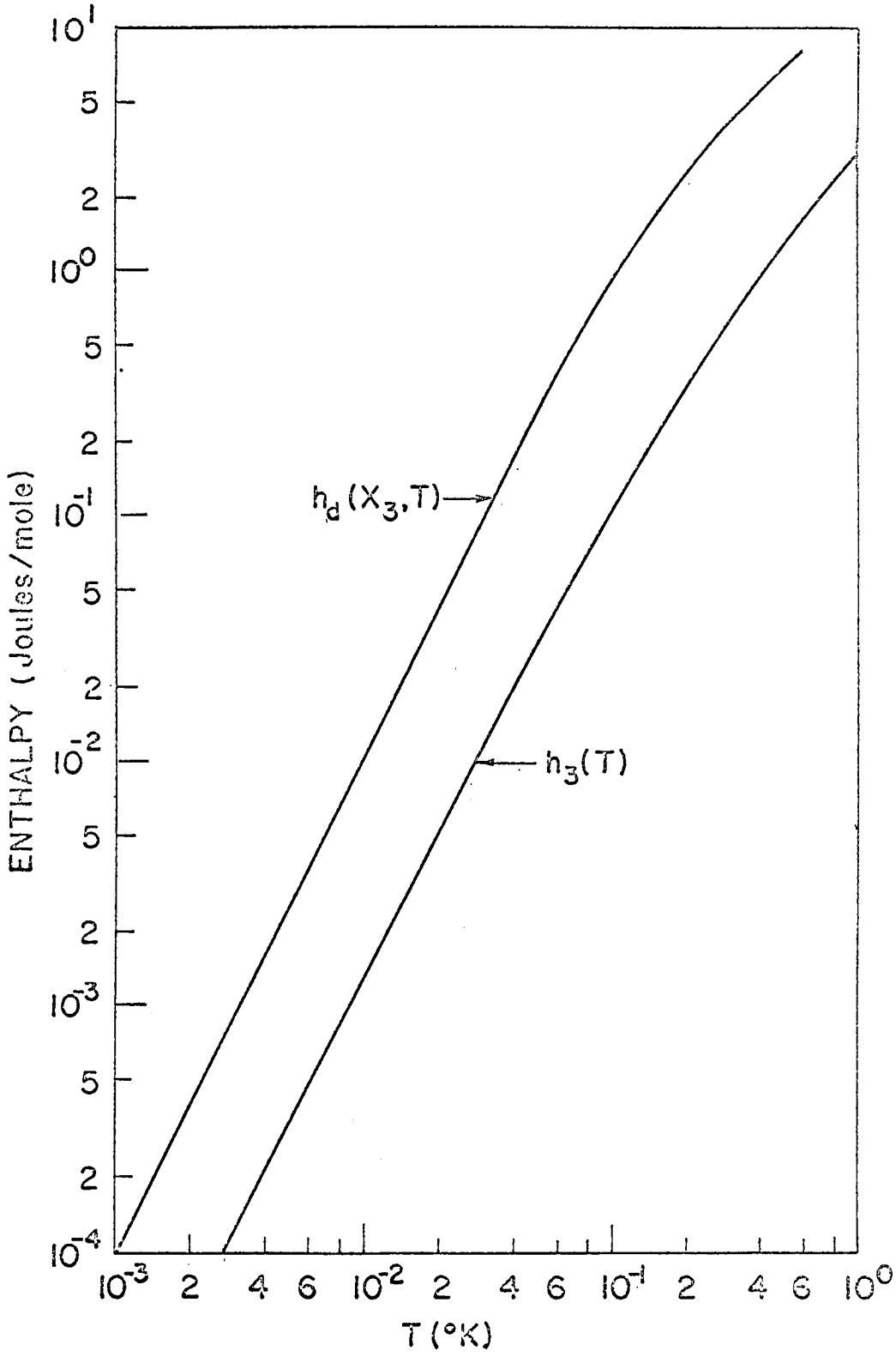

Figure 2.6 Molar enthalpyies of pure helium-3 and the equilibrium He^3-He^4 solution at low temperatures.

where h_{d3} is a binding energy of helium-3 atoms in superfluid helium-4. The h_{d3} is almost the same as the $h_{\sigma 3}$. The helium-3 in dilute phase is evaporated from a still and is exhausted by a pump. Therefore, a mole-number of outgoing helium-3 is almost constant. If we consider our vessel to be in thermal contact with a heat reservoir at a temperature T, then the rate of heat absorption $\dot{Q}$ that is drawn from the reservoir by the vessel is just

$$\dot{Q} = 10.6\ n_3 RT^2 \quad \text{(J/mole)} \tag{2.19}$$

where n_3 is a mole-number of outgoing helium-3 per second. Equation (2.10) gives the total heat extraction rate of a single cycle dilution cryostat in which helium-3 is withdrawn from the dilute phase but is not returned to the upper phase. Figure 2.6 shows a complete enthalpy diagram for a dilution refrigerator.

We must stress the fact that n_3 is not a function of T because the soluability is nearly independent of temperature below 40 mK.

$ 2.3.c Comparison of He^3 Refrigerator and Dilution Refrigerator

We now clearly see the difference between the dilution process and ordinary evaporation. In a dilution refrigerator the number of helium-3 atoms removed by the pump per unit time is independent of the temperature at mixing chamber but the cooling capacity, per helium-3 atom crossing the phase boundary. decreases propotionally to the temperature. In the evaporation type refrigerator the number of molecules removed from the vapor phase is propotional to the vapor pressure, which decreases exponentially with temperature, while the cooling capacity per atom removed remains approximately constant. This basic difference of the two types of refrigerators results in differences in their operational characteristics as emphasized in figure 2.7.

Therefore, the available cooling power of helium-3 evaporator and dilution refrigerator are

helium-3 evaporator

$$\dot{Q} = \dot{n}_3(T)\, L \qquad (J/sec) \qquad L = \text{constant},$$

dilution refrigerator (single shot type)

$$\dot{Q} = \dot{n}_3 \times 10.6\ RT^2 \quad (J/sec) \qquad \dot{n}_3 = \text{constant.}$$

Figure 2.6 shows the flow diagram of both type refrigerator. Figure 2.7 shows the cooling power of a He^3 evaporation refrigerator and of a He^3-He^4 dilution refrigerator as a function of temperature. It has been assumed the pump used can handle 5.0 (litres/sec). This corresponds in the dilution refrigerator to a helium-3 circulation rate of 20 (μ mole/sec) at all temperatures. In the He^3 refrigerator the same circulation rate is btained at 0.5 K. We can notice that in the temperature range $<$0.37 K the cooling capacity of a dilution refrigerator become larger than that of a evaporation refrigerator.

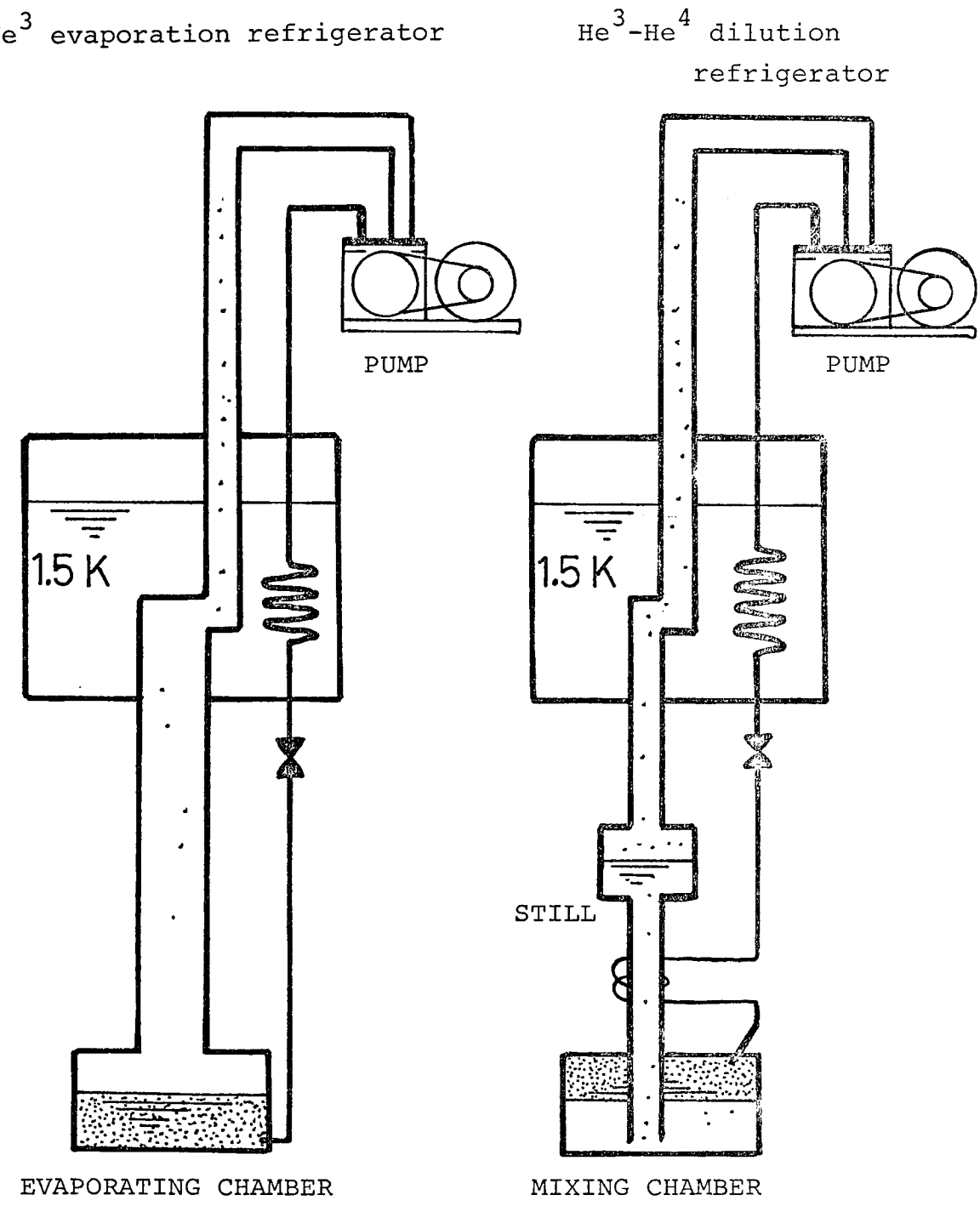

Figure 2.6 Schematic flow diagram of the He^3 evaporation refrigerator and He^3-He^4 dilution refrigerator.

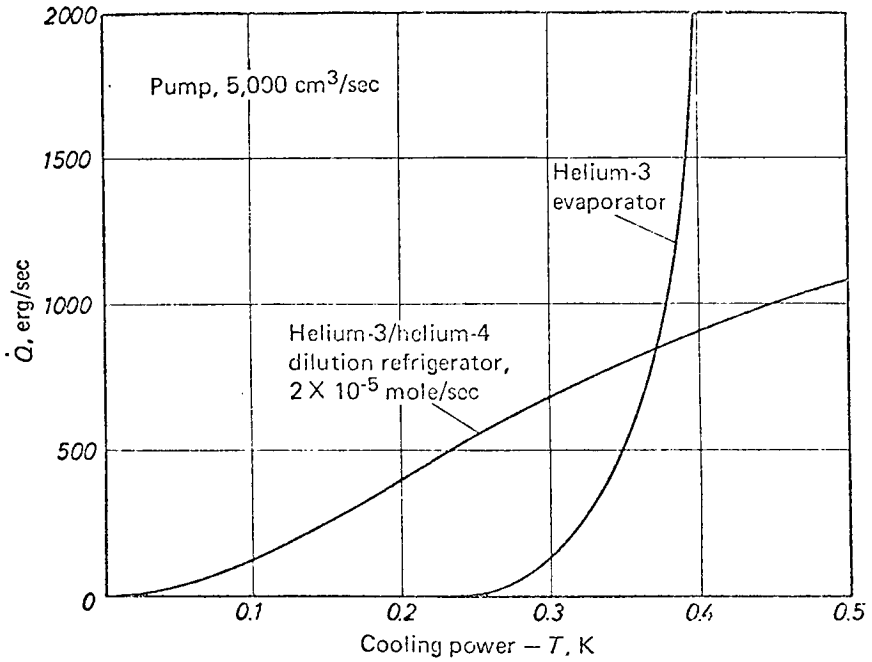

Figure 2.7 The cooling power of a He^3 evaporation refrigerator and of a He^3-He^4 dilution refrigerator as a functions of temperature. It has been assumed that the pump used can handle 5 (l/sec) of gas at all relevant pressure. This corresponds in the dilution refrigerator to a He^3 circulation rate of 20 (u mole/sec) at all temperatures. In the He^3 cryostate the same circulation ratio is obtained at 0.5 K.

$ 2.4 Continuous Dilution Refrigerator

There were basic ideas for realizing a continuously operating refrigerator, one was to circulate superfluid helium-4 and the other to circulate helium-3. In the beginning most work was done on the first idea and this was not very succesful. It lasted untill 1965 when the first dilution refrigerators based on the circulation of helium-3 were developed. but it did not cooled below 0,1 K. In 1966, Hall, Ford and Tompson reported on their first refrigerator with which they reached a temperature of about 70 mK,[17] at the same time, Neganov, Borisov and Liburg reported on a high cooling power refrigerator with a final temperature of 56 mK[18]. These refrigerators based on a circulation of helium-3. Today the refrigerators of this type is a standard one. The first dilution refrigerator based on the circulation of helium-4 was constructed by Taconis, Pennings, Das and Ouboter in 1971.

$ 2.4.a Dilution Refrigerator based on the Circuration of Helium-3

A schematic flow diagram of the dilution refrigerator is shown in figure 2.8. Concentrated helium-3 is condensed in a helium-4 bath at about 1.3 K at C. The liquid produced at C passes down a flow-limiting capillary, designed to produce adequate pressure drop for condensation to occur at C, to the still S. This capillary is taken from C to S inside the pumping tube from the still, so that the incoming liquid is cooled by heat exchanger with the vapor to the temperature of the still T_s. Between the still S and the mixing chamber M the liquid is further cooled in a heat exchanger H and in M heat is extracted from a load by the passeage of helium-3 atoms from the concentrated to the dilute phase. From M to S the helium-3 returns up the heat exchanger H through the stationary superfluid helium-4. In the still concentrated vapor is distilled from the dilute liquid and returned to C by a pump at room temperatures.

Since this is a stationary flow process, its orera-tion is most clearly understood by means of an enthalpy flow diagram, in fact the osmotic enthalpy defined by

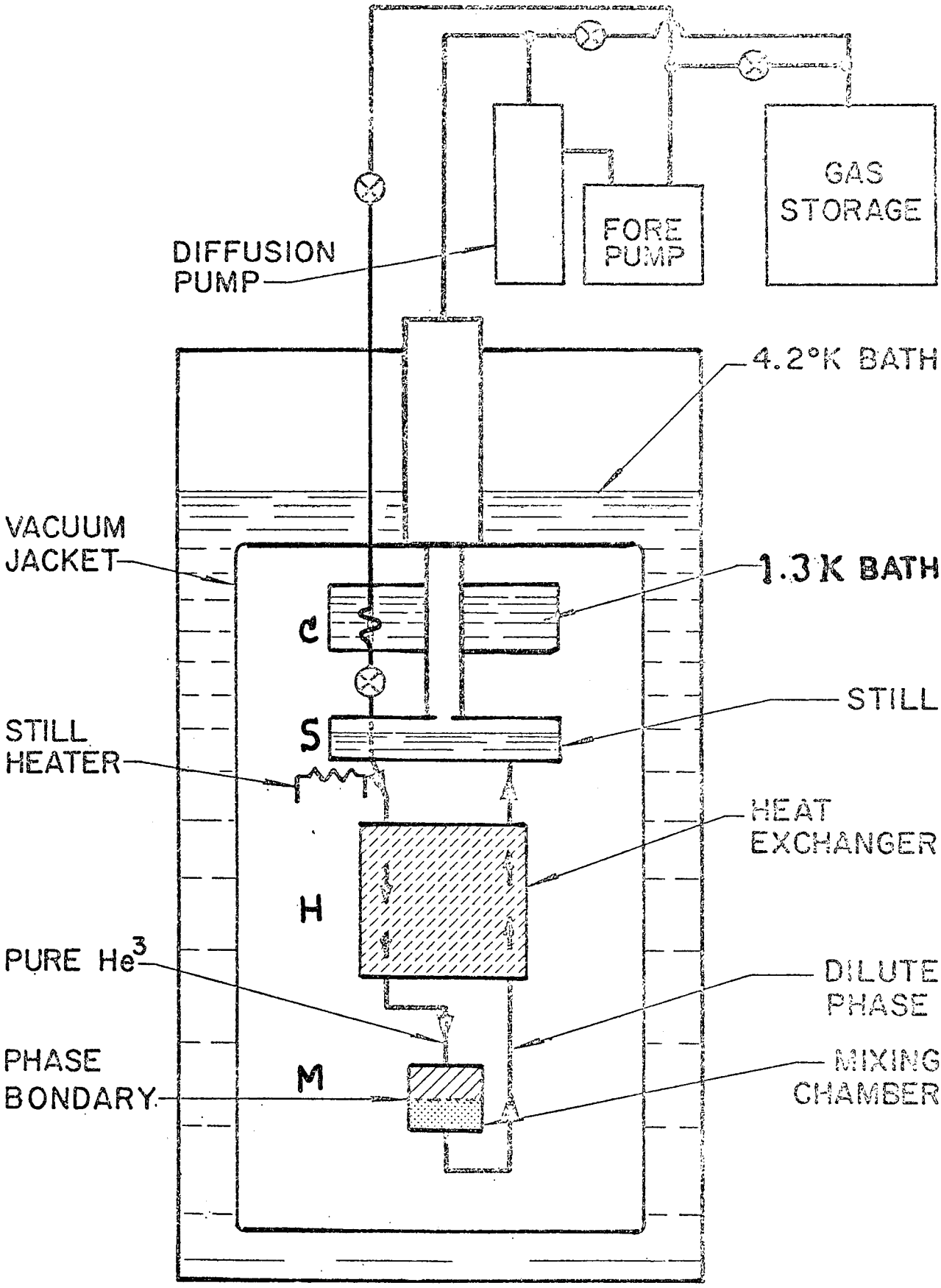

Figure 2.8 Schematic diagram of the continuous refrigerator based on the circulation of He^3

$ 2.4.b Dilution Refrigerator through which Helium-4 is circulated

Figure 2.9 shows a schematic drawing of the main part of the refrigerator through which helium-4 is circulated by Taconis et al.(see for example; ref.[30])
The lower (demixing) chamber (D) is kept at about 0.25 K by means of a helium-3 bath (B) to which it is mounted. The upper (mixing) chamber (M) is connected to the lower chamber (D) via a cupronickel capillary (C). There are two superleaks; the first (S_1), through which superfluid helium-4 is supplied, is brought in thermal contact with the helium-3 cryostat and goes to nearly the top of the upper chamber (M); the helium-4 is taken out through the second superleak (S_2) which goes from nearly the bottom of the lower chamber to outside the vacuum jacket. Above the vacuum jacket both superleaks are connected via capillaries to a helium-4 gas handling system outside the cryostat. The system can be filled with helium-3 by means of a capillary (F) to the lower chamber. The upper chamber and the capillary (C) are provided with cerous magnesium nitrate thermometers and a germanium thermometer (G) is mounted on the helium-3 cryostat.

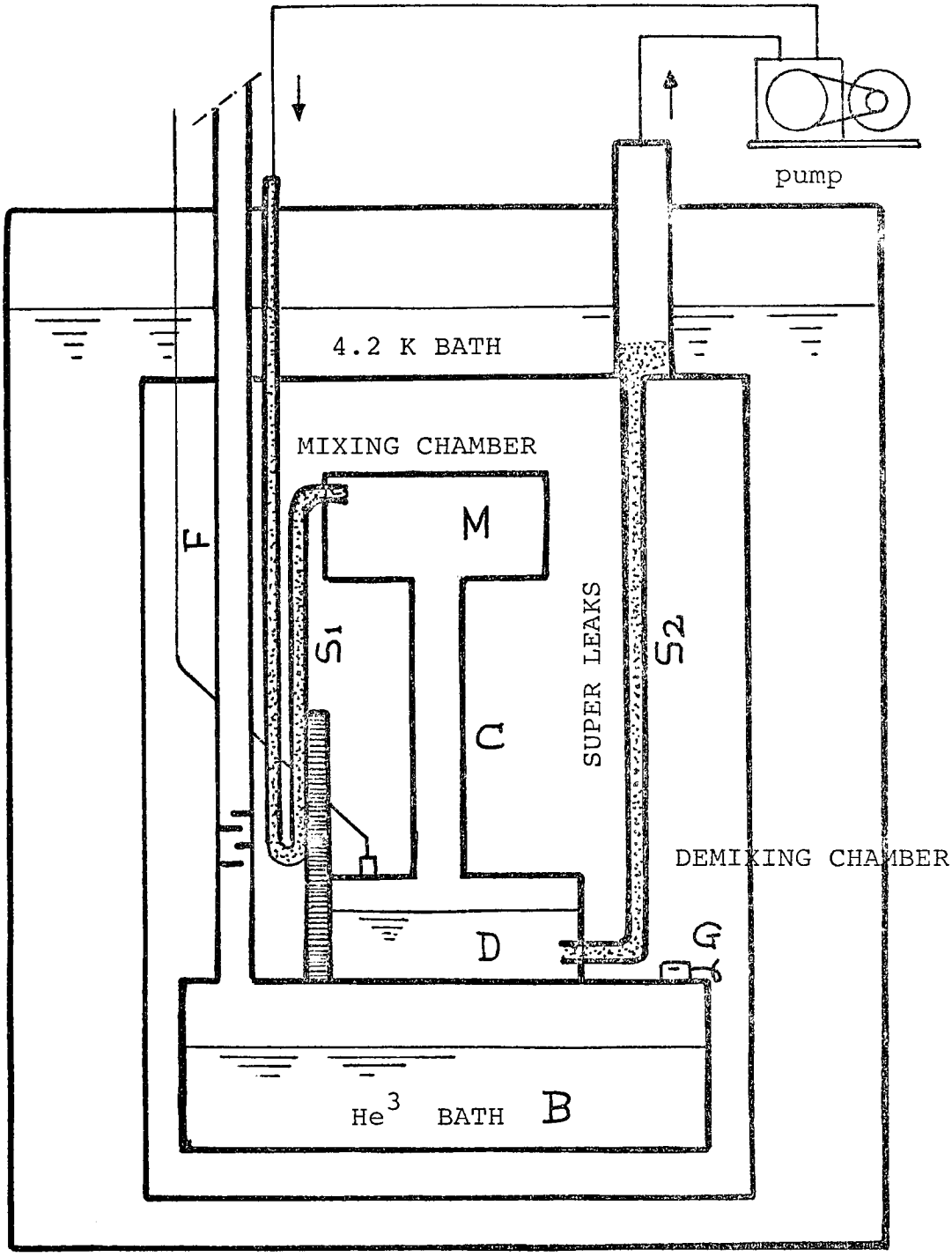

Figure 2.9 Schematic diagram of the continuous refrigerator based on the circulation of He^4.

$ 2.5 The Construction of Dilution Refrugerator

In this paragraph the aspects involved in the design of the various elements of the continuous dilution refrigerator will be considered in some detail.

$ 2.5.a The mixing chamber and ultimate temperature

First the thermodynamics involved at the mixing chamber will be considered when it is operating continuously at a temperature below 0.1 K. Let us assume that $\dot{n}_3$ moles per second of pure helium-3 is entering the top of the mixing chamber at a temperature T_i and the dilute phase is leaving the bottom of the chamber at a temperature T_m. Since T_i, which the concentrated phase leaves the heat exchanger, is greater than T_m, a significant part of heat load on the mixing chamber is just cooling in incoming helium-3 down to T_m. Assuming that all external heat inputs per second to the mixing chamber is $\dot{Q}_e$, the stationally condition is

$$10.6\ \dot{n}_3 T_m^2 = \dot{n}_3 [\ h_3(T_i) - h_3(T_m)\ ] + Q_e, \qquad (2.20)$$

where $h_3(T)$ is molar enthalpy of pure helium-3.

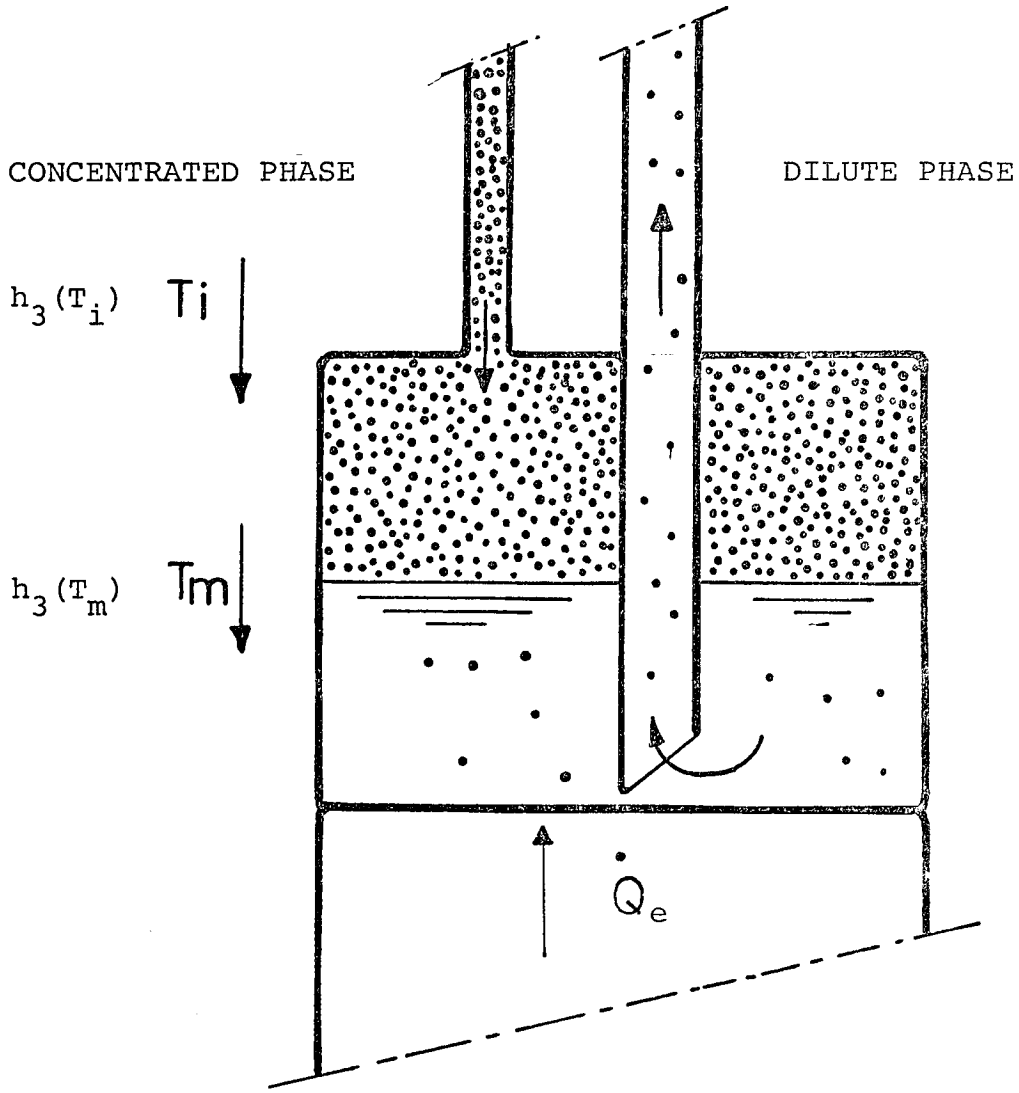

$$10.6\ \dot{n}_3 R\ T_m^2 = \dot{n}_3 [\ h_3(T_i) - h_3(T_m)\ ] + \dot{Q}_e$$

Figure 2.10 Schematic diagram illustrating the thermodynamics of the mixing chamber. Here h_3 is a molar enthalpy of pure helium-3 and T_i and T_m are the temperature of incoming helium-3 and mixing chamber, respectively.

From equation (2.11) ,in the temperature region below 0.1 K, $h_3(T)$ is given by

$$h_3(T) = h_{o3} + 1.35\,RT \tag{2.11}$$

where h_{o3} is the zero point enthalpy Substituting the equation(2.11) to equation (2.20), we get

$$10.6\,\dot{n}_3 R\,T_m^2 = \dot{n}_3[\,1.35RT_i^2 - 1.35RT_m^2\,] + \dot{Q}_e$$

$$T_m^2 = \frac{\dot{Q}_e + 1.35\,\dot{n}_3 R\,T_i^2}{11.95\,\dot{n}_3\,R} \tag{2.21}$$

In the temperature region above 0.1 K, equation (2.21) must be changed.

(1) Setting $\dot{Q}_e = 0$ in equation (2.11), we get the low temperature limit in continuous operation

$$T_m = 0.336\,T_i \tag{2.22}$$

and we see that this low temperature limit for T_m is determined by the efficiency of the heat exchanger, that is, the value of the incoming helium-3 can be reduced before it enters the mixing chamber.

(2) When the external heat input is constant and $T_i = T_m$, for example; 10^{-9} watt by a electrical resistor for temperature monitor(1000Ω-1μA) or a black body radiation ($5.7\times10^{-12}\ T^4$ watt/cm^2), equation(2.20) is rewritten

$$T_m = \sqrt{\frac{\dot{Q}_e}{10.6\ \dot{n}_3\ R}} \quad (K) \tag{2.23}$$

Here R = 8.31434 J/mol K, $\dot{Q}_e = 10^{-9}$ J/sec and $\dot{n}_3 = 10^{-5}$ mol /sec typically.

$$T_m = \sqrt{\frac{10^{-9}}{8.31434\ \ 10.6\ \ 10^{-5}}} \quad (K) \tag{2.24}$$

$$\simeq \quad 0.001 \quad (K)$$

Therefore, the lowest temperature is limited about 1.0 mK.

(3) It was first pointed out by Vilches, Wheatly and Abel [8] that viscous heating due to the flow of dilute phase from the mixing chamber might be a source of heating. Wheatly et al. pointed out that the viscous heating is the intrinsic temperature limit. We will consider a single cycle process where the helium-3 removed from the still is not returned.

Whennever a viscous fluid is caused to flow, a heat is given off because of mutual friction in the fluid. The fact that viscous heating becomes apparent only at the lowest temperatures results from the temperature dependence of the viscosity and the thermal conductivity of the dilute phase. Although no direct measurements of the viscosity has done, ultrasonic attenuation measurements by Abraham et al.[31] agree with the theory of Bayn and Ebner[32]. Roach[33] has used this theory, combined with that of Bardeen, Bayn and Pines [34], to calculate the limiting low temperature.

The viscosity at the low temperatures is

$$\eta_d = \frac{5\times10^{-7}}{T^2} \qquad \left[\frac{\text{dyne sec}}{\text{cm}^2} \right] \tag{2.25}$$

Abel, Johnson, Wheatley and Zimmerman[35] have measured the low temperature thermal conductivity, κ_d, of dilute He^3-He^4 solution and found that below about 0.01 K is

$$\kappa_d \cong \frac{30}{T^3} \quad \left[\frac{\text{erg}}{\text{sec cm K}} \right], \tag{2.26}$$

So we see that both the viscosity and thermal conductivity start to become appreciable as T approaches zero. A approximate analysis of the viscous heating will be given here.

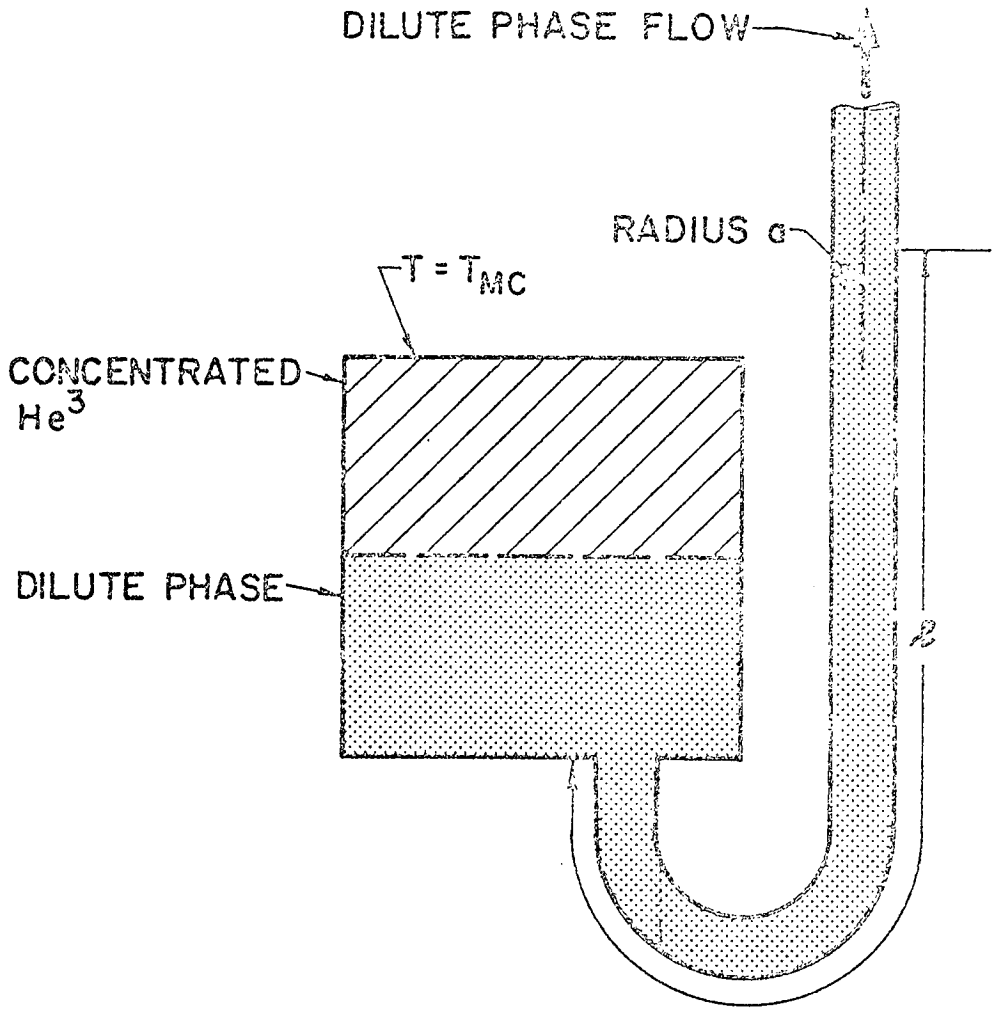

Figure 2.11 Diagram for viscous heating analysis

The situation is shown in figure 2.11. A tube of radius a conducts the dilute phase from the mixing chamber. We shall calculate the heat generated in length ℓ of this tube by viscous flow and assume this heat must be removed by the mixing chamber. It is also assumed that the length ℓ is isothermal due to the high thermal conductivity of the dilute phase.

The rate of viscous heating $\dot{Q}_v$ in this section of tube is geven by

$$\dot{Q}_v = \dot{V}_d \Delta P \tag{2.27}$$

where V_d and P are volume flow rate of the dilute phase and pressure drop across the length of tubing, respectively. Assuming Poiseille flow (i.e. no turbulence) we have

$$\Delta P = \frac{8 \dot{V}_d \ell \eta_d}{\pi a^4} \tag{2.28}$$

(see Landau and Liphshitz; Fluid Mechnics)
Now $\dot{V}_d$ can be weitten in terms of the molar flow rate of helium-3, $\dot{n}_3$. For concentration 6.3% this is

$$\dot{V}_d = \dot{n}_3 V_d / 0.063 \qquad (2.29)$$

where V_d is molar volume of dilute phase. Taking V_d = 28 cc/mole[27], equation(2.27) becomes

$$\dot{Q}_v = \frac{8X28^2}{0.063^2} \frac{\ell \eta_d \dot{n}_3^2}{\pi a^4 T^2} \qquad [erg/sec] \qquad (2.30)$$

Setting this equal to the total heat that can be removed, which is given in equation(2.21) we have for the temperature limit due to viscous heating

$$T_m = \left| \frac{0.79 \dot{n}_3 \ell}{10.6 \pi R} \right|^{\frac{1}{4}} \frac{1}{a} \quad [K] \qquad (2.31)$$

We see that T_m is not greatly dependent upon the length ℓ we take. Putting in tylical values for the parameters involved, $\dot{n}_3 = 10^{-5}$ moles/sec, ℓ = 1.0 cm and a = 0.05 cm, respectively,we get

$$T_m = 0.005 \quad [K] \quad (=T_{limiting}) \qquad (2.32)$$

This value agrees well with that deduced by Wheatley et al.[8]

We see from equation(2.30) that we shuld be able to reduce T_{lim} by increasing the radius of the dilute phase

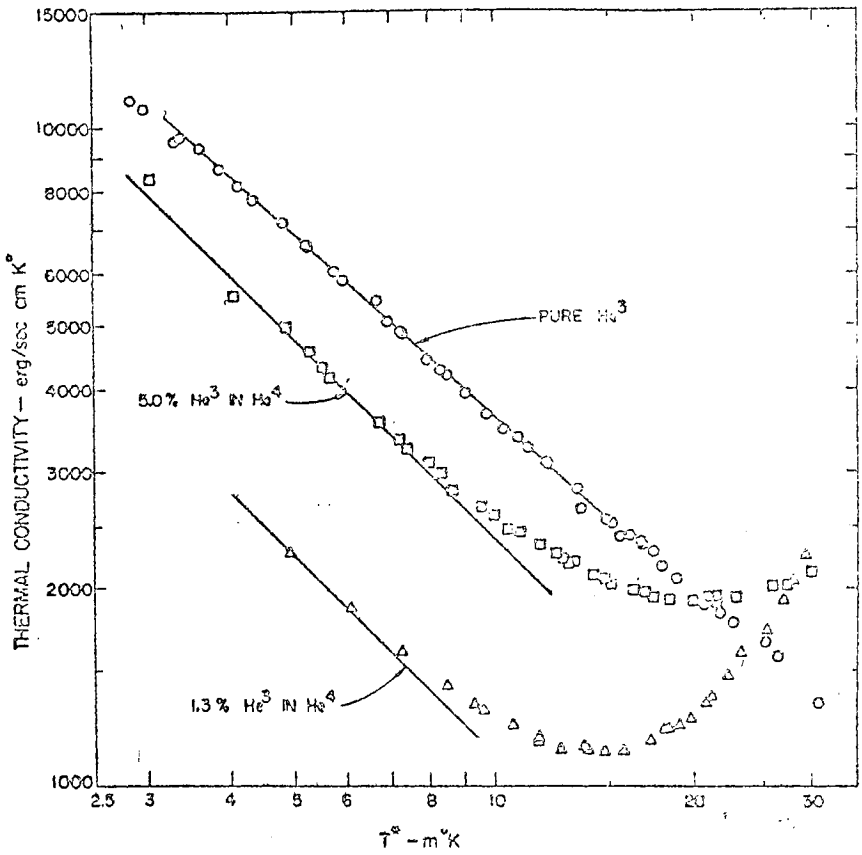

Figure 2.12 Thermal conductivity coefficient for dilute solutions of He^3 in He^4 of normal concentration; 1.3%, 5,0% and at saturated vapor pressure.

tube. However, we cannot increase this radius without limit for two main reasons. The first is fairly simple. Increasing the size of the tubing increases the conduction heat leak down the metal of the tube itself, unless the wall thickness can be made proportionally smaller Since the wall thickness of the tubing used is almost always made as small as possible anyway, this constitutes a problem.

The second is due to an effect noticed by H.London and mentioned by Hall et al.[17] If the osmotic pressure is constant, then the concentration of helium-3 at the top near the still is less than at the bottom. Hence, there may be a tendency towards a gravitational instability. London notes that such an instability would be damped by the flow of helium-3 in the tube and estimated a critical diameter of about 1 mm for typical operating conditions.

$ 2.5.b Heat exchanger

The heat exchanger finally determined the performance of the dilution refrigerator. In the temperature region below 1.0 K it becomes very difficult to achieve good thermal contact between two streams for two main reasons; (a) the thermal conductivities of most materials that can used to separate the two streams become very small below 0.1 K. and (b) the thermal contact between liquid helium and solid surfaces is hampered by the Kapitza boundary resistance.

For the concentrated side the Kpitza-resistance between copper and helium-3 is given by

$$R(He^3\text{-}Cu) = 2\times10^{-5}\ T^{-3}\ \ \text{sec cm}^2\ \text{K}^4/\text{erg}, \qquad (2.33)$$

The boundary resistance in the dilute phase is more complicated. Wheatly suggested that it is most probable that in the dilute phase energy is first transferred from the walls into the helium-3 quasiparticles via a helium-3 quasiparticle-helium-4 phonon interaction. Since the amount of heat that must be transferred in the exchangers diminishes

with T^2 and boundary resistance rise with the third power of T, the effective surfaces of the exchanger should be linearly increased with falling temperature.

Usually the heat exchanger is of the following two types; (I) a continuous tube-in-tube heat exchanger[36] and (II) discrete heat exchanger [8] The refrigerator of the auther has a simple continuous heat exchanger with a tube-in-tube type.

(I) Continuous tube-in-tube heat exchanger

The heat exchangers on the first successful refrigerators[17] were of the continuous type. In this type of heat exchanger an attempt is made to keep the two counterflowing streams in thermal contact continuously while maintaining a low heat flow along the direction parallel to the flow.

Let us consider the efficiency of such a heat exchanger. Figure 2.13 shows a small elements of our continuous heat exchanger. It is assumed that the limit to the thermal contact between the two streams is the Kapitza registant of the area elements dA. On the concentrated side the helium-3, flowing at a rate $\dot{n}_3$, has its tempe-

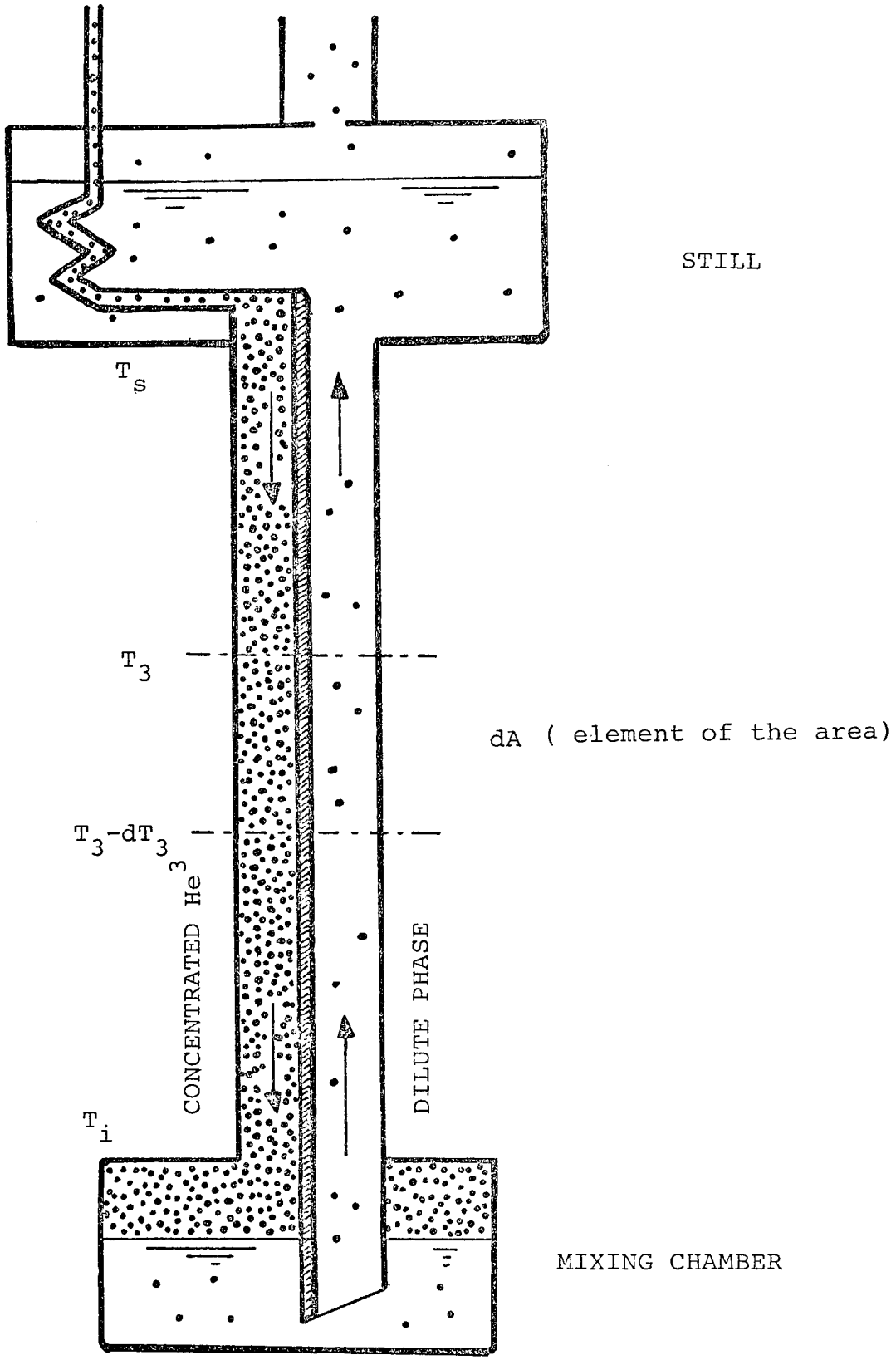

Figure 2.13 Differential element of the continuous heat exchanger.

rature reduced by the amount dT_3 so that equating the amount of heat its takes to do this to the amount of heat flowing through the serfaces element dA, we get

$$\dot{n}_3 c_3^P \, dT_3 = \alpha (T_3^4 - T_d^4) \, dA$$
$$= \alpha T_3^4 \, [\, 1 - (T_d/T_3)^4 \,] \, dA \, , \qquad (2.34)$$

The right hand side of equation (2.34) is based on the Anderson, Connolly and Wheatley[37] where we have neglected the difference between the Kapitza resistance for pure He^3 and the dilute mixture. c_3^P is the molar heat capacity of pure helium-3, T_3 and T_d are the respective temperatures of the concentrated phase and dilute phase. For simplicity we assume T_d is considerably lower than T_3, then the total area of the heat exchanger is

$$A = \frac{\dot{n}_3}{\alpha} \int_{T_S}^{T_i} \frac{c_3 \, dT_3}{T_3^4} \qquad (2.35)$$

where Ts is the temperature of the still and T_i is the outlet temperature from the heat exchanger

Figure 2.5 shows the specific heat of pure helium-3. We see that it is not unreasonable approximation to devide this curve into two temperature ranges, $T < 0.17$ K and

$T > 0.17$ K and c_3 is assumed to be linear in each region as shown in figure 2.5. We get

$$c_3 = 2.25\times10^8\ T \qquad [\frac{erg}{mole\ K}] \qquad T_i < 0.17 \qquad (2.36)$$

$$c_3 = 7.77\times10^7\ T + 2.5\times10^7 \qquad [\frac{erg}{mole\ K}] \qquad T_i > 0.17 \qquad (2.37)$$

Inserting these in equation( ) and integrating, we get

$$A = \frac{\dot{n}_3}{\alpha}\left[\frac{1.94\times10^7}{T_i^4} + \frac{5\times10^6}{T_i^5}\right] \quad cm^2 \qquad T_i < 0.17\ K \qquad (2.38)$$

$$A = \frac{\dot{n}_3}{\alpha}\left[\frac{5.63\times10^7}{T_i^4} - 4.07\times10^{10}\right] \quad cm^2 \qquad T_i > 0.17\ K \qquad (2.39)$$

Both of equations assumed that $T_s >> T_i$. In equation(2.38) we can make the further simplification that the second term is only a small correction. Then inverting equation (2.38, 39) we get

$$T_i^4 = \frac{1.94\times10^7}{A}\dot{n}_3 \qquad T_i < 0.17 \qquad (2.40)$$

$$T_i^4 = \frac{5.63\times10^7}{4.07\times10^{10} + A/\dot{n}_3} \qquad T_i > 0.17 \qquad (2.41)$$

Let us take $1/\alpha = 10^{-5}$ sec K^4 cm^2/erg which makes the Kapitza resistance involved about a factor of 10 higher than that measured by Wheatley et al.). Then we get

$$T_i = \left[\frac{1.94\times10^2\ \dot{n}_3}{A}\right]^{1/4} K \qquad A/\dot{n}_3 < 2.5\times10^5\left[\frac{cm^2\ sec}{mole}\right] \tag{2.42}$$

$$T_i = \left[\frac{5.63\times10^2\ \dot{n}_3}{4.07\times10^5\ A}\right]^{1/4} K \qquad A/\dot{n}_3 > 2.5\times10^5\left[\frac{cm^2\ sec}{mole}\right] \tag{2.43}$$

From equation(2.42) we see that if n_3 is too large then T_i becomed high and low temperature can not be achieved.

In our refrigerator $\dot{n}_3$ is about 10^{-4}mole/sec and A is about 10 cm^2(inner tube 0.64×0.33×1000 mm). Inserting this $A/\dot{n}_3=10^5 cm^2$sec/mole in equation(2.42), we get

$$T_i = [1.94\times10^{-3}]^{1/4}\ K \cong\ 0.209\ K \tag{2.44}$$

If we assume external heat leak is zero, from equation(2.22) in §2.5.a we get

$$T_m = 0.336\ T_i \cong 0.070\ \ K. \tag{2.45}$$

This value is almost the same as the value measured by

Mössbauer thermometer in our experiment(0.080 K).

Equations(2.42) and (2.43) are actually more restrictive of the total surface area A than $\dot{n}_3$ since $\dot{n}_3$ must be large enough to maintain a high heat extraction rate above the limiting temperature.

(II) Step Heat Exchanger

The preceding analysis has shown that it is very desirable to make the heat exchanger surface area as large as possible. It turns out that such a large surface area is easier to achieve if we allow the heat echanger process to take place in a stepwise manner rather than continuously. Such a modular heat exchanger is shown schematically in figure 2.14. In this type of heat exchanger the two counterflowing streams are brought into thermal contact at discrete points. The heat exchange modules are separated by regions of low thermal conduction in order to maintain a low heat flow along the respective directions of flow of the two streams.

The simplest means of attaining very large surface area with a resonably small volume is to use very finely divided particles.

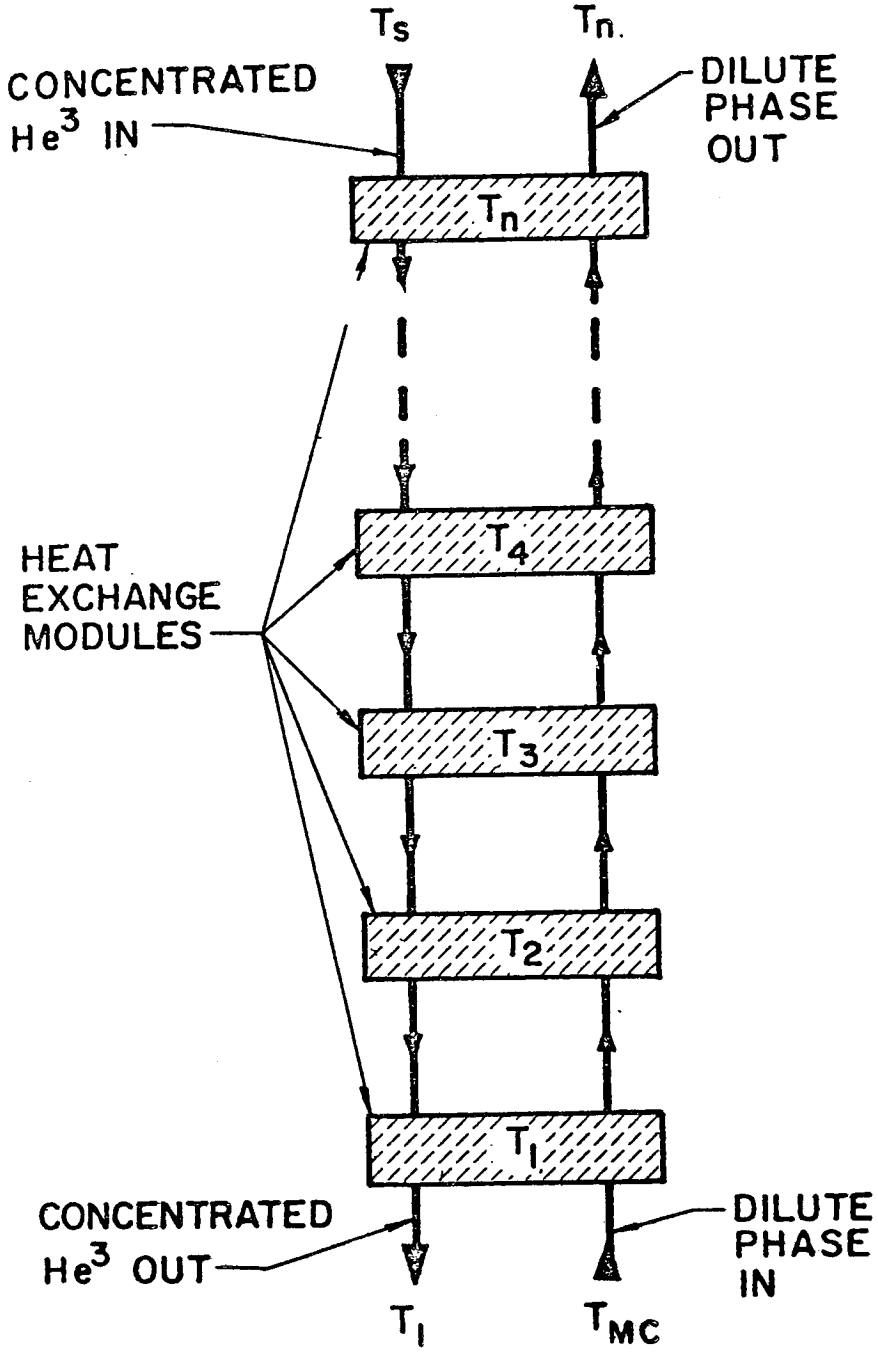

Figure 2.14 Schematic diagram of step heat exchangers

$ 2.5.c The Still

The helium-3 is evaporated from the still to maintain the flow. Assuming no helium-3 is evaporated, then the partial chemical potentials must be equal in the mixing chamber and still, and no osmotic pressure gradient can exist. But, since still and mixing chamber are at different temperatures, there must exist a gradient in concentration x_d, which is in a first approximation given by

$$P_{osm} = (T_m X_{dm} - T_s X_{ds})\ R/V_4 = 0, \qquad (2.46)$$

where X_{dm} and X_{ds} are concentration of helium-3 in the dilute phase of the mixing chamber and in the still, respectively. With X_{dm}=0.064 we get for a still temparsture of 0.7 K, X_{ds}=0.008. This small concentration is still lowered when helium-3 is evaporated from the still. Then osmotic pressure gradient is built up , which acts as the driving force for the helium-3 atoms to cross the phase boundary in the mixing chamber and produce cooling.

For a still temperature of 0.7 K, the pumped gas should cotain about 96 % helium-3. In practice the result is worse, acording to the superfluid film flow in the still. The enrichment of helium-3 gets better

with lower still temperatures and higher flow rates. Most refrigerators work with still temperatures between 0.6 and 0.8 K and helium-3 concentrations between 70 and 80 %.

Provided the heat exchanger is good, the helium-4 admixture in the concenterated side has only a small effect on the final temperature of the refrigerator. The helium-4 admixture causes an aditional load mainly on the warm end of the heat exchanger, where phase separation occurs. At temperatures below 0.15 K nearly no further separation takes places, since the concentration of the dilute phase remains practically constant below this temperature and no further heat of mixing must be handled if the exchanger.

Some provision must be made in the still for keeping the film flow rate low. Since the film flow rate is propotional to the smallest perimeter over which it must flow, the usual method taken to decrease the film flow is to install a small orifice in the top of the still. This orifice should be small enough to keep the film flow but large enough so as not to impede the flow of concentrated helium-3 gas from the still. Another method for reducing the film flow is discussed by Whitmore et al.[38] which involves heating the orifice.

$ 2.6 Experimental Apparatus

In this section, the apparatus of the dilution refrigerator is described. This system was constructed by Osaka Sanso Kogyo Co.

$2.6.a Circulation System of He^3-He^4 Dilution Refrigerator. (shown in figure 2.15)

(1) Pumping system

The concentrated helium-3 is removed from the still via a pump tube which runs through the 1.27 K bath and the main helium-4 bath. This tube was designed to have a conductance for helium-3 of about 5.6×10^{-4} (moles /sec) when the pressure at the still is 2×10^{-2} (torr). It diameter increases in three steps from $6\phi \times 0.5$ at the still to 2 inches at room temperature region.

The pumping system for the vapor removal is an Edwards model E02 (150 l/sec) backed by a ULVAC model PVD-150 (150 l/min) mechanical rotary pump. This rotary pump was completely sealed and this sysytem is capable of a maximum circulation rate of about 5.6×10^{-4} moles of He^3 /sec.

^{3}He-DILUTION REFRIGERATOR FLOW DIAGRAM FOR MÖSSBAUER STUDY

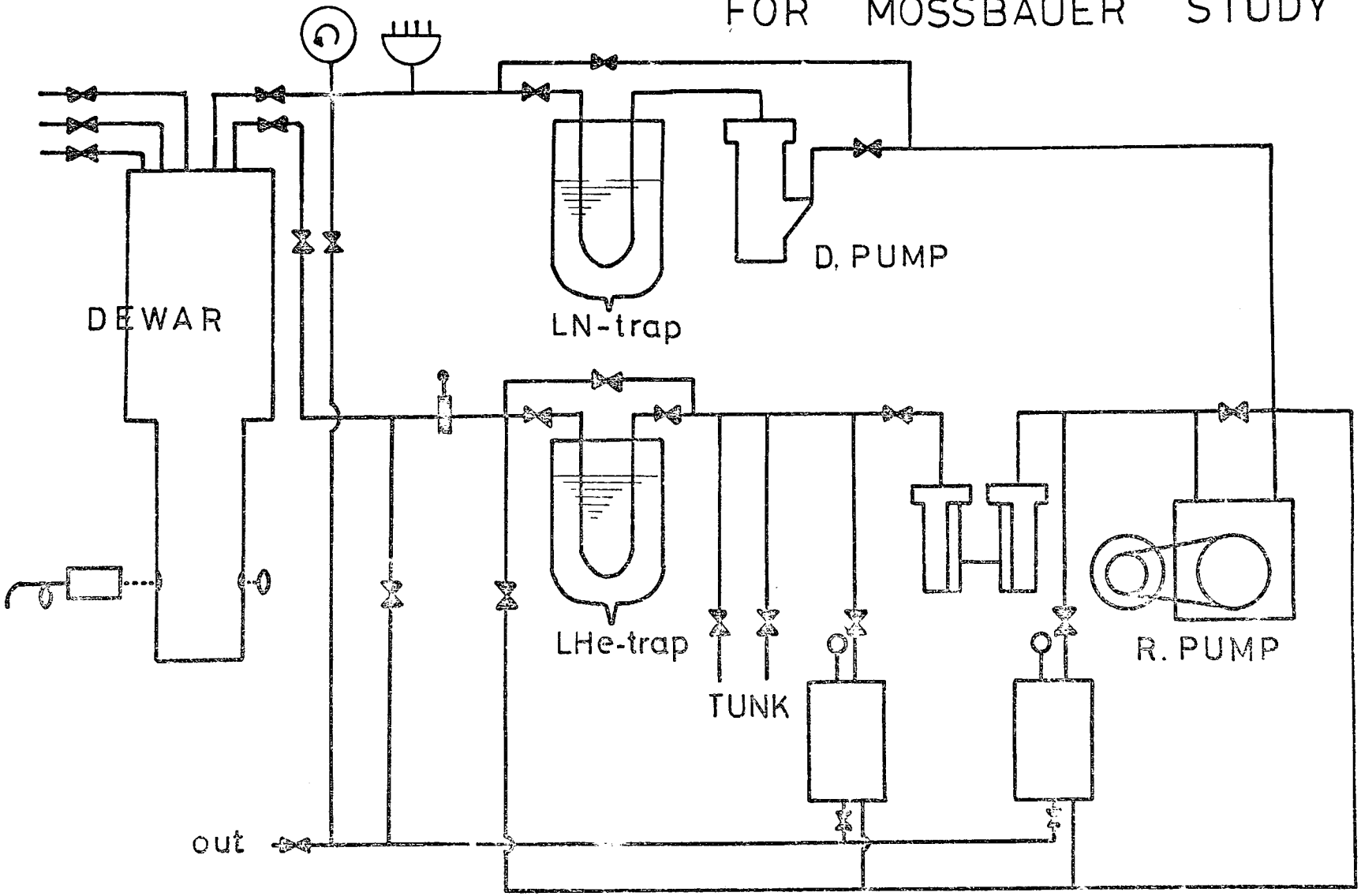

In our experiments to reduce back-streaming of oil from the diffusion pump into refrigerator, a nitrogen cooled trap is placed between the diffusion pump and the dewar system.

(2) Gas mixing and handling system

The gas handling system consists of 3-storage tanks with appropriate valves, interconnecting tubing, and pressure measuring devices. Two tanks have a volume of 10 liters and the other 20 liters but only 20 liters tunk is used.

Provisions are made in the gas handling system for introducing the mixture of helium-3 and helium-4 to the refrigerator either through the returen line or through the pumping tube. In early experiments, a molecular sheave trap was used in the system for removing the air from the helium gas, but it has no efficiency. So instead of a molecular sheave, a liquid helium-4 trap is used. When the helium gas is flowed through the liquid helium trap, which is held at liquid helium temperature, the air in the gas is absorbed by the cold trap. Once the helium gas has been so cleaned, the trap may be warmed to room temperature. It is then ready for use again.

(3) Return line for the concentrated helium-3

The concentrated helium-3 gas is flowed through the liquid helium trap, maintained at 4.2 K, before it is conducted back to the refrigerator This removes any air that may get into the gas. After leaving the trap the gas is conducted to the dewar top plate via a flexible stainless steel tube.

The line that carries the concentrated helium-3 gas passes through the nitrogen bath, the main helium bath and 1.0 K bath, maintaining the thermal contuct.

Below the 1.0 K bath a constriction is put in the return line. The purpose of the constriction is to maintain the pressure of the returning helium-3 at a high enough value so that it will recondense in the i.0 K bath. A flow limiting cappilary tube (0.05 cm o.d./ 0.0025 cm wall / 50 cm) was used for the constriction.

$ 2.6.b Main parts and Operating Characteristic of the Dilution Refrigertor

The refrigerator of the auther has a single heat exchanger with tube-in-tube type and only 20 minutes for the cooling from 1.3 K to 0.08 K. A schematic of the refrigerator assembly is shown in figure 2.16.

(1) Main parts of the dilution refrigerator

The still is a cylinder made of OFHC copper and has a volume of 11.8cm^3 (πX3.4X3.4X3.1/4 cm^3). The heat exchanger to cool the returning helium-3 to the temperature of the still is wound into a coil which passes through the still. Inside the rop of still, near the pump tube, a small diameter orifice is machined to limit the superfluid film flow. The heater which is necesseary to regulate the still temperature is a 300 Ω manganese wire resistor But it was not used because the temperature of the still became 0.8 K without this heater The temperature of the sill is monitered with a 100 Ω Speer resistor attached to the still with Apiezon N greese. Typical power input to the resistor during measurement is 10^{-11} watt.

Figure 2.16 Principal part of the dilution refrigerator

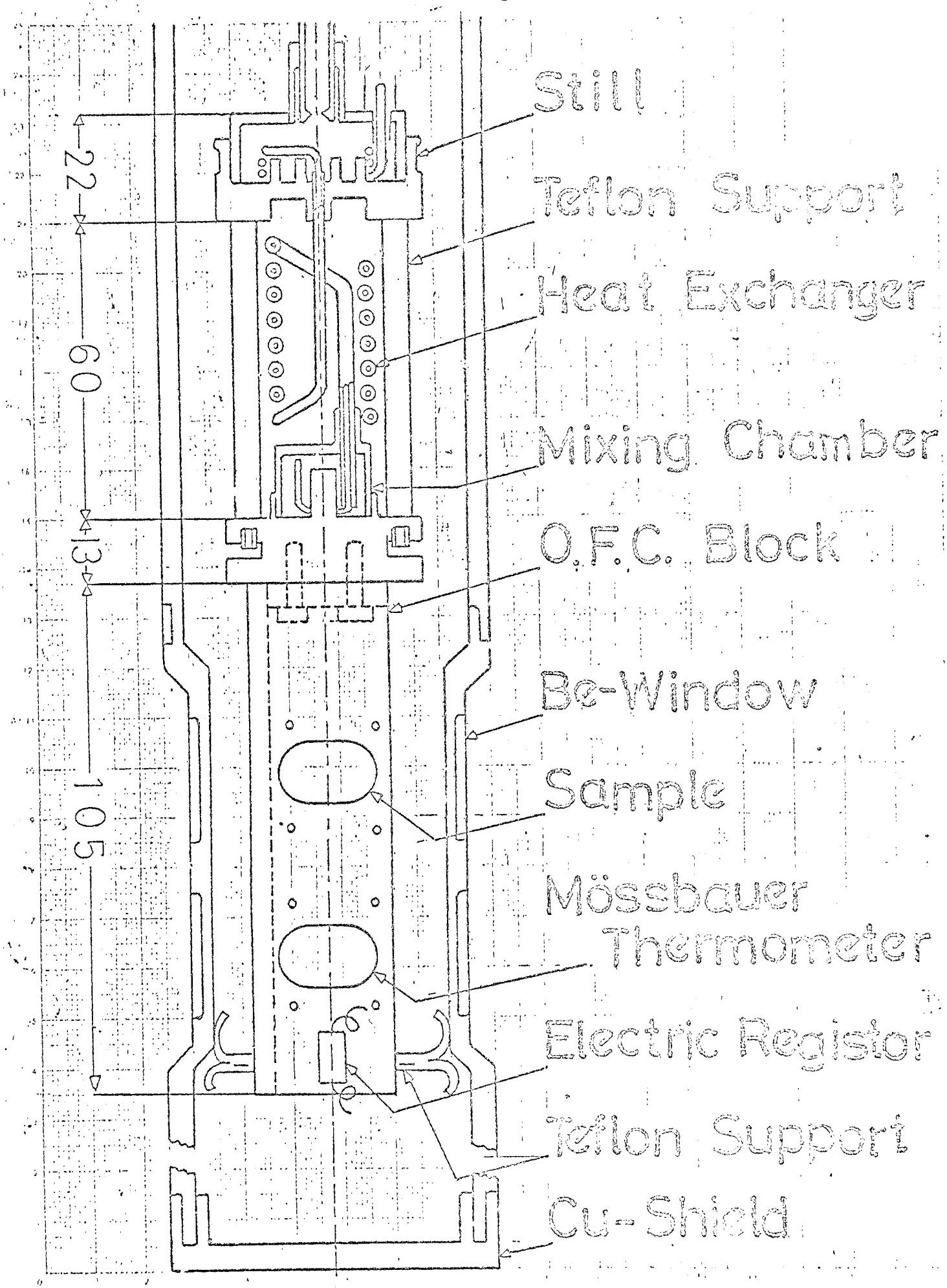

The mixing chamber is a cylinder made of OFHC copper and has a volume of 2.3 cm^3. The temperature of the mixing chamber is monitered by a 100 Ω [illegible] resistor that have been previously calibrated in [illegible] 0.08 K to 1.27 K against the Mössbauer thermometer. The resistance thermometer on the mixing chamber was mounted in exactly the same manner as the still heater.

The heat exchanger is of the tube-in-tube type and have a surface of 4.3 cm^2. The two streams in this tube counterflow in thermal contact continuously while maintaining a low heatflow along the direction parallel to the flow. In the proceeding section, it was stated that the temperature of the concentrated helium-3 outgoing from the exchanger become 0.209 K with the effective surface of 4.3 cm^2 and the flow rate of 3.8×10^{-4} moles/sec, theoretically.

Operating ch cte ic of the d ion refri erator

liquid nitroge reserv by putting 10 litres of heliu in The cooldown to liquid nitroge emperature takes about 1 hours.

Once the apparatus reac s at 77 K, the heliu exchange gas of about 10^{-4} tor are introduced to the xchange room and the liquid helium transfer is begun. The lium transfer usually takes about 2.5 hours by which time the apparatus inside the vacuum can has been cooled to 4.2 K by means of the exchange gas.

After the dewar is filled by liquid helium-4, the helium in 1 K can is evaporated. At the same time the exchange ga is pumped out and the He^3-He^4 mixture is introduced into the dilution refrigerator to condence.

After one hour for pumpin out the exchange gas, the He^3-He^4 mixture is circulated. If the initial gas mixture was properly chosen, the mixing chamber reaches its lowest temperatur

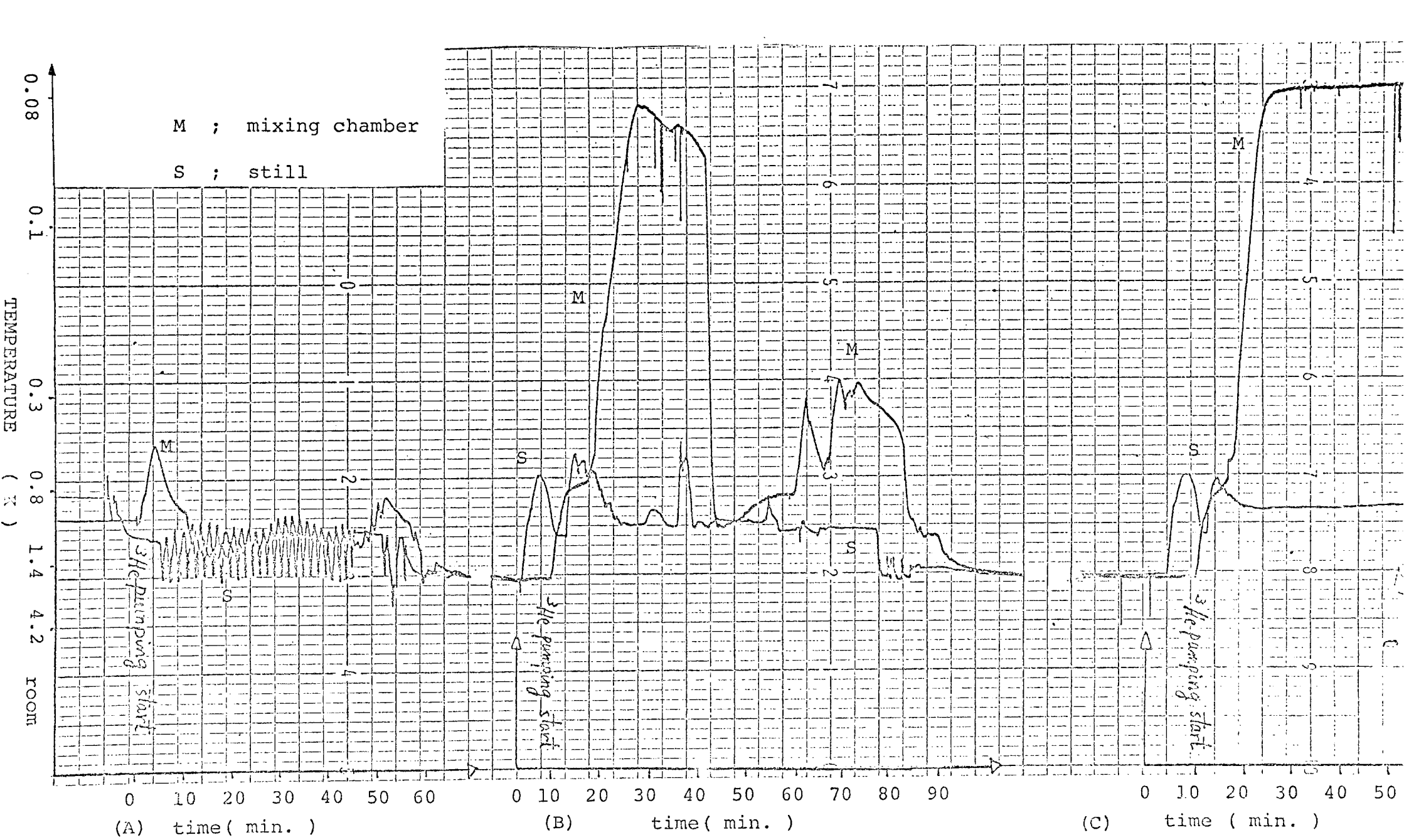

Figure 2.17 Cooling curve for the dilution refrigerator. (A) shows the operation with very small quantities of He^3, (B) rather small and (C) suitable.

in about 20 minutes. If the initial mixture was not properly chosen, the temperature at the mixing chamber and at the still becomes unstable. Figure 2.17 shows the cooling process for the dilution refrigerator with some quantities of He^3 applied. In the case of (A) in figure 2.17, the quantity of applied He^3 was very small. The temperature at the still showed the vibrating behavior curiously. In the case of (B) in figure 2.17, the quantity of an applied He^3 is somewhat small and the temperature at the mixing chamber was not stable. In the case of (C) in figure 2.17, since the quantity of an applied He^3 was suitable, the temperature at the mixing chamber and the still were very stable. The lowest temperature at the mixing chamber was about 0.08 K by the Mössbauer thermometer.

The equilibliumproperties of dilution refrigerator are given in Table 2.1 under no external load.

The heat extraction curves for no still heater are given in figure 2.18 . The curve by Wheatley et al. is shown for comparison.

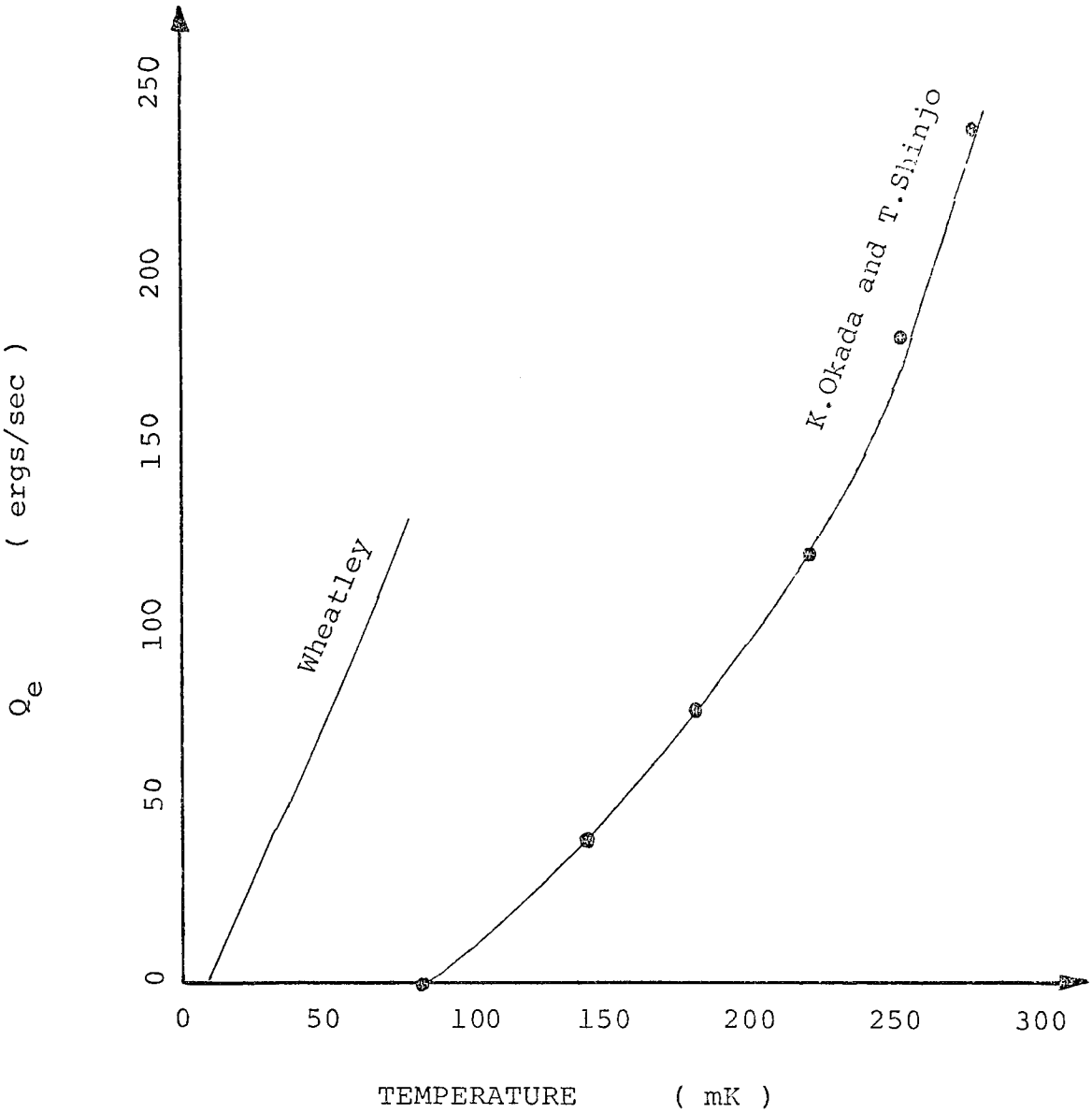

Figure 2.18 Heat extraction curve for dilution refrigerator The horizontal axis expresses the absolute temperature of the mixing chamber and the vertical axis expresses the heat applied to the mixing chamber.

Table 2.1 Equilibrium Properties of He^3-He^4 Dilution Refrigerator

Still heater	0	
Circulating rate	3.8×10^{-4}	moles/sec
Pressure at the still	0.002	tor
Pressure at the inlet line	20-30	tor
Quantity of applied He^3	1.7	liters/STP
Quantity of applied He^4	4.2	liters/STP

CHAPTER III

NUCLEAR POLARIZATION AND THE EFFECT OF THE MÖSSBAUER SPECTRUM AT VERY LOW TEMPERATURES

Among the recent fundamental scientific discoveries the Mössbauer effect has the distinction of having been one of the most fruitful. Today, the domain of Mössbauer effect which originally included only low energy nuclear physics, had expanded to include relativity, magnetism, metallurgy, chemistry, and even biophysics.

In this chapter, it will be stated that the nuclear polarization occurs at very low temperatures and it has a serious effect on the Mössbauer spectrum. A concise explanation to a β-transition of nucleus will be also be presented.

$ 3.1 Introduction

There are many reasons for pursuing Mössbauer experiments at very low temperatures. We should first mention studies of hyperfine intractions as a function of temperature in substances with magnetic transitions well below 1.0 K. Second, experiments which make use of nuclear polarization can only conducted at temperatures at which the thermal energy kT is comparable with the hyperfine interaction energy. A valuable feature of polarization experiments using the Mössbauer technique is that macroscopic orientation of the nuclei is not necessary. Finally, we should mention relaxation phenomena and localized moments in dilute alloys, in particular the Kondo-effect, as possible candidates for Mössbauer studies at very low temperatures.

At low temperatures a serious problem is radioactive heating. For a 10 mC Co^{57} source the total heating power is 80 ergs/sec, a load which if absorbed by the mixing chamber, is sufficient for preventing the refrigerator from cooling below 0.07 K[40]. In absorber experiments raioactive heating is generally very small, and calculations show that one should be able to reduced the temperature at least an order of magnitude further.

$ 3.2 Review of Mössbauer Spectroscopy

Mössbauer spectroscopy has become a standard spectroscopic tool in the decade since its discovery. Numerous texts and papers describing its principles and applications are to be found in the literature.[41-44] Consequently, we shall just briefly discuss some of the features of Mössbauer spectra particularly relevant to our experiment.

The parameters of the Mössbauer transition on Fe^{57} are indicated on figure 3.1 which shows the effects of three electromagnetic perturbations on the energy levels, the isomer shift, quadrupole and Zeeman splittings. We shall describe the Mössbauer line width and the recoilless fractions, then proceed to discussions of these perturbations.

$ 3.2.a Emission from bounded atoms and recoilless-fraction

In 1956 and 1957, R.L.Mössbauer was studying the scattering of gamma rays at the Max Plank Institute for Medical Research in Heidelberg. While comparing the scattering of the 129 eV gamma ray of Ir^{191} by Ir and Pt he found an increase in scattering in Ir at low temperatures which was counter to classical predictions.

To understand the new idea that Mössbauer brought to bear in the analysis of the emission and scattering of gamma rays by atoms bounded in solids, three different cases should be distinguished;

1. If the free-atom recoil energy is large compared to the binding energy of the atom in solid, the atom will be dislodged from its lattice site. The minimum energy required to displace an atom is known from radiation-damage investigations and generally falls in the range from 15 to 30 eV. Under these circumstances, the free-atom analysis given above is applicable.

2. If the free—atom recoil energy is larger than the characteristic energy of the lattice vibrations, the phonon energy, but less than the displacement energy, the atom will remain in its site and will dissipate its recoil energy by heating the lattice.

3. If the recoil energy is less than the phonon energy, a new effect arises becauce the lattice is a quantized system which cannot be excited in an arbitrary fashion. This effect is responsible for the unexcited increase in the scattering of gamma rays at low temperature first by Mössbauer.

This phenomenon is most readily understood in the case of an Einstein solid. At a given instant, the solid may be characterized by the quantum numbers of its oscillatiors. The only possible changes in its state are an increase or decrease in one or more of the quantum numbers. These correspond to the absorption or emission of quanta of energy $\hbar\omega_E$ which in real solids is characteristically of the order of 10^{-2} eV. The emission of a gamma ray is now accompanied by the transfer of integral multiples of this phnon energy to the lattice.

It has been shown by Lipkin[44] that when an average is taken over many emission processes, the energy transferred per event is exactly the free-atom recoil energy. Using this fact we may write an expression which leads derectly to the fraction of events, f, which takes place without lattice exitation. Since E_r is much less than $\hbar\omega_E$, typically $E_r = 1.943 \times 10^{-3}$ eV $\ll \hbar\omega_E = 10^{-2}$ eV, two quantum transitions can be neglected and as a result f is

$$E_r = (1 - f) \hbar\omega_E, \tag{3.1}$$

or

$$f = 1 - E_r/\hbar\omega_E. \tag{3.2}$$

Only these events gives rise to the Mössbauer effect. The f is often called the Lamb-Mössbauer coefficient.

This discussion is equally applicable to the scattering of X-rays or neutrons by atoms, where the distinction between elastic and inelastic processes is well known. Elastic scattering is equivalent to scattering without lattice excitation. A general expression for the fraction of elastic or zero-phonon processes is

$$f = \exp[-4\pi^2 \langle u^2 \rangle / \lambda^2] \tag{3.3}$$

where λ is the wavelength of the gamma quantum and $\langle u^2 \rangle$ is the component of the mean square vibrational amplitude of the emitting nucleus in the direction of the gamma ray. In order to obtain a value of f close to unity, we require $4\pi^2\langle u^2\rangle/\lambda^2 \ll 1.0$, which in turn requires that the rms displacement of the nucleus must be small compared to the wavelength of the gamma ray.

The pysical significance of this requirement is apparant. If the period of the motion of the atom in the lattice is short compared to the time associated with the emession of the gamma ray and the amplitude comparable to the emitted wavelength, then the phase of the emitted wave will be strongly modulated. Such a phase modulated wave is not monochromatic and a resonator tuned to the unmodulated wave is not readily excited because the excitation of the passing wave train is not coherent.

Equation (3.3) can be obtained in microscopic derivation The interaction Hamiltonian between the nucleus and gamma-rays, H_{int}, is quantum mechanically

$$H_{int} = \sum_p \left(- \frac{q}{m_p c} \mathbb{A}(x_p)\ p_p + q\phi(x_p) \right) - \sum_{p,n} \mu_i \times [\nabla \times \mathbb{A}(x_i)] \tag{3.4}$$

where, m, p, q and μ are mass, momentum, charge and the magnetic moment of the nucleus. And the suffix p and n denote a proton and a nutron. A(x) and $\Phi(x)$ are the potential of gamma-rays at the position, x. The transition probability, W_{i-f} from a initial state $|in\rangle$ to a final state $|fi\rangle$ is drawn by

$$W_{i-f} \propto |\langle in|H_{int}|fi\rangle|^2 \qquad (3.5)$$

Since the atomic motion is independent of the motion of nucleus, $|in\rangle$ and $|fi\rangle$ can be devided into two parts, that is, the state of a nucleus $|N\rangle$ and the state of lattice $|L\rangle$.

$$|in\rangle = |N_{in}\rangle\ |L_{in}\rangle \quad \text{and} \quad |fi\rangle = |N_{fi}\rangle\ |L_{fi}\rangle . \qquad (3.6)$$

The $\mathbb{x}$ can be expressed with a vector of a position $\mathbb{X}_L$ from the center of lattice to the center of a nuclear-mass and a vector of a position $\mathbb{X}_N$ from the center of a nuclear-mass to a nucleon. The momentum corresponsing to $\mathbb{x}$ can also be expressed with $\mathbb{P}_L$ and $\mathbb{P}_N$, namely

$$\begin{aligned} \mathbb{x} &= \mathbb{X}_L + \mathbb{X}_N , \\ \mathbb{p} &= \mathbb{P}_L + \mathbb{P}_N . \end{aligned} \qquad (3.7)$$

Since the expectation value of $\mathbb{P}_L$ is 5-orders of magnitude smaller than that of $\mathbb{P}_N$, we get

$$\mathbb{P} \cong \mathbb{P}_N. \tag{3.8}$$

The gamma-ray is represented with a plane wave, which has

$$A(\mathbb{x}) = A_o \exp(i\mathbb{k}\mathbb{x}) = A_o \exp(i\mathbb{k}\mathbb{X}_N) \exp(i\mathbb{k}\mathbb{X}_L) \tag{3.9}$$

$$\Phi(\mathbb{x}) = \Phi_o \exp(i\mathbb{k}\mathbb{x}) = \Phi_o \exp(i\mathbb{k}\mathbb{X}_N) \exp(i\mathbb{k}\mathbb{X}_L)$$

Substituting the equation (3.8) and (3.9) to (3.6), we get

$$\langle in|H_{int}|fi\rangle = \langle N_{in}|C|N_{fi}\rangle \langle L_{in}|\exp(ikX_L)|L_{fi}\rangle \tag{3.10}$$

where $\langle N_{in}|C|N_{fi}\rangle$ is independent of the lattice vibration. A part of the fraction of recoil-free process is

$$f = \frac{|\langle in|H_{int}|in\rangle|^2}{\sum_f |\langle fi|H_{int}|in\rangle|^2} = \frac{|\langle L_{in}|e^{ikX_L}|L_{in}\rangle|^2}{\sum_f |\langle L_{fi}|e^{ikX_L}|L_{fi}\rangle|^2}$$

$$= |\langle L_{in}|e^{i\mathbb{k}\mathbb{X}_L}|L_{in}\rangle|^2 . \tag{3.11}$$

We introduce the displacement vector $\mathbb{u}$ from a lattice point

$\mathfrak{L}$, and $\mathfrak{X}_L = \mathfrak{L} + \mathfrak{u}$. If the temperature is finite, then equation(3.11) must be replaced by its thermal average

$$f = \frac{\sum_i |\langle L_{in}|e^{i\mathfrak{k}\mathfrak{u}}|L_{in}\rangle|^2 e^{-Ei/kT}}{\sum_i e^{Ei/kT}} \qquad (3.12)$$

Using the expansion of the exponential function, e^{iku}, we get

$$|\langle L_{in}|e^{i\mathfrak{k}\mathfrak{u}}|L_{in}\rangle|^2 = 1 - \mathfrak{k}^2 |\langle L_{in}|\mathfrak{u}^2|L_{in}\rangle \qquad (3.13)$$

Therefore, substituting equation(3.13) to (3.12), we get

$$f = \exp(-k^2\langle u^2\rangle) \text{ or } = \exp(-4\pi^2\langle u^2\rangle/\lambda^2) \qquad (3.14)$$

Where $\langle u^2\rangle$ is the thermal average of u^2 and λ is the wavelength of gamma-ray.

Q.E.D.

Table 3.1 shows the recoilless fraction of a Einstein-model solid and a Debye-model solid.[45]

Table 3.1 The specific heat and the recoilless fraction of a Einstein-model solid and a Debye-model solid.

	Einstein	Debye
specific heat		
low temp.	$R\frac{\Theta_E^2}{T^2}\exp(-\frac{\Theta_E}{T})$	$\frac{12\pi^4 R}{5\Theta_D^3}T^3$
high temp.	3R	3R
recoilless fraction		
low temp.	$\exp(-\frac{E_r}{k\Theta_E})$	$\exp(-\frac{3E_r}{2k\Theta_D^2})$
high temp.	$\exp(-\frac{2E_r}{k\Theta_E^2}T)$	$\exp(-\frac{6E_r}{k\Theta_D^2}T)$

$ 3.2.b Width of Gamma-ray Spectrum and Why the Mössbauer effect is valuable

More important on the Mössbauer effect is the fact that the linewidth of gamma-ray transition is smaller than characteristic values for the magnetic dipole and electric quadrupole interactions of nuclei with surrounding electrons.

Lipkin calculated the spectrum of emitted gamma-ray from free atoms with Maxwell distribution. Figure 3.2.A shows a typical gamma-ray apectrum from free atoms, where E_r and E_e are the recoil energy and the excited energy of a nucleus. The gamma-ray spectrum is centered the value E_e-E_r and has a width propotional to the mean square velocity in the initial distribution which is charasteric of the Doppler broadening of a spectral line due to the thermal motion of emitting atoms.

Next consider a solid where the nucleus is not free, but is moving in one dimentiona in a harmonic oscillator potential(Einstein model). This is not exactly the same as the motion of an atom in a crystal. The energy of emitted gamma-ray can differ from the energy E_e by an integral number of oscillator quanta with an uncertainly

given by the linewidth which is very small. The gamma-ray spectrum therefore consists of a set of spikes. For the weak binding, the spectrum approach that of free atoms as shown in figure 3.2.B.

The more interesting case is that of strong binding (here $\hbar\omega_E=2E_r$). In this case the spectrum consists of spikes at E_e, $E_r\pm2E_r$ and other spikes further out as shown in figure 3.2.C. However there can be no gamma-ray emitted with an energy between E_e and E_r-2E_r.

In the case of a real crystal, the spectrum of a low-energy gamma-ray transition in a solid consists of a zero-phonon, full-emergy line plus a phonon-accompanied energy shifted component. The latter is necesserily much broader , not only because the linewidth of the phonons is greater than that of gamma transition, but also because the energy of a phonon is a function of its propagation vector. An acoustic phonon may generally have any energy from zero at k=0.0 to a maximum at the boundary of the Brilloun zone. As a concrete example, consider the spectrum of 129 keV gamma-ray of Ir^{191} 44). Figure 3.2.d shows the real spectrum of a solid Ir^{191} which shows the narrow recoil free component at the energy of the nuclear transition plus broad "phonon wing" to borrow a term that has gained acceptance

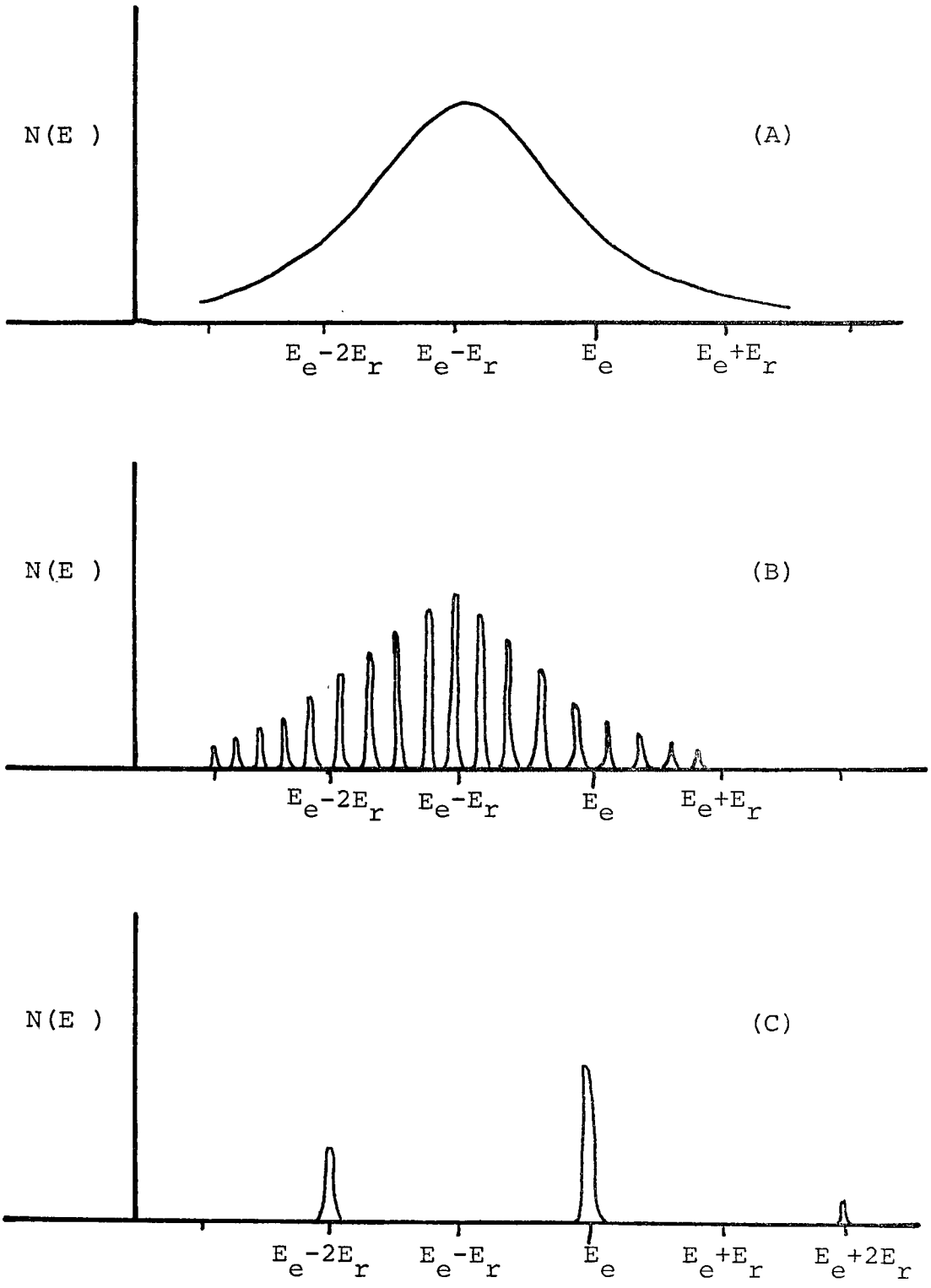

Figure 3.2 The gamma-rays emission spectra

(A) from the free atoms with thermal motion.

(B) from the weakly bounded atoms in Einstein solid

(C) from the strongly bounded atoms in Einstein solid

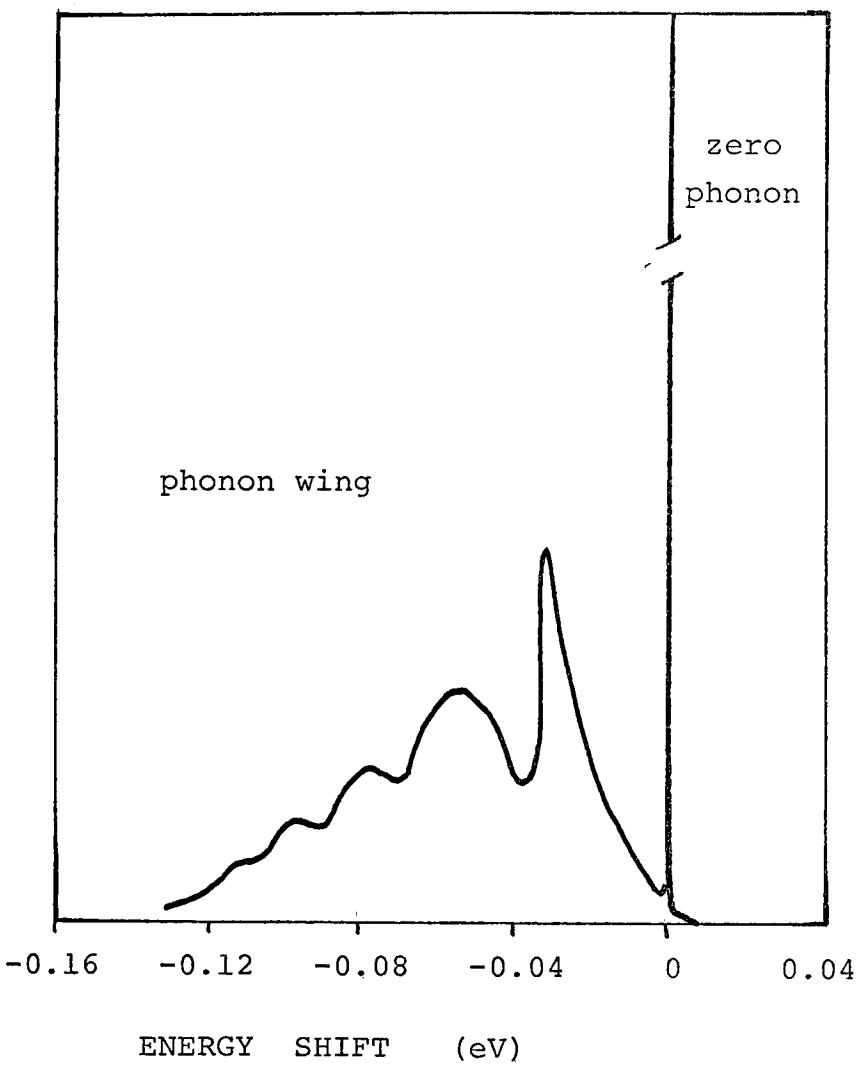

Figure 3.2.D The theoretical spectrum of the 129 keV gamma-ray of Ir^{191} emitted by an atom in iridium metal at low temperature[46]. The Mössbauer spectrometer is sensitive only to the narrow, recoil-free line at zero energy shift which contain 5.7% of the total area under the curve.

in optical spectroscopy. The width of zero phonon line is 10^{-5} eV. The natural line width of Ir^{191} is 3.5×10^{-6} eV($=0.693\,\hbar/t_{1/2}$, where $\hbar=1.05\times10^{-27}$ergs sec, $t_{1/2}=0.13\times10^{-9}$ sec). Thus, the width of zero phonon line is almost the same as the natural line width of the nucleus.

It is interesting to consider how momentum is transmitted to the lattice to make these zero-phonon events possible. The velocity with which momentum can travel through the lattice is the velocity of sound. The time available is the decay time of the damped oscillator which represents the radiating nucleus. Sonic velocities in solid are characteristically 10^{-5}cm/sec. So that during 1.4×10^{-7}sec lifetime of Fe^{57} the impulse travels 1.4×10^{-2}cm, while during the 1.4×10^{-10}sec lifetime of Ir^{191} the impulse travels 1.4×10^{-5} cm. Thus, even in the irdium experiment there is the time for 3×10^{8} nearby atoms to become involved in the recoil-free process. As a result, the recoil energy becomes 3×10^{8} times of magnitude smaller than that in the case of a free atom. Therefore, the linewidth by Doppler broadening becomes very small.

More important, however, is the fact that this linewidth is smaller than characteristic values for the magnetic dipole and electric quadrupole interactions of nuclei with their surrounding electrons. For example, the linewidth of Fe^{57}

zero-phonon line is 10^{-8}eV and the magnetic hyperfine interaction the field of 100 kOe is 10^{-6}eV. Therefore, Mössbauer experiment makes the study of a hyperfine structure of a nucleus to be possible.

In practice, the energy of gamma-rays emitted from RI source can be varied by the convenient modulation technique based on the Dopper effect. To obtain a hyperfine spectrum, one proceeds as follows. The radioactive material which will constitute the source is incorporated into a host where its nuclear levels remain unsplit. Any cubic, diamagnetic metal will be a good choice provided the radioisotope enters the lattice substitutionally. This source is then mounted on the "velocity modulator".

A stationary absorber is now placed between the source and the detector. If the nuclear levels in the absorber are split by hyperfine interaction, there will be a number of different energies at which absorption takes place.

The most advantageous properties for Mössbauer experiment is found in Fe^{57} which has been used in more experiments than all other isotopes. Its properties are summarized in Table 3.2. Next , consideration must be given to the cross section, σ_0, for absorption of the gamma ray by the resonant isotope,which is given by

$$\sigma_o = \frac{\lambda^2}{2\pi} \times \frac{1+2I_e}{1+2I_g} / \frac{1}{1+\alpha} \qquad (3.15)$$

where I_e and I_g are the nuclear spins of the excited state and the ground state, respectively, and α is the internal conversion coefficient of the gamma transition. In Fe^{57} this cross section is 2.2×10^{-18} cm^2, which is about 200 times greater than that for the next most important process, photoelectric absorption. As a result, the resonant absorption process can dominate even when the resonant isotope is a minor constituent of the absorption solid. The energy dependence of the absorption cross section is given by the Breit-Wigner formula. If the linewidth is related to the lifetime , the Lorentzian line shape applies both to the emitted radiation and to the absorption cross section. For thin absorbers, the experimentally observed line shape is given by

$$\sigma_{exp}(E) = \sigma_o / [\, 1 + 4 (\frac{E-E_e}{W_s+W_a})^2]^{-1} \qquad (3.16)$$

where W_s and W_a are the linewidth of the source and the absorber. In other words the linewidth of the source and the absorber are additive. If the natural linewidth is realized in both, the Mössbauer effect linewidth is just twice the linewidth of the gamma-ray.

Table 3.2 Properties of Fe^{57}

	Ground state	First excited state
Energy (keV)	0	14.36
Spin and Parity	$1/2^-$	$3/2^-$
Magnetic moment (nm)	0.0903	-0.153
Quadrupole moment (barns)	0	0.29
Mean life time (sec)	stable	1.4×10^{-7}
Internal conversion coefficient		9.7 ± 0.2

$ 3.2.c Study of Hyperfine Structure

The parameters of the Mössbauer transition if Fe^{57} are indicated in figure 3.1, showing the effects of three electromagnetic perturbations on the energy levels, the isomer shift, quadrupole and Zeeman splittings. We shall describe the origins and magnitudes of these perturbations, briefly.

Isomer Shift

The isomer shift, also known as the chemical shift, whcih exhibits itself as a change in position of the centroid of the Mössbauer spectra, arises from two effects. One is purely nuclear, caused ny the difference in the size of the nucleus in its excited and ground state. The other represents the interaction of the nucleus with the electronic charge that interpenetrates it. This interaction, being a function of electronic density at the nuclear site is dependent upon the chemical environment. Since Mössbauer spectra arise from a resonance between source and absorber , the observed isomer shift is

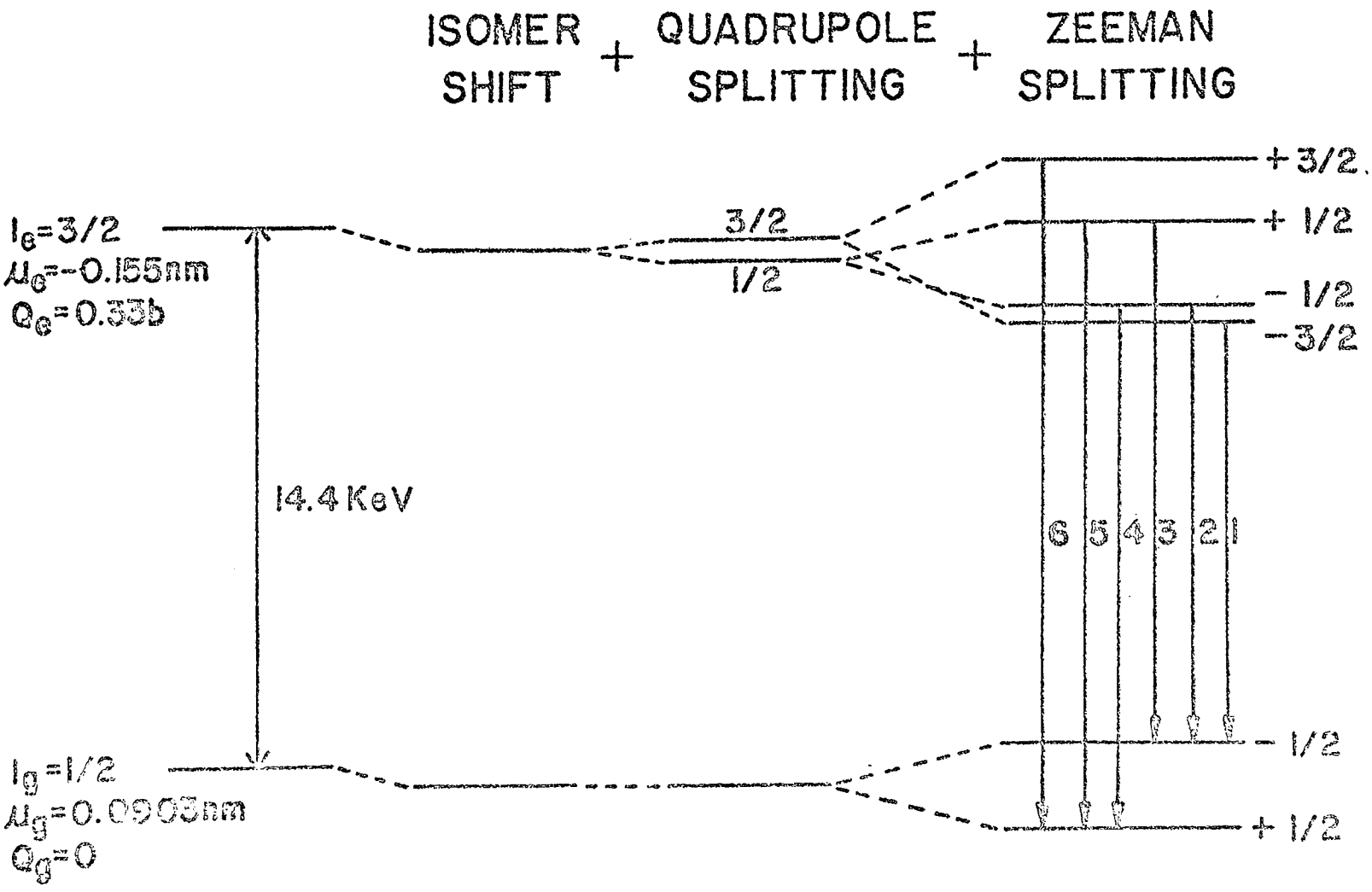

Figure 3.1 Perturbation of 14.4 keV and ground state energylevels of Fe^{57} b isomer shift, quadrupole coupling and magnetic hyperfien field.

$$I.S. = \frac{2\pi}{5} Ze^2 \left[|\psi_a(0)|^2 - |\psi_s(0)|^2 \right] [R_{ex}^2 - R_{gd}^2] \quad (3.17)$$

where $|\psi_a(0)|^2$ and $|\psi_s(0)|^2$ are electronic densities at the nuclear site for the source and absorber respectively, R_{ex} and R_{gd} the nuclear radius in the excited state and ground state respectively. One of the uses of the isomer shift is an indication of the oxidation state of Mössbauer isotope. For example, as the 3d electrons by the d electrons and their density at the nuclear site increase. This results in the isomer shift becoming more negative as the oxidation state increases($R_{ex} < R_{gd}$)

Quadrupole Splitting

The quadrupole coupling is the electrostatic interaction of the nuclear quadrupole moment, Q, with the electric field gradient, (EFG) at the nucleus. It is well known that the quadrupole interaction Hamiltonian is

$$H = \frac{eqQ}{4I(2I-1)} \left[3I_z^2 - I(I+1) + \frac{\eta}{2}(I_+^2 + I_-^2) \right] \quad (3.18)$$

with eigenvalues

$$E_q = \frac{eqQ}{4I(2I-1)} \left[3m^2 - I(I+1) \right] \left[1+\eta^2/3\right]^{1/2} \quad m=I,,-I \qquad (3.19)$$

where $eq = V_{zz}$ and η is asymmetry factor. In the case of Fe^{57} in axial symmetry, the ground state (I=1/2) is unaffected while the excited state (I=3/2) is split into the energy levels

$$E_q(m=3/2) = eqQ/4 \quad \text{and} \quad E_q(-m) = -eqQ/4 \qquad (3.20)$$

The splitting is thus $E_q = eqQ/2$.

Zeeman Splitting

The interaction of the nuclear magnetic dipole moment, u, with the magnetic hyperfine field at the nucleus H results in the splitting of the nuclear levels into 2I+1 sublevels each separated by an energy of uH/I. For magnetic dipole radiation $m=0,\pm1$ in the case of Fe^{57}, we have only six transition as shown in figure 3. . The line intensities have the following angular distributions;

Transition	Line Assignment	Angular distribution
-3/2...-1/2	1	$3(1+\cos^2\theta)$
-1/2...-1/2	2	$4\sin^2\theta$
+1/2...-1/2	3	$(1+\cos^2\theta)$
-1/2...+1/2	4	$(1+\cos^2\theta)$

+1/2...+1/2	5	$4 \sin^2\theta$
+3/2...+1/2	6	$3(1+\cos^2\theta)$

Here θ is the angle between the effective magnetic field at the nucleus and the gamma-ray propagation. Thus the ratio of the line intensities is 3:x:1:x:3 where x from 0, when the effective field is parallel to the gamma-ray direction, to 4 when the two direction are perpendicular.

In general case of combined magnetic and electric hyperfine effects, all eight transition are made possible due to the mixing of the magnetic substates by the quadrupole interaction. For this general situation a solution cannot be written in closed form. However, the important feature is that the information of Fe^{57} nucleus can be obtained in both a Mössbauer experiment used Fe^{57} absorber and a Mössbauer a Mössbauer experiment used Co^{57} source.

$ 3.3 Nuclear polarization and the effect on the Mössbauer spectrum

Nuclear polarization is one of the characteristic phenomena at very low temperature. Significant polarization occurs only at temperatures where the thermal energy kT is comparable with the hyperfine interaction energy, which is usually lower than 0.1 K. For example, let us consider a sample embeded a most popular Mössbauer source Co^{57}. The Co^{57} nucleus has a large magnetic moment (+4.58 nm) which is for instance, fifty times as large as the moment of the daughter nucleus, Fe^{57}. It is expected that Co^{57} nuclei located in a large hyperfine field, of the order of 100 kOe, will show a remarkable polarization at the temperatures range at 0.1 K. It is well known that an Fe^{57} Mössbauer spectrum in the presence of a magnetic field shows a 6-line splitting whose intensity ratio is usually 3:2:1:1:2:3. Figure 3.2.a shows the Mössbauer spectrum of a standard source of Co^{57} in a Fe thin foil at high temperature, 300 K. Those intensity ratio deviates from 3:2:1:1:2:3, because the source is a thin foil.

In the presence of a hyperfine field a nuclear state of Co^{57} (I=7/2) separetes into 8-sublevells which are characterized by the magnetic quautum number m_I. The magnetic interaction energy is $-\mu_I H m_I/I$. Here $\mu_I = g\mu_N I$ is the magnetic moment of the nuclear state with spin =I and μ_N is the nuclear magneton. Thus, we have for the separation of two successeve levells ($\Delta m_I=1$)

$$\Delta E = -\mu_I H/I = -g_I \mu_N H. \qquad (3.21)$$

The total magnetic splitting of the nuclear state I is $2\mu_I H$. The population of each level is given by the Boltzmann factor

$$P(m_I) = \frac{\exp(-m_I \Delta E/kT)}{\sum_{m_I} \exp(-m_I \Delta E/kT)} \qquad (3.22)$$

At higher temperatures, where the thermal energy is much larger than the magnetic energy, i.e. $kT \ll 2\mu_I H$, the individual sublevels are equally populated. But at low temperatures where $kT \leq 2\mu_I H$, those will no longer be equally populated. Since in the case of Co^{57} nucleus, the quadrupole interaction is considered to be less than a few percents of the magnetic interaction in general.

it may be neglected.

In Mössbauer experiment, the resonantly absorbed gamma-rays are emitted by the transition from the first excited state of Fe^{57}, I_e, produced after the β-decay of Co^{57} to the ground state, I_g. In the presence of hyperfine splitting of Fe^{57} nucleus, this process will occur between the sublevels m_e and m_g. The relative absorption $A(m_e, m_g)$ due to such a transition, as observed in a Mössbauer spectrum, is propotional to

$$A(m_e, m_g) \propto P(Fe^{57}, I=3/2, I_z=m_e)\ C(m_e, m_g), \qquad (3.23)$$

where $C(m_e, m_g)$ is the squave of the appropriate normalized Clebsch-Gordon coefficient and $P(Fe^{57}, I=3/2, I_z=m_e)$ is the population of a first excited state m_e of Fe^{57}. The P is related the polarization of Co^{57} nucleus through the β-transition and the magnetic dipole transition. Consequently, the A can be related to the source temperature and the hiperfine field at Co^{57} nucleus. In the case of a pure magnetic interaction at Fe^{57} nucleus, the sublevels of Fe^{57} first excited state are fully characterized by a magnetic quantum number m_e. Since $C(m_e, m_g)=C(-m_e, -m_g)$, we obtain for the intensity ratio R of two lines

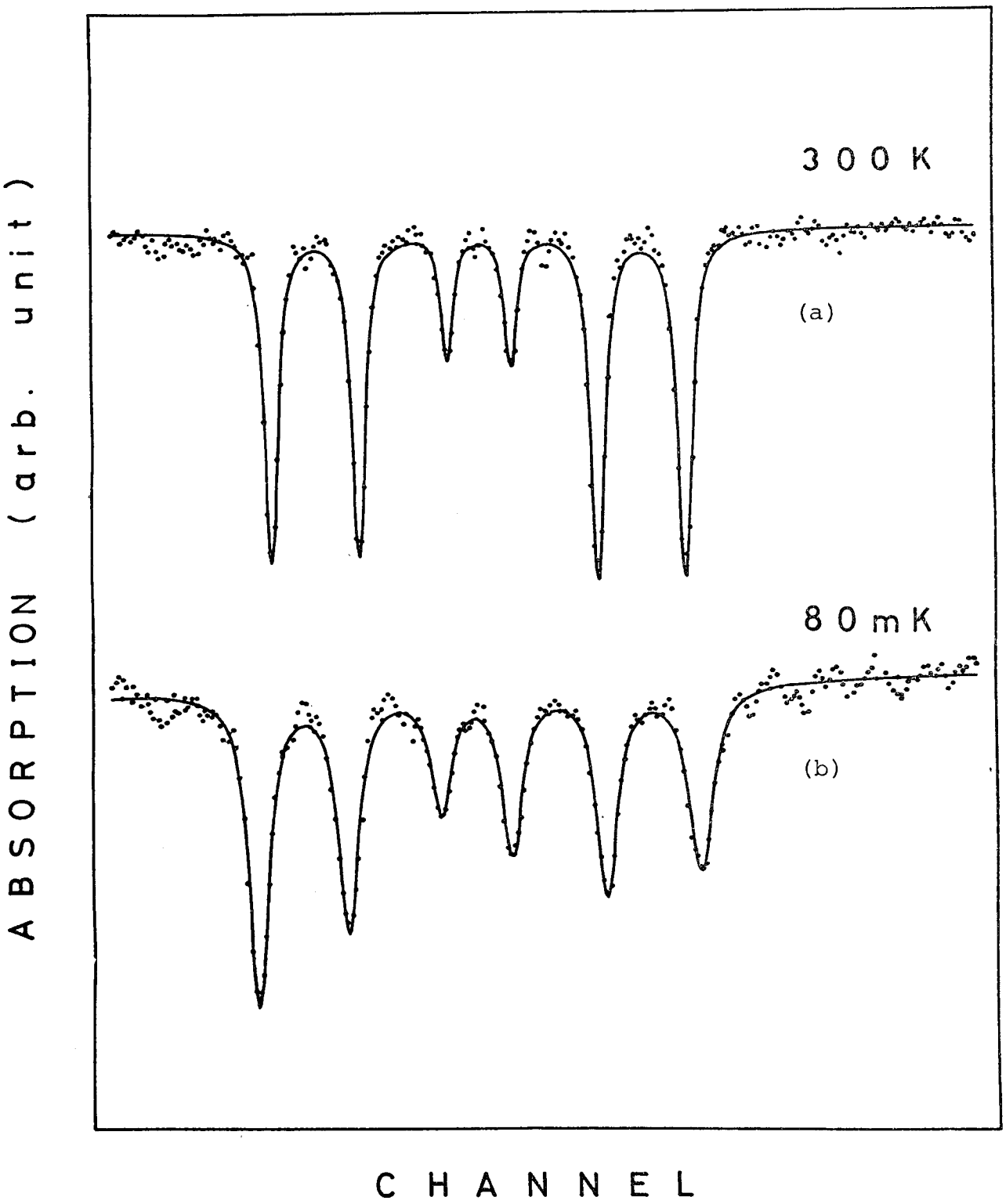

Figure 3.2 The Mössbauer spectrum of Co^{57} in Fe metal. The (a) is the spectrum at 300 K and (b) at 0.08 K. The spectrum at 300 K has the intensity ratio to deviate from 3;2;1;1;2;3. because the surce is a thin foil.

$$R = \frac{A(+m_e,+m_g)}{A(-m_e,-m_g)} = \frac{P(Fe^{57},I=3/2,I_z=+m_e)}{P(Fe^{57},I=3/2,I_z=-m_e)} \qquad (3.24)$$

If the Co^{57} nuclei are polarized, the value of this R is not equal to 1.0 . That is, the spectrum is no more symmetric and the most striking is the difference of the intensities at the outermost peaks. Figure 3.2.b shows the Mössbauer spectrum of Co^{57} in Fe metal at 0.08 K which shows a remarkable asymmetry.

§ 3.4 Mössbauer thermometer

The polarization of the source nuclei, Co^{57}, which is a function of $\mu_I H/IkT$, can be determined from the Fe^{57} Mössbauer spectrum, because the decay time of the nucleus, from Co^{57} to Fe^{57}, is much shorter than the relaxation time of the nuclear magnetic spins.

When the hyperfine field is already known, the temperature can be determined from the degree of nuclear polarization. For a cobalt nucleus dissolved in iron matrix, the hyperfine field has been determined to be -290 kOe by a NMR experiment[47]. Therefore, from the polarization of Co^{57} nuclei in Fe observed in the Mössbauer spectrum, the absolute temperature can be determined.

This method of temperature determination, Mössbauer source thermometry[48], may not be useful so generally, mainly because of the instrumental condition, but at least for Mössbauer spectroscopic studies at very low temperatures from 0.03 to 0.5 K, it is a very easy and reliable method. In the present work, this Co^{57} thermometer was used for the absolute temperature determination.

It is, of course, also possible to utilize the nuclear

polarization in a absorber spectrum splitted at very low temperatures. In this arrangement, the source is a unsplitted single line emitter. This thermometer can be classified as "absorber thermometer". The absorber thermometer supplies its own calibration, but its accuracy is limitted by thickness effects, which must be determined separately. Both types of thermometer require rather sophisticated experimental equipment, and the measurement of one temperature may involve counting times up to an hour.

Another difficulty arises besause the β-transition probability must be known. This problem will be discussed in more detail below. Let us state here that a priori the value of such probability is known only allowed β-decays($\Delta I=0,\pm 1$ and no parity change). Table 3.3 shows the intensity ratios between each line as a function of the absolute temperature in the case of Co^{57} nuclei in thin Fe metal, which was calculated with a computer, Facom 270/30, at the Data Processing Center, Kyoto University. Table 3.4 shows the intensity ratios as a universal function of H/T, where H is a magnetic hyperfine field at Co^{57} nucleus and T is the absolute temperature.

On the other hand, if the temperature of the sample is determined, the magnetic hyperfine field at Co^{57} nucleus

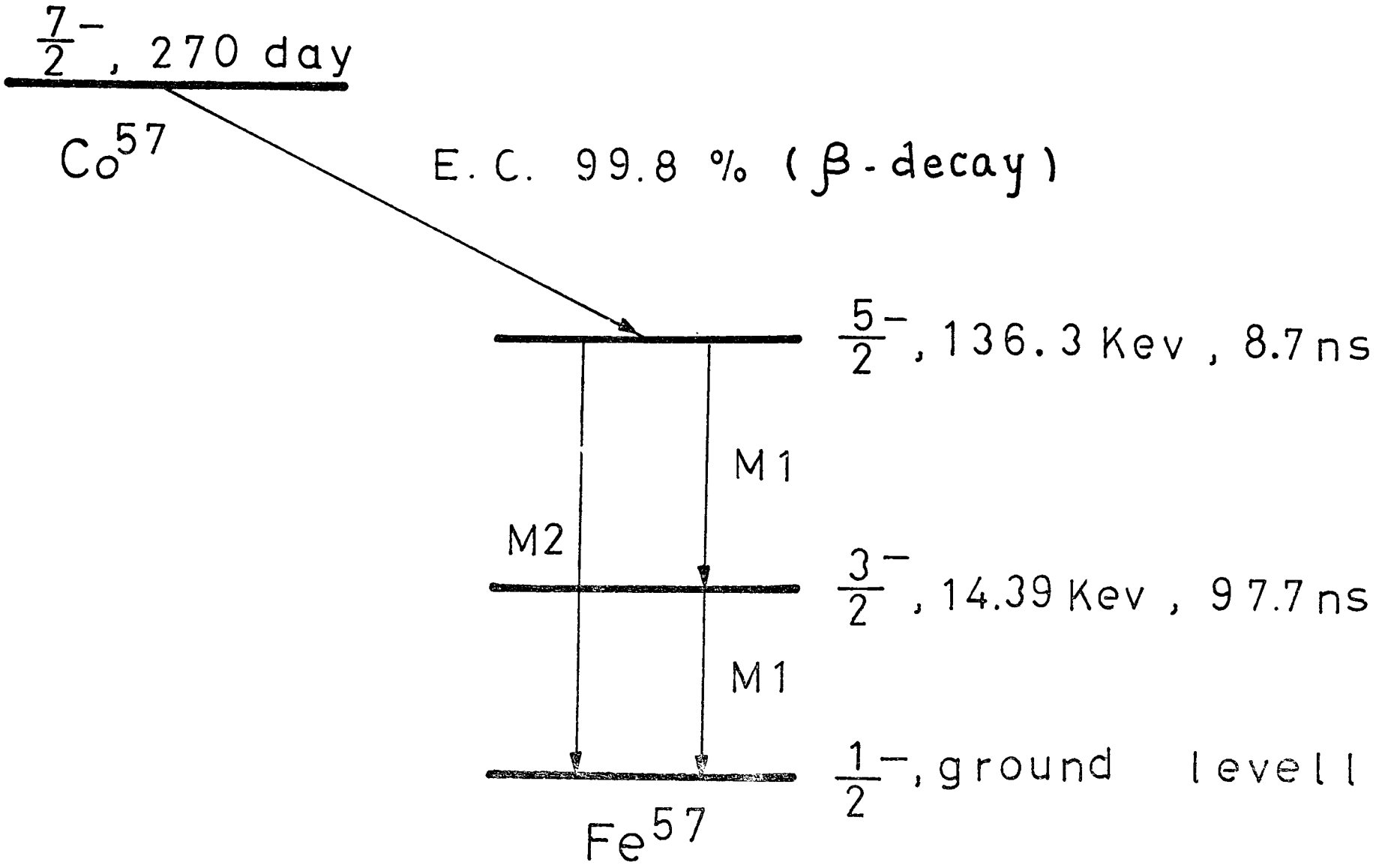
7/2−, 270 day
Co57
E. C. 99.8 % (β-decay)
5/2−, 136.3 Kev, 8.7 ns
M1
M2
3/2−, 14.39 Kev, 97.7 ns
M1
1/2−, ground level
Fe57

can be estimated from the nuclear polarization. Using this technique, Finnish group has estimated the hyperfine fields at dilute cobalt in Pd and Pt matrics and the observed values were +280 kOe and -119 kOe respectively[49,50]. This new method is especially useful to estimate the hyperfine fields in antiferromagnetic substances because the application of NMR is technically difficult.

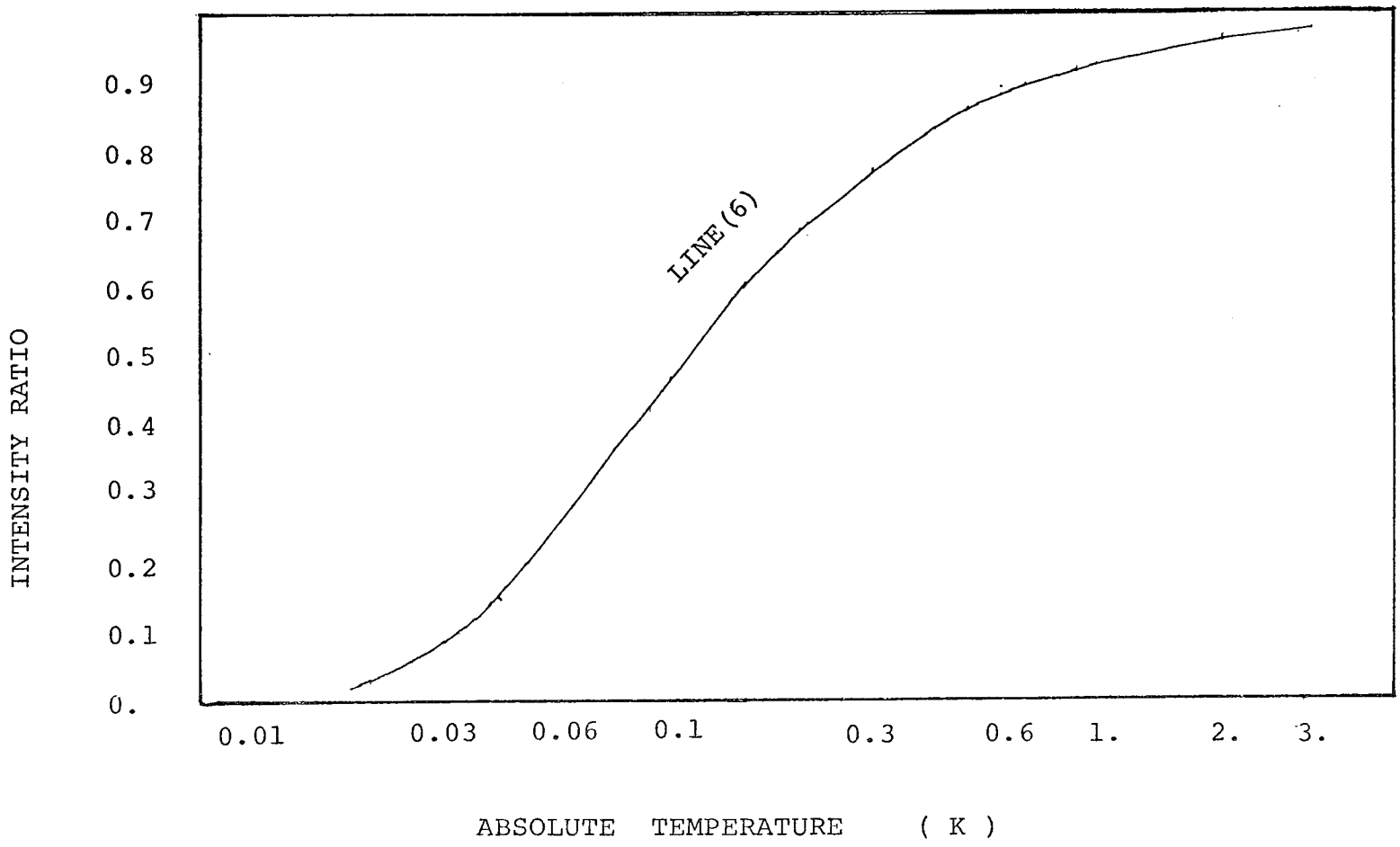

Figure 3.3 The intensity ratio of Mössbauer thermometer(Co^{57}in Fe metal). versus temperature.

*****MAGNETIC FIELD ***** = 289.00 kOe

Table 3.3 The intensity ratios of 6-lines in Mössbauer thermometer (Co^{57} in Fe metal). Here LINE(1) = 1.0

TEMPERATURE (K)	LINE(2)	LINE(3)	LINE(4)	LINE(5)	LINE(6)
0.1000E-01	0.8295E-01	0.4881E-02	0.4147E-01	0.9761E-02	0.1119E-02
0.1100E-01	0.9645E-01	0.6721E-02	0.4822E-01	0.1344E-01	0.1871E-02
0.1200E-01	0.1097E+00	0.8839E-02	0.5487E-01	0.1768E-01	0.2917E-02
0.1300E-01	0.1227E+00	0.1121E-01	0.6137E-01	0.2241E-01	0.4301E-02
0.1400E-01	0.1354E+00	0.1380E-01	0.6772E-01	0.2759E-01	0.6053E-02
0.1500E-01	0.1478E+00	0.1658E-01	0.7389E-01	0.3316E-01	0.8198E-02
0.1600E-01	0.1597E+00	0.1953E-01	0.7987E-01	0.3906E-01	0.1075E-01
0.1700E-01	0.1713E+00	0.2261E-01	0.8566E-01	0.4522E-01	0.1370E-01
0.1800E-01	0.1825E+00	0.2581E-01	0.9126E-01	0.5162E-01	0.1706E-01
0.1900E-01	0.1933E+00	0.2909E-01	0.9667E-01	0.5819E-01	0.2081E-01

TEMPERATURE (K)	LINE(2)	LINE(3)	LINE(4)	LINE(5)	LINE(6)
0.2000E-01	0.2038E+00	0.3245E-01	0.1019E+00	0.6489E-01	0.2493E-01
0.2100E-01	0.2138E+00	0.3585E-01	0.1069E+00	0.7170E-01	0.2941E-01
0.2200E-01	0.2235E+00	0.3929E-01	0.1118E+00	0.7858E-01	0.3421E-01
0.2300E-01	0.2329E+00	0.4274E-01	0.1164E+00	0.8549E-01	0.3932E-01
0.2400E-01	0.2419E+00	0.4621E-01	0.1209E+00	0.9242E-01	0.4471E-01
0.2500E-01	0.2506E+00	0.4967E-01	0.1253E+00	0.9934E-01	0.5036E-01
0.2600E-01	0.2589E+00	0.5311E-01	0.1295E+00	0.1062E+00	0.5623E-01
0.2700E-01	0.2670E+00	0.5654E-01	0.1335E+00	0.1131E+00	0.6230E-01
0.2800E-01	0.2748E+00	0.5994E-01	0.1374E+00	0.1199E+00	0.6856E-01
0.2900E-01	0.2823E+00	0.6331E-01	0.1411E+00	0.1266E+00	0.7497E-01

TEMPERATURE (K)	LINE(2)	LINE(3)	LINE(4)	LINE(5)	LINE(6)
0.3000E-01	0.2895E+00	0.6663E-01	0.1447E+00	0.1333E+00	0.8151E-01
0.3100E-01	0.2965E+00	0.6992E-01	0.1482E+00	0.1398E+00	0.8817E-01
0.3200E-01	0.3032E+00	0.7317E-01	0.1516E+00	0.1463E+00	0.9493E-01
0.3300E-01	0.3097E+00	0.7636E-01	0.1549E+00	0.1527E+00	0.1018E+00
0.3400E-01	0.3160E+00	0.7951E-01	0.1580E+00	0.1590E+00	0.1087E+00
0.3500E-01	0.3221E+00	0.8261E-01	0.1610E+00	0.1652E+00	0.1156E+00
0.3600E-01	0.3279E+00	0.8565E-01	0.1640E+00	0.1713E+00	0.1226E+00
0.3700E-01	0.3336E+00	0.8865E-01	0.1668E+00	0.1773E+00	0.1296E+00
0.3800E-01	0.3391E+00	0.9159E-01	0.1696E+00	0.1832E+00	0.1366E+00
0.3900E-01	0.3444E+00	0.9448E-01	0.1722E+00	0.1890E+00	0.1436E+00

TEMPERATURE (K)	LINE(2)	LINE(3)	LINE(4)	LINE(5)	LINE(6)
0.4000E-01	0.3496E+00	0.9732E-01	0.1748E+00	0.1946E+00	0.1507E+00
0.4100E-01	0.3545E+00	0.1001E+00	0.1773E+00	0.2002E+00	0.1576E+00
0.4200E-01	0.3594E+00	0.1028E+00	0.1797E+00	0.2057E+00	0.1646E+00
0.4300E-01	0.3640E+00	0.1055E+00	0.1820E+00	0.2110E+00	0.1716E+00
0.4400E-01	0.3686E+00	0.1081E+00	0.1843E+00	0.2163E+00	0.1785E+00
0.4500E-01	0.3730E+00	0.1107E+00	0.1865E+00	0.2214E+00	0.1853E+00
0.4600E-01	0.3773E+00	0.1132E+00	0.1886E+00	0.2265E+00	0.1922E+00
0.4700E-01	0.3814E+00	0.1157E+00	0.1907E+00	0.2314E+00	0.1989E+00
0.4800E-01	0.3854E+00	0.1182E+00	0.1927E+00	0.2363E+00	0.2057E+00
0.4900E-01	0.3893E+00	0.1205E+00	0.1947E+00	0.2411E+00	0.2123E+00

TEMPERATURE (K)	LINE(2)	LINE(3)	LINE(4)	LINE(5)	LINE(6)
0.5000E-01	0.3932E+00	0.1229E+00	0.1966E+00	0.2457E+00	0.2189E+00
0.5100E-01	0.3968E+00	0.1252E+00	0.1984E+00	0.2503E+00	0.2255E+00
0.5200E-01	0.4004E+00	0.1274E+00	0.2002E+00	0.2548E+00	0.2320E+00
0.5300E-01	0.4039E+00	0.1296E+00	0.2020E+00	0.2592E+00	0.2384E+00
0.5400E-01	0.4073E+00	0.1318E+00	0.2037E+00	0.2635E+00	0.2447E+00
0.5500E-01	0.4107E+00	0.1339E+00	0.2053E+00	0.2678E+00	0.2510E+00
0.5600E-01	0.4139E+00	0.1360E+00	0.2069E+00	0.2719E+00	0.2572E+00
0.5700E-01	0.4170E+00	0.1380E+00	0.2085E+00	0.2760E+00	0.2634E+00
0.5800E-01	0.4201E+00	0.1400E+00	0.2100E+00	0.2800E+00	0.2695E+00
0.5900E-01	0.4231E+00	0.1420E+00	0.2115E+00	0.2839E+00	0.2755E+00

TEMPERATURE (K)	LINE(2)	LINE(3)	LINE(4)	LINE(5)	LINE(6)
0.6000E-01	0.4260E+00	0.1439E+00	0.2130E+00	0.2878E+00	0.2814E+00
0.6100E-01	0.4288E+00	0.1458E+00	0.2144E+00	0.2915E+00	0.2873E+00
0.6200E-01	0.4316E+00	0.1476E+00	0.2158E+00	0.2952E+00	0 2931E+00
0.6300E-01	0.4343E+00	0.1494E+00	0.2171E+00	0.2989E+00	0.2988E+00
0.6400E-01	0.4369E+00	0.1512E+00	0.2185E+00	0.3024E+00	0.3045E+00
0.6500E-01	0.4395E+00	0.1530E+00	0.2197E+00	0.3059E+00	0.3100E+00
0.6600E-01	0.4420E+00	0.1547E+00	0.2210E+00	0.3094E+00	0.3156E+00
0.6700E-01	0.4445E+00	0.1564E+00	0.2222E+00	0.3127E+00	0.3210E+00
0.6800E-01	0.4469E+00	0.1580E+00	0.2234E+00	0.3160E+00	0.3264E+00
0.6900E-01	0.4492E+00	0.1596E+00	0.2246E+00	0.3193E+00	0.3317E+00

TEMPERATURE (K)	LINE(2)	LINE(3)	LINE(4)	LINE(5)	LINE(6)
0.7000E-01	0.4515E+00	0.1612E+00	0.2258E+00	0.3225E+00	0.3369E+00
0.7100E-01	0.4537E+00	0.1628E+00	0.2269E+00	0.3256E+00	0.3421E+00
0.7200E-01	0.4559E+00	0.1643E+00	0.2280E+00	0.3287E+00	0.3472E+00
0.7300E-01	0.4581E+00	0.1659E+00	0.2290E+00	0.3317E+00	0.3522E+00
0.7400E-01	0.4602E+00	0.1673E+00	0.2301E+00	0.3347E+00	0.3572E+00
0.7500E-01	0.4622E+00	0.1688E+00	0.2311E+00	0.3376E+00	0.3621E+00
0.7600E-01	0.4642E+00	0.1702E+00	0.2321E+00	0.3405E+00	0.3670E+00
0.7700E-01	0.4662E+00	0.1716E+00	0.2331E+00	0.3433E+00	0.3718E+00
0.7800E-01	0.4681E+00	0.1730E+00	0.2341E+00	0.3460E+00	0.3765E+00
0.7900E-01	0.4700E+00	0.1744E+00	0.2350E+00	0.3488E+00	0.3812E+00

TEMPERATURE (K)	LINE(2)	LINE(3)	LINE(4)	LINE(5)	LINE(6)
0.8000E-01	0.4719E+00	0.1757E+00	0.2359E+00	0.3514E+00	0.3858E+00
0.8100E-01	0.4737E+00	0.1770E+00	0.2368E+00	0.3541E+00	0.3903E+00
0.8200E-01	0.4755E+00	0.1783E+00	0.2377E+00	0.3567E+00	0.3948E+00
0.8300E-01	0.4772E+00	0.1796E+00	0.2386E+00	0.3592E+00	0.3992E+00
0.8400E-01	0.4789E+00	0.1809E+00	0.2395E+00	0.3617E+00	0.4036E+00
0.8500E-01	0.4806E+00	0.1821E+00	0.2403E+00	0.3642E+00	0.4079E+00
0.8600E-01	0.4822E+00	0.1833E+00	0.2411E+00	0.3666E+00	0.4122E+00
0.8700E-01	0.4838E+00	0.1845E+00	0.2419E+00	0.3690E+00	0.4164E+00
0.8800E-01	0.4854E+00	0.1857E+00	0.2427E+00	0.3713E+00	0.4205E+00
0.8900E-01	0.4870E+00	0.1868E+00	0.2435E+00	0.3736E+00	0.4246E+00

TEMPERATURE (K)	LINE(2)	LINE(3)	LINE(4)	LINE(5)	LINE(6)
0.9000E-01	0.4885E+00	0.1879E+00	0.2442E+00	0.3759E+00	0.4287E+00
0.9100E-01	0.4900E+00	0.1891E+00	0.2450E+00	0.3781E+00	0.4327E+00
0.9200E-01	0.4915E+00	0.1902E+00	0.2457E+00	0.3803E+00	0.4366E+00
0.9300E-01	0.4929E+00	0.1912E+00	0.2464E+00	0.3825E+00	0.4405E+00
0.9400E-01	0.4943E+00	0.1923E+00	0.2472E+00	0.3846E+00	0.4443E+00
0.9500E-01	0.4957E+00	0.1934E+00	0.2479E+00	0.3867E+00	0.4481E+00
0.9600E-01	0.4971E+00	0.1944E+00	0.2485E+00	0.3888E+00	0.4519E+00
0.9700E-01	0.4984E+00	0.1954E+00	0.2492E+00	0.3908E+00	0.4556E+00
0.9800E-01	0.4997E+00	0.1964E+00	0.2499E+00	0.3928E+00	0.4593E+00
0.9900E-01	0.5010E+00	0.1974E+00	0.2505E+00	0.3948E+00	0.4629E+00

TEMPERATURE (K)	LINE(2)	LINE(3)	LINE(4)	LINE(5)	LINE(6)
0.1000E+00	0.5023E+00	0.1984E+00	0.2512E+00	0.3967E+00	0.4664E+00
0.1100E+00	0.5139E+00	0.2074E+00	0.2570E+00	0.4147E+00	0.4998E+00
0.1200E+00	0.5239E+00	0.2152E+00	0.2620E+00	0.4304E+00	0.5295E+00
0.1300E+00	0.5325E+00	0.2220E+00	0.2663E+00	0.4441E+00	0.5560E+00
0.1400E+00	0.5400E+00	0.2281E+00	0.2700E+00	0.4562E+00	0.5798E+00
0.1500E+00	0.5466E+00	0.2335E+00	0.2733E+00	0.4670E+00	0.6012E+00
0.1600E+00	0.5525E+00	0.2383E+00	0.2762E+00	0.4767E+00	0.6206E+00
0.1700E+00	0.5577E+00	0.2427E+00	0.2789E+00	0.4854E+00	0.6383E+00
0.1800E+00	0.5624E+00	0.2466E+00	0.2812E+00	0.4933E+00	0.6544E+00
0.1900E+00	0.5667E+00	0.2502E+00	0.2833E+00	0.5004E+00	0.6691E+00

TEMPERATURE (K)	LINE(2)	LINE(3)	LINE(4)	LINE(5)	LINE(6)
0.2000E+00	0.5705E+00	0.2535E+00	0.2853E+00	0.5070E+00	0.6827E+00
0.2100E+00	0.5740E+00	0.2565E+00	0.2870E+00	0.5130E+00	0.6952E+00
0.2200E+00	0.5773E+00	0.2592E+00	0.2886E+00	0.5185E+00	0.7068E+00
0.2300E+00	0.5802E+00	0.2618E+00	0.2901E+00	0.5236E+00	0.7175E+00
0.2400E+00	0.5829E+00	0.2642E+00	0.2915E+00	0.5283E+00	0.7275E+00
0.2500E+00	0.5855E+00	0.2663E+00	0.2927E+00	0.5327E+00	0.7368E+00
0.2600E+00	0.5878E+00	0.2684E+00	0.2939E+00	0.5368E+00	0.7455E+00
0.2700E+00	0.5900E+00	0.2703E+00	0.2950E+00	0.5406E+00	0.7537E+00
0.2800E+00	0.5920E+00	0.2721E+00	0.2960E+00	0.5441E+00	0.7613E+00
0.2900E+00	0.5939E+00	0.2737E+00	0.2970E+00	0.5474E+00	0.7685E+00

TEMPERATURE (K)	LINE(2)	LINE(3)	LINE(4)	LINE(5)	LINE(6)
0.3000E+00	0.5957E+00	0.2753E+00	0.2978E+00	0.5506E+00	0.7753E+00
0.3100E+00	0.5973E+00	0.2768E+00	0.2987E+00	0.5535E+00	0.7817E+00
0.3200E+00	0.5989E+00	0.2781E+00	0.2995E+00	0.5563E+00	0.7877E+00
0.3300E+00	0.6004E+00	0.2795E+00	0.3002E+00	0.5589E+00	0.7934E+00
0.3400E+00	0.6018E+00	0.2807E+00	0.3009E+00	0.5614E+00	0.7988E+00
0.3500E+00	0.6031E+00	0.2819E+00	0.3016E+00	0.5637E+00	0.8040E+00
0.3600E+00	0.6044E+00	0.2830E+00	0.3022E+00	0.5660E+00	0.8089E+00
0.3700E+00	0.6055E+00	0.2840E+00	0.3028E+00	0.5681E+00	0.8135E+00
0.3800E+00	0.6067E+00	0.2850E+00	0.3033E+00	0.5701E+00	0.8180E+00
0.3900E+00	0.6077E+00	0.2860E+00	0.3039E+00	0.5720E+00	0.8222E+00

TEMPERATURE (K)	LINE(2)	LINE(3)	LINE(4)	LINE(5)	LINE(6)
0.4000E+00	0.6087E+00	0.2869E+00	0.3044E+00	0.5738E+00	0.8262E+00
0.4100E+00	0.6097E+00	0.2878E+00	0.3049E+00	0.5756E+00	0.8301E+00
0.4200E+00	0.6106E+00	0.2886E+00	0.3053E+00	0.5772E+00	0.8338E+00
0.4300E+00	0.6115E+00	0.2894E+00	0.3058E+00	0.5788E+00	0.8373E+00
0.4400E+00	0.6124E+00	0.2902E+00	0.3062E+00	0.5804E+00	0.8407E+00
0.4500E+00	0.6132E+00	0.2909E+00	0.3066E+00	0.5818E+00	0.8439E+00
0.4600E+00	0.6139E+00	0.2916E+00	0.3070E+00	0.5832E+00	0.8470E+00
0.4700E+00	0.6147E+00	0.2923E+00	0.3073E+00	0.5846E+00	0.8500E+00
0.4800E+00	0.6154E+00	0.2929E+00	0.3077E+00	0.5858E+00	0.8529E+00
0.4900E+00	0.6161E+00	0.2935E+00	0.3080E+00	0.5871E+00	0.8557E+00

TEMPERATURE (K)	LINE(2)	LINE(3)	LINE(4)	LINE(5)	LINE(6)
0.5000E+00	0.6167E+00	0.2941E+00	0.3084E+00	0.5883E+00	0.8584E+00
0.5100E+00	0.6174E+00	0.2947E+00	0.3087E+00	0.5894E+00	0.8609E+00
0.5200E+00	0.6180E+00	0.2953E+00	0.3090E+00	0.5905E+00	0.8634E+00
0.5300E+00	0.6186E+00	0.2958E+00	0.3093E+00	0.5916E+00	0.8658E+00
0.5400E+00	0.6191E+00	0.2963E+00	0.3096E+00	0.5926E+00	0.8681E+00
0.5500E+00	0.6197E+00	0.2968E+00	0.3098E+00	0.5936E+00	0.8704E+00
0.5600E+00	0.6202E+00	0.2973E+00	0.3101E+00	0.5946E+00	0.8725E+00
0.5700E+00	0.6207E+00	0.2978E+00	0.3104E+00	0.5955E+00	0.8746E+00
0.5800E+00	0.6212E+00	0.2982E+00	0.3106E+00	0.5964E+00	0.8766E+00
0.5900E+00	0.6217E+00	0.2986E+00	0.3108E+00	0.5973E+00	0.8786E+00

TEMPERATURE (K)	LINE(2)	LINE(3)	LINE(4)	LINE(5)	LINE(6)
0.6000E+00	0.6221E+00	0.2991E+00	0.3111E+00	0.5981E+00	0.8805E+00
0.6100E+00	0.6226E+00	0.2995E+00	0.3113E+00	0.5989E+00	0.8823E+00
0.6200E+00	0.6230E+00	0.2999E+00	0.3115E+00	0.5997E+00	0.8841E+00
0.6300E+00	0.6234E+00	0.3002E+00	0.3117E+00	0.6005E+00	0.8858E+00
0.6400E+00	0.6238E+00	0.3006E+00	0.3119E+00	0.6012E+00	0.8875E+00
0.6500E+00	0.6242E+00	0.3010E+00	0.3121E+00	0.6020E+00	0.8892E+00
0.6600E+00	0.6246E+00	0.3013E+00	0.3123E+00	0.6027E+00	0.8907E+00
0.6700E+00	0.6250E+00	0.3017E+00	0.3125E+00	0.6033E+00	0.8923E+00
0.6800E+00	0.6254E+00	0.3020E+00	0.3127E+00	0.6040E+00	0.8938E+00
0.6900E+00	0.6257E+00	0.3023E+00	0.3129E+00	0.6046E+00	0.8952E+00

TEMPERATURE (K)	LINE(2)	LINE(3)	LINE(4)	LINE(5)	LINE(6)
0.7000E+00	0.6260E+00	0.3026E+00	0.3130E+00	0.6053E+00	0.8966E+00
0.7100E+00	0.6264E+00	0.3029E+00	0.3132E+00	0.6059E+00	0.8980E+00
0.7200E+00	0.6267E+00	0.3032E+00	0.3133E+00	0.6065E+00	0.8994E+00
0.7300E+00	0.6270E+00	0.3035E+00	0.3135E+00	0.6070E+00	0.9007E+00
0.7400E+00	0.6273E+00	0.3038E+00	0.3137E+00	0.6076E+00	0.9019E+00
0.7500E+00	0.6276E+00	0.3041E+00	0.3138E+00	0.6081E+00	0.9032E+00
0.7600E+00	0.6279E+00	0.3043E+00	0.3139E+00	0.6087E+00	0.9044E+00
0.7700E+00	0.6282E+00	0.3046E+00	0.3141E+00	0.6092E+00	0.9056E+00
0.7800E+00	0.6284E+00	0.3049E+00	0.3142E+00	0.6097E+00	0.9067E+00
0.7900E+00	0.6287E+00	0.3051E+00	0.3144E+00	0.6102E+00	0.9079E+00

TEMPERATURE (K)	LINE(2)	LINE(3)	LINE(4)	LINE(5)	LINE(6)
0.8000E+00	0.6290E+00	0.3053E+00	0.3145E+00	0.6107E+00	0.9090E+00
0.8100E+00	0.6292E+00	0.3056E+00	0.3146E+00	0.6111E+00	0.9100E+00
0.8200E+00	0.6295E+00	0.3058E+00	0.3147E+00	0.6116E+00	0.9111E+00
0.8300E+00	0.6297E+00	0.3060E+00	0.3149E+00	0.6121E+00	0.9121E+00
0.8400E+00	0.6300E+00	0.3062E+00	0.3150E+00	0.6125E+00	0.9131E+00
0.8500E+00	0.6302E+00	0.3065E+00	0.3151E+00	0.6129E+00	0.9141E+00
0.8600E+00	0.6304E+00	0.3067E+00	0.3152E+00	0.6133E+00	0.9150E+00
0.8700E+00	0.6306E+00	0.3069E+00	0.3153E+00	0.6137E+00	0.9160E+00
0.8800E+00	0.6309E+00	0.3071E+00	0.3154E+00	0.6141E+00	0.9169E+00
0.8900E+00	0.6311E+00	0.3073E+00	0.3155E+00	0.6145E+00	0.9178E+00

TEMPERATURE (K)	LINE(2)	LINE(3)	LINE(4)	LINE(5)	LINE(6)
0.9000E+00	0.6313E+00	0.3075E+00	0.3156E+00	0.6149E+00	0.9186E+00
0.9100E+00	0.6315E+00	0.3076E+00	0.3157E+00	0.6153E+00	0.9195E+00
0.9200E+00	0.6317E+00	0.3078E+00	0.3158E+00	0.6157E+00	0.9203E+00
0.9300E+00	0.6319E+00	0.3080E+00	0.3159E+00	0.6160E+00	0.9212E+00
0.9400E+00	0.6321E+00	0.3082E+00	0.3160E+00	0.6164E+00	0.9220E+00
0.9500E+00	0.6322E+00	0.3084E+00	0.3161E+00	0.6167E+00	0.9228E+00
0.9600E+00	0.6324E+00	0.3085E+00	0.3162E+00	0.6171E+00	0.9235E+00
0.9700E+00	0.6326E+00	0.3087E+00	0.3163E+00	0.6174E+00	0.9243E+00
0.9800E+00	0.6328E+00	0.3089E+00	0.3164E+00	0.6177E+00	0.9250E+00
0.9900E+00	0.6330E+00	0.3090E+00	0.3165E+00	0.6180E+00	0.9258E+00

TEMPERATURE (K)	LINE(2)	LINE(3)	LINE(4)	LINE(5)	LINE(6)
0.1000E+01	0.6331E+00	0.3092E+00	0.3166E+00	0.6183E+00	0.9265E+00
0.1100E+01	0.6346E+00	0.3106E+00	0.3173E+00	0.6211E+00	0.9329E+00
0.1200E+01	0.6359E+00	0.3117E+00	0.3179E+00	0.6235E+00	0.9383E+00
0.1300E+01	0.6370E+00	0.3127E+00	0.3185E+00	0.6255E+00	0.9429E+00
0.1400E+01	0.6379E+00	0.3136E+00	0.3189E+00	0.6272E+00	0.9469E+00
0.1500E+01	0.6387E+00	0.3144E+00	0.3193E+00	0.6287E+00	0.9504E+00
0.1600E+01	0.6394E+00	0.3150E+00	0.3197E+00	0.6300E+00	0.9534E+00
0.1700E+01	0.6400E+00	0.3156E+00	0.3200E+00	0.6312E+00	0.9561E+00
0.1800E+01	0.6406E+00	0.3161E+00	0.3203E+00	0.6322E+00	0.9585E+00
0.1900E+01	0.6411E+00	0.3166E+00	0.3205E+00	0.6331E+00	0.9606E+00

TEMPERATURE (K)	LINE(2)	LINE(3)	LINE(4)	LINE(5)	LINE(6)
0.2000E+01	0.6415E+00	0.3170E+00	0.3207E+00	0.6340E+00	0.9625E+00
0.2100E+01	0.6419E+00	0.3174E+00	0.3209E+00	0.6347E+00	0.9643E+00
0.2200E+01	0.6423E+00	0.3177E+00	0.3211E+00	0.6354E+00	0.9659E+00
0.2300E+01	0.6426E+00	0.3180E+00	0.3213E+00	0.6360E+00	0.9673E+00
0.2400E+01	0.6429E+00	0.3183E+00	0.3215E+00	0.6366E+00	0.9687E+00
0.2500E+01	0.6432E+00	0.3186E+00	0.3216E+00	0.6371E+00	0.9699E+00
0.2600E+01	0.6434E+00	0.3188E+00	0.3217E+00	0.6376E+00	0.9711E+00
0.2700E+01	0.6437E+00	0.3190E+00	0.3218E+00	0.6381E+00	0.9721E+00
0.2800E+01	0.6439E+00	0.3193E+00	0.3220E+00	0.6385E+00	0.9731E+00
0.2900E+01	0.6441E+00	0.3194E+00	0.3221E+00	0.6389E+00	0.9740E+00

TEMPERATURE (K)	LINE(2)	LINE(3)	LINE(4)	LINE(5)	LINE(6)
0.3000E+01	0.6443E+00	0.3196E+00	0.3222E+00	0.6393E+00	0.9749E+00
0.3100E+01	0.6445E+00	0.3198E+00	0.3222E+00	0.6396E+00	0.9757E+00
0.3200E+01	0.6447E+00	0.3200E+00	0.3223E+00	0.6399E+00	0.9764E+00
0.3300E+01	0.6448E+00	0.3201E+00	0.3224E+00	0.6402E+00	0.9771E+00
0.3400E+01	0.6450E+00	0.3203E+00	0.3225E+00	0.6405E+00	0.9778E+00
0.3500E+01	0.6451E+00	0.3204E+00	0.3226E+00	0.6408E+00	0.9784E+00
0.3600E+01	0.6453E+00	0.3205E+00	0.3226E+00	0.6410E+00	0.9790E+00
0.3700E+01	0.6454E+00	0.3206E+00	0.3227E+00	0.6413E+00	0.9796E+00
0.3800E+01	0.6455E+00	0.3208E+00	0.3228E+00	0.6415E+00	0.9801E+00
0.3900E+01	0.6456E+00	0.3209E+00	0.3228E+00	0.6417E+00	0.9806E+00

TEMPERATURE (K)	LINE(2)	LINE(3)	LINE(4)	LINE(5)	LINE(6)
0.4000E+01	0.6457E+00	0.3210E+00	0.3229E+00	0.6419E+00	0.9811E+00
0.4100E+01	0.6458E+00	0.3211E+00	0.3229E+00	0.6421E+00	0.9815E+00
0.4200E+01	0.6459E+00	0.3212E+00	0.3230E+00	0.6423E+00	0.9820E+00
0.4300E+01	0.6460E+00	0.3212E+00	0.3230E+00	0.6425E+00	0.9824E+00
0.4400E+01	0.6461E+00	0.3213E+00	0.3231E+00	0.6427E+00	0.9828E+00
0.4500E+01	0.6462E+00	0.3214E+00	0.3231E+00	0.6428E+00	0.9832E+00
0.4600E+01	0.6463E+00	0.3215E+00	0.3231E+00	0.6430E+00	0.9835E+00
0.4700E+01	0.6464E+00	0.3216E+00	0.3232E+00	0.6431E+00	0.9839E+00
0.4800E+01	0.6464E+00	0.3216E+00	0.3232E+00	0.6433E+00	0.9842E+00
0.4900E+01	0.6465E+00	0.3217E+00	0.3233E+00	0.6434E+00	0.9845E+00

TEMPERATURE (K)	LINE(2)	LINE(3)	LINE(4)	LINE(5)	LINE(6)
0.5000E+01	0.6466E+00	0.3218E+00	0.3233E+00	0.6435E+00	0.9848E+00
0.5100E+01	0.6466E+00	0.3218E+00	0.3233E+00	0.6437E+00	0.9851E+00
0.5200E+01	0.6467E+00	0.3219E+00	0.3234E+00	0.6438E+00	0.9854E+00
0.5300E+01	0.6468E+00	0.3219E+00	0.3234E+00	0.6439E+00	0.9857E+00
0.5400E+01	0.6468E+00	0.3220E+00	0.3234E+00	0.6440E+00	0.9860E+00
0.5500E+01	0.6469E+00	0.3221E+00	0.3234E+00	0.6441E+00	0.9862E+00
0.5600E+01	0.6469E+00	0.3221E+00	0.3235E+00	0.6442E+00	0.9865E+00
0.5700E+01	0.6470E+00	0.3222E+00	0.3235E+00	0.6443E+00	0.9867E+00
0.5800E+01	0.6471E+00	0.3222E+00	0.3235E+00	0.6444E+00	0.9869E+00
0.5900E+01	0.6471E+00	0.3223E+00	0.3236E+00	0.6445E+00	0.9871E+00

TEMPERATURE (K)	LINE(2)	LINE(3)	LINE(4)	LINE(5)	LINE(6)
0.6000E+01	0.6472E+00	0.3223E+00	0.3236E+00	0.6446E+00	0.9874E+00
0.6100E+01	0.6472E+00	0.3223E+00	0.3236E+00	0.6447E+00	0.9876E+00
0.6200E+01	0.6472E+00	0.3224E+00	0.3236E+00	0.6448E+00	0.9878E+00
0.6300E+01	0.6473E+00	0.3224E+00	0.3236E+00	0.6449E+00	0.9880E+00
0.6400E+01	0.6473E+00	0.3225E+00	0.3237E+00	0.6449E+00	0.9881E+00
0.6500E+01	0.6474E+00	0.3225E+00	0.3237E+00	0.6450E+00	0.9883E+00
0.6600E+01	0.6474E+00	0.3225E+00	0.3237E+00	0.6451E+00	0.9885E+00
0.6700E+01	0.6474E+00	0.3226E+00	0.3237E+00	0.6452E+00	0.9887E+00
0.6800E+01	0.6475E+00	0.3226E+00	0.3237E+00	0.6452E+00	0.9888E+00
0.6900E+01	0.6475E+00	0.3227E+00	0.3238E+00	0.6453E+00	0.9890E+00

TEMPERATURE (K)	LINE(2)	LINE(3)	LINE(4)	LINE(5)	LINE(6)
0.7000E+01	0.6476E+00	0.3227E+00	0.3238E+00	0.6454E+00	0.9891E+00
0.7100E+01	0.6476E+00	0.3227E+00	0.3238E+00	0.6454E+00	0.9893E+00
0.7200E+01	0.6476E+00	0.3228E+00	0.3238E+00	0.6455E+00	0.9894E+00
0.7300E+01	0.6477E+00	0.3228E+00	0.3238E+00	0.6456E+00	0.9896E+00
0.7400E+01	0.6477E+00	0.3228E+00	0.3238E+00	0.6456E+00	0.9897E+00
0.7500E+01	0.6477E+00	0.3228E+00	0.3239E+00	0.6457E+00	0.9899E+00
0.7600E+01	0.6477E+00	0.3229E+00	0.3239E+00	0.6457E+00	0.9900E+00
0.7700E+01	0.6478E+00	0.3229E+00	0.3239E+00	0.6458E+00	0.9901E+00
0.7800E+01	0.6478E+00	0.3229E+00	0.3239E+00	0.6458E+00	0.9903E+00
0.7900E+01	0.6478E+00	0.3230E+00	0.3239E+00	0.6459E+00	0.9904E+00

TEMPERATURE (K)	LINE(2)	LINE(3)	LINE(4)	LINE(5)	LINE(6)
0.8000E+01	0.6479E+00	0.3230E+00	0.3239E+00	0.6460E+00	0.9905E+00
0.8100E+01	0.6479E+00	0.3230E+00	0.3239E+00	0.6460E+00	0.9906E+00
0.8200E+01	0.6479E+00	0.3230E+00	0.3240E+00	0.6460E+00	0.9907E+00
0.8300E+01	0.6479E+00	0.3230E+00	0.3240E+00	0.6461E+00	0.9908E+00
0.8400E+01	0.6480E+00	0.3231E+00	0.3240E+00	0.6461E+00	0.9909E+00
0.8500E+01	0.6480E+00	0.3231E+00	0.3240E+00	0.6462E+00	0.9911E+00
0.8600E+01	0.6480E+00	0.3231E+00	0.3240E+00	0.6462E+00	0.9912E+00
0.8700E+01	0.6480E+00	0.3231E+00	0.3240E+00	0.6463E+00	0.9913E+00
0.8800E+01	0.6481E+00	0.3232E+00	0.3240E+00	0.6463E+00	0.9914E+00
0.8900E+01	0.6481E+00	0.3232E+00	0.3240E+00	0.6464E+00	0.9915E+00

TEMPERATURE (K)	LINE(2)	LINE(3)	LINE(4)	LINE(5)	LINE(6)
0.9000E+01	0.6481E+00	0.3232E+00	0.3240E+00	0.6464E+00	0.9916E+00
0.9100E+01	0.6481E+00	0.3232E+00	0.3241E+00	0.6464E+00	0.9916E+00
0.9200E+01	0.6481E+00	0.3232E+00	0.3241E+00	0.6465E+00	0.9917E+00
0.9300E+01	0.6482E+00	0.3233E+00	0.3241E+00	0.6465E+00	0.9918E+00
0.9400E+01	0.6482E+00	0.3233E+00	0.3241E+00	0.6466E+00	0.9919E+00
0.9500E+01	0.6482E+00	0.3233E+00	0.3241E+00	0.6466E+00	0.9920E+00
0.9600E+01	0.6482E+00	0.3233E+00	0.3241E+00	0.6466E+00	0.9921E+00
0.9700E+01	0.6482E+00	0.3233E+00	0.3241E+00	0.6467E+00	0.9922E+00
0.9800E+01	0.6483E+00	0.3233E+00	0.3241E+00	0.6467E+00	0.9922E+00
0.9900E+01	0.6483E+00	0.3234E+00	0.3241E+00	0.6467E+00	0.9923E+00

$ 3.5 Matrix Element of the β-transition

To estimate the nuclear polarization from the intensity ratio of two lines in a Mössbauer spectrum, a β-transition probability must be known. In this section, the β-transition will be summarized concisely.

The interaction Hamiltonian used to describe the decay was first proposed by Fermi(1933). The interaction is involved an weak interaction whose strength is 10^{-11} orders of magnitude smaller than that of the electromagnetic interaction. The genaral forms of the β-decay Hamiltonian is given by

$$H_\beta = \frac{1}{\sqrt{2}} \int dr^3 \; [\, J_u^+ \, j_u + \text{h.c.}] \; . \tag{3.25}$$

where J_u and j_u are the current density of nucleons and leptons in four dimentions. In the present theory of the β-decay, it is a fact that all existing data on the β-decay are in good agreement with a combination of the vector and axial vector interactions. That is, the Hamiltonian is written by

$$H_\beta = \frac{1}{\sqrt{2}} \int dr^3 \; [\, g_v (\overset{+}{\psi}_N \gamma_u \psi_N) \; (\overset{+}{\psi}_1 \gamma_u (1+\gamma_5) \psi_1)$$

$$+ g_A (\overset{+}{\psi}_N \gamma_u \gamma_5 \psi_N) (\overset{+}{\psi}_1 \gamma_u \gamma_5 (1+\gamma_5) \psi_1) + \text{h.c.}] \quad (3.26)$$

where γ_i is the Dirac matrix and ψ_N and ψ_1 are the operators of field of nucleons and leptons. The first term is the vector type interaction and the second term is the axial vector type interaction. The coupling coefficient of g_V and g_A from the experimental data are

$$g_V = (1.40 \pm 0.20)/10^{-49} \; (\text{erg.cm}^3) \; , \quad (3.27)$$

$$g_A/g_V \cong -1.23 \; . \quad (3.28)$$

After the nonrelativistic approximation, the Hamiltonian H_β can be expanded into multipoles by the same way it is done in the case of gamma-transition. However, in the β-decay it is generally not true that only moultipoles of lowest possible order have to be considered. Table 4.3 lists the nuclear matrix elements of different rank for allowed and first forbidden β-decay togetger with their selection rules. The lowest order Hamiltonian is given by

$$H_\beta \cong \frac{g_V}{\sqrt{2}} \int dr^3 \sum_i (\psi_N^+ \tau(i) \delta(r-r_i) \psi_N)\ (\psi_1^+ \psi_1)$$

$$+ \frac{g_A}{\sqrt{2}} \int dr^3 \sum_i (\psi_N^+ \tau(i) \delta(r-r_i \quad\quad) \quad (3.29)$$

$$+h.c.$$

where ϕ_i and ϕ are the Pauli spin matrix to operate on the nucleon and the lepton, respectively. The first term of Hamiltonian (3.29) is called the Fermi transition and the second term the Gamow-Teller transition. Both transitions are allowed transitions. The pure Fermi transition(I=0; no parity change) and the mixed Fermi-Gamow-Teller transitions ($I_i - I_f = 0$; no parity change) are of little interest here. A pure Gamow-Teller decay is found for several Mössbauer soures, in paticular for Co^{57}.

The transition probability for the β-decay is given by using the formula derived in the first-order time-dependent perturbation theory

$$W(i,f) = \frac{2\pi}{\hbar} |\langle f|H_\beta|i\rangle|^2 \quad (3.30)$$

where W is the transition probability. In the case of Co^{57}, since the Hamiltonian is found to be a Gamow-Teller transition, the transition operator blongs to a first rank tensor.

Table 3.3 Nuclear Matrix Elements for the β-Decay

Decay type	matrix element	tensor rank	selection rules $I_i - I_f$	selection rules $\Pi_i \Pi_f$
Allowed Fermi	$\int 1$	0	0	1
Allowed G-T.	$\int \sigma$	1	0,1;no 0-0	1
First forbidden	$\int \gamma_5$	0	0	-1
	$\int (\sigma \cdot r)$	0	0	-1
	$\int r$	1	0,1;no 0-0	-1
	$\int \alpha$	1	0,1;no 0-0	-1
	$\int (\sigma \times r)$	1	0,1;no 0-0	-1
	$\int B_{ij}$	2	0,1,2; no 0-0 no 1/2-1/2 no 0-1	-1

Therefore, the probability W between two magnetic hyoerfine levels with the Wigner-Ekart theorem is given by

$$W(m_i,m_f) = C^{(1)}(m_i,m_f) \; |\langle \|V\| \rangle|^2 \qquad (3.31)$$

where

$$C^{(1)}(m_i,m_f) = |\langle I_f,m_f,1,(m_f-m_i)|\, I_i,1,I_i,m_i\rangle|^2 \qquad (3.32)$$

is the square of the Clebsch-Gordon coefficient for dipoler radiation and $\langle\|V\|\rangle$ is a reduced matrix element. Using the relation (3.31), the calculation of the intensity ratio of two lines in a Mössbauer spectrum can be explicitly performed for the case of Co^{57}

In a forbidden β-transition generally all six matrix elements will be present unless some of them are excluded by the selection rules. That is, matrix elements of 3-type transitions (rank zero(scalar), $W^{(0)}$, rank one(vector) $W^{(1)}$ and rank two (tensor) $W^{(2)}$) is needed. The relative strength of $W^{(0)}$, $W^{(1)}$ and $W^{(2)}$ are not known a priori. However, the observation of the population of the different hyperfine levels in the daughter nucleus with the Mössbauer effect may give direct evidence as to the relative strengths of the different reduced matrix

elements. It is customary to define mixing ratios of the reduced matrix elements in the following manner;

$$\delta^2 = \frac{|\langle \|V\| \rangle|^2}{|\langle \|S\| \rangle|^2} \quad \text{or} \quad \frac{|\langle \|T\| \rangle|^2}{|\langle \|V\| \rangle|^2} \tag{3.33}$$

By evaluating the Clebsch-Gordan coefficients we will be able to obtain the mixing ratios from Mössbauer measurements on polarized sources which decay by first forbidden β-transition. Two experiments of this type have been performed so far. By He^3 refrigerator, the Munich group has studied Tm^{169}, which is populated by the β-decay of Er^{169}.[51,52]

$ 3.6 Exact Expression of Intensity Ratio as a Function of H/T

In the case of Co^{57}, we will discuss the exact expression of the intensity ratios as a function of nuclear polarization or H/T, where H and T are the magnetic hyperfine field and the absolute temperature at Co^{57}.

When the nuclear spins of Co^{57}(I=7/2, parity-) in the presence of a magnetic field H are in a thermal equilibrium, the population of each sublevel,n, is given by the Boltzmann factor,

$$P(Co^{57}, I=7/2, I_z=n) = \exp(-n\mu H/IkT) / \sum_m \exp(-m\mu H/IkT) \quad (3.34)$$

where k, μ, I and T represent the Boltzmann constant, the nuclear moment of Co^{57}(+4.58 nm), the spin of the nucleus (I=7/2) and the absolute temperature, respectively.

At higher temperatures, where the thermal enargy is much larger than the magnetic energy, i.e. $kT \rangle\rangle 2\mu H$, the individual sublevels are equally populated. But at low temperatures, where $kT \lesssim 2\mu H$, those will no longer be equally populated. Here it is assumed that the

electric quadrupole interaction is much smaller than the magnetic hyperfine interaction and can be neglected. Substituting the values of $u(=4.58\times5.0505\times10^{-24}\ erg.g^{-1})$ and $k(=1.38054\times10^{-16}\ erg.K^{-1})$ to the equation(4.13), P is

$$\left(X = 4.787 \times 10^{-8}\ [K^{-1}Oe^{-1}]\right) \tag{3.35}$$

$$P(Co^{57}, I=7/2, I_z=n) = \exp(-nXH/T) / \sum_{n'} \exp(-nXH/T). \tag{3.36}$$

In the preceding section it was stated that The β-transition probability between two hyperfine levels can be calculated with the Clebsch-Gordon coefficients.

The β-decay (K electron capture) will lead to six sublevels of the second excited state of Fe^{57} (I=5/2,parity-). The population of a sublevel, m, in the second excited state of the daughter nuclei, after integration over all directions and lepton spins, is given by

$$P(Fe^{57}, I=5/2, I_z=m) = K_1\ C(n,m)\ P(Co^{57}, I=7/2, I_z=n) \tag{3.37}$$

where K_1 is the propotional coefficient and C(n,m)

$$C(n,m) = |\langle\ 7/2\ n,1\ (m-n)|\ 7/2\ 1,5/2\ m\rangle|^2$$

$$<J_1M_1J_2M_2|JM>^{\dagger}.$$

一般式

$$\begin{aligned}<J_1M_1J_2M_2|JM> &= \delta(M,\ M_1+M_2)\sqrt{2J+1}\ \Delta(J_1J_2J)\\ &\times\sqrt{(J_1+M_1)!(J_1-M_1)!(J_2+M_2)!(J_2-M_2)!(J+M)!(J-M)!}\\ &\times\sum_z(-)^z[z!(J_1+J_2-J-z)!(J_1-M_1-z)!(J_2+M_2-z)!\\ &\times(J-J_2+M_1+z)!(J-J_1-M_2+z)!]^{-1}\end{aligned}\qquad (C.1)$$

ただし,

$$\Delta(J_1J_2J)=\sqrt{(J_1+J_2-J)!(J+J_1-J_2)!(J+J_2-J_1)!/(J_1+J_2+J+1)!}.\qquad (C.2)$$

$[J_2=\frac{1}{2}]$ $\qquad <J_1\ M-M_2\ \frac{1}{2}\ M_2|JM>$

	$M_2=\frac{1}{2}$	$M_2=-\frac{1}{2}$
$J=J_1+\frac{1}{2}$	$\sqrt{\left(J_1+M+\frac{1}{2}\right)\Big/(2J_1+1)}$	$\sqrt{\left(J_1-M+\frac{1}{2}\right)\Big/(2J_1+1)}$
$J=J_1-\frac{1}{2}$	$-\sqrt{\left(J_1-M+\frac{1}{2}\right)\Big/(2J_1+1)}$	$\sqrt{\left(J_1+M+\frac{1}{2}\right)\Big/(2J_1+1)}$

(C.3)

$[J_2=1]$ $\qquad <J_1\ M-M_2\ 1\ M_2|JM>$

	$M_2=1$	$M_2=0$	$M_2=-1$
$J=J_1+1$	$\sqrt{\frac{(J_1+M)(J_1+M+1)}{(2J_1+1)(2J_1+2)}}$	$\sqrt{\frac{(J_1-M+1)(J_1+M+1)}{(2J_1+1)(J_1+1)}}$	$\sqrt{\frac{(J_1-M)(J_1-M+1)}{(2J_1+1)(2J_1+2)}}$
$J=J_1$	$-\sqrt{\frac{(J_1+M)(J_1-M+1)}{2J_1(J_1+1)}}$	$\frac{M}{\sqrt{J_1(J_1+1)}}$	$\sqrt{\frac{(J_1-M)(J_1+M+1)}{2J_1(J_1+1)}}$
$J=J_1-1$	$\sqrt{\frac{(J_1-M)(J_1-M+1)}{2J_1(2J_1+1)}}$	$-\sqrt{\frac{(J_1-M)(J_1+M)}{J_1(2J_1+1)}}$	$\sqrt{\frac{(J_1+M+1)(J_1+M)}{2J_1(2J_1+1)}}$

(C.4)

ウィグナー係数の性質として (4.63) にあげた関係式

$$<J_2M_2J_1M_1|JM>=(-)^{J_1+J_2-J}<J_1M_1J_2M_2|JM>$$

---

† ウィグナーの $3j$ 記号 $\begin{pmatrix}J_1 & J_2 & J\\ M_1 & M_2 & M\end{pmatrix}$ とこの係数の関係は次のとおりである.

$$\begin{pmatrix}J_1 & J_2 & J\\ M_1 & M_2 & M\end{pmatrix}=(-)^{J_1-J_2-M}(2J+1)^{-1/2}<J_1M_1J_2M_2|J-M>.$$

これらについては数表もつくられている.

Table 3.4 Clebsch-Gordon coefficient

is the square of the Clebsch-Gordon coefficient. Table 4.4 shows the Clebsch-Gordon coefficient and with this Table 4.4 we get

$$P(Fe,\tfrac{5}{2},\tfrac{5}{2}) = K_1[\ 21P(Co,\tfrac{7}{2},\tfrac{7}{2})+ 6P(Co,\tfrac{7}{2},\tfrac{5}{2})+ P(Co,\tfrac{7}{2},\tfrac{3}{2})\ ]$$

$$P(Fe,\tfrac{5}{2},\tfrac{3}{2}) = K_1[\ 15P(Co,\tfrac{7}{2},\tfrac{5}{2})+ 5P(Co,\tfrac{7}{2},\tfrac{3}{2})+ 3P(Co,\tfrac{7}{2},\tfrac{1}{2})]$$

$$P(Fe,\tfrac{5}{2},\tfrac{1}{2}) = K_1[\ 10P(Co,\tfrac{7}{2},\tfrac{3}{2})+ 12P(Co,\tfrac{7}{2},\tfrac{1}{2})+ 6P(Co,\tfrac{7}{2},-\tfrac{1}{2})]$$

$$P(Fe,\tfrac{5}{2},-\tfrac{1}{2}) = K_1[\ 10P(Co,\tfrac{7}{2},-\tfrac{3}{2})+ 12P(Co,\tfrac{7}{2},-\tfrac{1}{2})+ 6P(Co,\tfrac{7}{2},\tfrac{1}{2})]$$

$$P(Fe,\tfrac{5}{2},-\tfrac{3}{2}) = K_1[\ 15P(Co,\tfrac{7}{2},-\tfrac{5}{2})+ 5P(Co,\tfrac{7}{2},-\tfrac{3}{2})+ 3P(Co,\tfrac{7}{2},-\tfrac{1}{2})]$$

$$P(Fe,\tfrac{5}{2},-\tfrac{5}{2}) = K_1[\ 21P(Co,\tfrac{7}{2},-\tfrac{7}{2})+ 6P(Co,\tfrac{7}{2},-\tfrac{5}{2})+ P(Co,\tfrac{7}{2},-\tfrac{3}{2})]$$

(3.38)

where $P(Fe,\frac{5}{2},m)$ and $P(Co,\frac{7}{2},n)$ are the population of the second excited state of Fe^{57} and the state of Co^{57}.

After the β-decay, the following transition occurs which is the magnetic dipole transition from the second excited state to the first excited state of Fe^{57} (I=3/2, parity -). The interaction Hamiltonian is known to

belong to a first rank tensor. Therefore, after integration over all the direction, the population of a sublevel,i, in the first excited state is given by

$$P(Fe^{57},\ I=3/2,\ I_z=i) = K_2\ C(m,i)\ P(Fe^{57},\ I=5/2,\ I_z=m) \quad (3.39)$$

where K_2 is the propotional coefficient and C(m,i)

$$C(m,i) = |\langle 5/2\ m,1(m-i)|5/2\ 1,3/2\ i\rangle|^2$$

is the square of the Clebsch-Gordon coefficient for the dipole radiation. Using Table 4.4, we get

$$P(Fe,\tfrac{3}{2},\tfrac{3}{2}) = K_2[\ 10P(Fe,\tfrac{5}{2},\tfrac{5}{2}) + 4P(Fe,\tfrac{5}{2},\tfrac{3}{2}) + P(Fe,\tfrac{5}{2},\tfrac{1}{2})\ ]$$

$$P(Fe,\tfrac{3}{2},\tfrac{1}{2}) = K_2[\ 6P(Fe,\tfrac{5}{2},\tfrac{3}{2}) + 6P(Fe,\tfrac{5}{2},\tfrac{1}{2}) + 3P(Fe,\tfrac{5}{2},-\tfrac{1}{2})\ ]$$

$$P(Fe,\tfrac{3}{2},-\tfrac{1}{2}) = K_2[\ 6P(Fe,\tfrac{5}{2},-\tfrac{3}{2}) + 6P(Fe,\tfrac{5}{2},-\tfrac{1}{2}) + 3P(Fe,\tfrac{5}{2},\tfrac{1}{2})\ ]$$

$$P(Fe,\tfrac{3}{2},-\tfrac{3}{2}) = K_2[\ 10P(Fe,\tfrac{5}{2},-\tfrac{5}{2}) + 4P(Fe,\tfrac{5}{2},-\tfrac{3}{2}) + P(Fe,\tfrac{5}{2},-\tfrac{1}{2})\ ]$$

(3.40)

where $P(Fe,\frac{3}{2},i)$ and $P(Fe,\frac{5}{2},m)$ are the population of the first excited state and the second excited state of Fe^{57}.

Finally, the transition from the first excited state to the ground state of Fe^{57} (I=1/2, parity -) occurs, which is the same magnetic dipole transition as above and is used for the Mössbauer effect. When the nucleus Fe^{57} is only in a magnetic field, then, the Mössbauer spectrum has six lines. Assuming that the sample is powder and the intensity of the line, which is correspodence to the transition from the state of $Fe^{57}(I=3/2, I_z=3/2)$ to $Fe^{57}(I=1/2, I_z=1/2)$, is unity. the intensity ratios of six lines are written by

$$R(3/2,3/2) = 1.0$$

$$R(1/2,1/2) = \frac{2}{3} P(Fe,\frac{3}{2},\frac{1}{2})/P(Fe,\frac{3}{2},\frac{3}{2})$$

$$R(-1/2,1/2) = \frac{1}{3} P(Fe,\frac{3}{2},-\frac{1}{2})/ P(Fe,\frac{3}{2},\frac{3}{2})$$

$$R(1/2,-1/2) = \frac{1}{3} P(Fe,\frac{3}{2},\frac{1}{2})/ P(Fe,\frac{3}{2},\frac{3}{2})$$

$$R(-1/2,-1/2) = \frac{2}{3} P(Fe,\frac{3}{2},-\frac{1}{2})/ P(Fe,\frac{3}{2},\frac{3}{2})$$

$$R(-3/2,-3/2) = P(Fe,\frac{3}{2},-\frac{3}{2}) / P(Fe,\frac{3}{2},\frac{3}{2}) \qquad (3.41)$$

Whenever the nucleus Fe^{57} is only in a magnetic field, those R can be represented as a universal function of H/T, where H is the magnetic field at the parent nucleus Co^{57} and T is the absolute temperature. Table 4.5 and figure 4.2 show the intensity ratio.

If the nucleus Fe^{57} has both the magnetic interaction and the electoric quadrupole interaction, the sublevels of the second excited state of Fe^{57} nucleus are not characterized by the magnetic quautum number, m_I. In this case, for example Fe^{57} in CoO, the mixing effect of wave function has been taken into consideration. It is tacitly assumed that the depolarization effect is neglected because the nuclear spin-lattice relaxation time is very long.

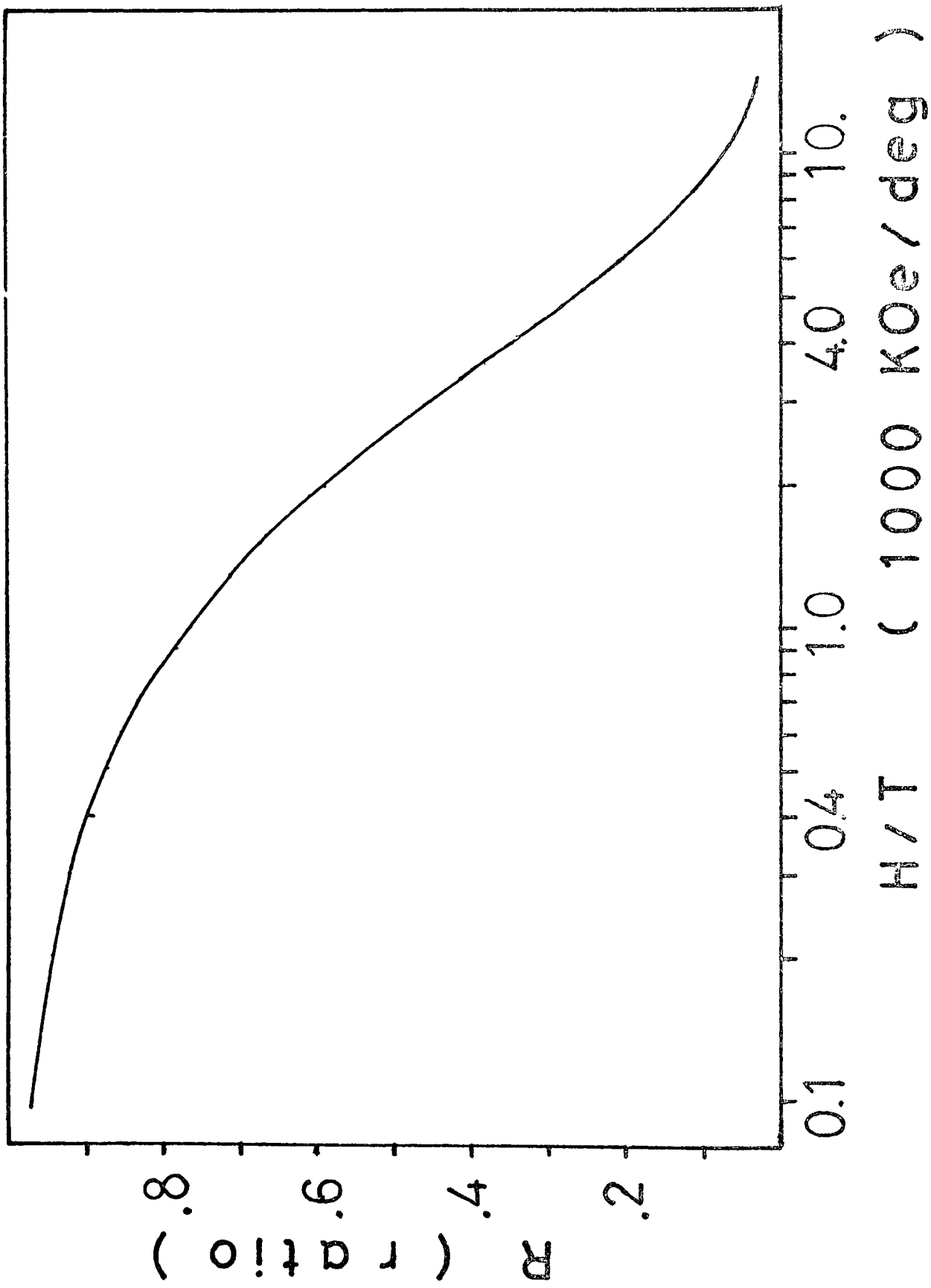

Figure 3.4 Intensity-ratio of LINE(6) versus H/T.

Table 3.5 the intensity ratio versus H/T.

***** H/T ***** paramemeter

H/T (KOE/K)	LINE(2)	LINE(3)	LINE(4)	LINE(5)	LINE(6)
0.1000E+02	0.6494E+00	0.3244E+00	0.3247E+00	0.6489E+00	0.9974E+00
0.1100E+02	0.6493E+00	0.3244E+00	0.3247E+00	0.6488E+00	0.9971E+00
0.1200E+02	0.6493E+00	0.3243E+00	0.3246E+00	0.6487E+00	0.9968E+00
0.1300E+02	0.6492E+00	0.3243E+00	0.3246E+00	0.6485E+00	0.9966E+00
0.1400E+02	0.6492E+00	0.3242E+00	0.3246E+00	0.6484E+00	0.9963E+00
0.1500E+02	0.6491E+00	0.3242E+00	0.3246E+00	0.6483E+00	0.9960E+00
0.1600E+02	0.6491E+00	0.3241E+00	0.3245E+00	0.6482E+00	0.9958E+00
0.1700E+02	0.6490E+00	0.3240E+00	0.3245E+00	0.6481E+00	0.9955E+00
0.1800E+02	0.6489E+00	0.3240E+00	0.3245E+00	0.6480E+00	0.9953E+00
0.1900E+02	0.6489E+00	0.3239E+00	0.3244E+00	0.6479E+00	0.9950E+00

H/T (KOE/K)	LINE(2)	LINE(3)	LINE(4)	LINE(5)	LINE(6)
0.2000E+02	0.6488E+00	0.3239E+00	0.3244E+00	0.6478E+00	0.9947E+00
0.2100E+02	0.6488E+00	0.3238E+00	0.3244E+00	0.6476E+00	0.9945E+00
0.2200E+02	0.6487E+00	0.3238E+00	0.3243E+00	0.6475E+00	0.9942E+00
0.2300E+02	0.6486E+00	0.3237E+00	0.3243E+00	0.6474E+00	0.9939E+00
0.2400E+02	0.6486E+00	0.3237E+00	0.3243E+00	0.6473E+00	0.9937E+00
0.2500E+02	0.6485E+00	0.3236E+00	0.3243E+00	0.6472E+00	0.9934E+00
0.2600E+02	0.6485E+00	0.3235E+00	0.3242E+00	0.6471E+00	0.9932E+00
0.2700E+02	0.6484E+00	0.3235E+00	0.3242E+00	0.6470E+00	0.9929E+00
0.2800E+02	0.6483E+00	0.3234E+00	0.3242E+00	0.6469E+00	0.9926E+00
0.2900E+02	0.6483E+00	0.3234E+00	0.3241E+00	0.6467E+00	0.9924E+00

H/T (KOE/K)	LINE(2)	LINE(3)	LINE(4)	LINE(5)	LINE(6)
0.3000E+02	0.6482E+00	0.3233E+00	0.3241E+00	0.6466E+00	0.9921E+00
0.3100E+02	0.6482E+00	0.3233E+00	0.3241E+00	0.6465E+00	0.9918E+00
0.3200E+02	0.6481E+00	0.3232E+00	0.3241E+00	0.6464E+00	0.9916E+00
0.3300E+02	0.6480E+00	0.3232E+00	0.3240E+00	0.6463E+00	0.9913E+00
0.3400E+02	0.6480E+00	0.3231E+00	0.3240E+00	0.6462E+00	0.9911E+00
0.3500E+02	0.6479E+00	0.3230E+00	0.3240E+00	0.6461E+00	0.9908E+00
0.3600E+02	0.6479E+00	0.3230E+00	0.3239E+00	0.6460E+00	0.9905E+00
0.3700E+02	0.6478E+00	0.3229E+00	0.3239E+00	0.6459E+00	0.9903E+00
0.3800E+02	0.6478E+00	0.3229E+00	0.3239E+00	0.6457E+00	0.9900E+00
0.3900E+02	0.6477E+00	0.3228E+00	0.3238E+00	0.6456E+00	0.9897E+00

H/T (KOE/K)	LINE(2)	LINE(3)	LINE(4)	LINE(5)	LINE(6)
0.4000E+02	0.6476E+00	0.3228E+00	0.3238E+00	0.6455E+00	0.9895E+00
0.4100E+02	0.6476E+00	0.3227E+00	0.3238E+00	0.6454E+00	0.9892E+00
0.4200E+02	0.6475E+00	0.3226E+00	0.3238E+00	0.6453E+00	0.9890E+00
0.4300E+02	0.6475E+00	0.3226E+00	0.3237E+00	0.6452E+00	0.9887E+00
0.4400E+02	0.6474E+00	0.3225E+00	0.3237E+00	0.6451E+00	0.9884E+00
0.4500E+02	0.6473E+00	0.3225E+00	0.3237E+00	0.6450E+00	0.9882E+00
0.4600E+02	0.6473E+00	0.3224E+00	0.3236E+00	0.6448E+00	0.9879E+00
0.4700E+02	0.6472E+00	0.3224E+00	0.3236E+00	0.6447E+00	0.9877E+00
0.4800E+02	0.6472E+00	0.3223E+00	0.3236E+00	0.6446E+00	0.9874E+00
0.4900E+02	0.6471E+00	0.3223E+00	0.3236E+00	0.6445E+00	0.9871E+00

H/T (KOE/K)	LINE(2)	LINE(3)	LINE(4)	LINE(5)	LINE(6)
0.5000E+02	0.6470E+00	0.3222E+00	0.3235E+00	0.6444E+00	0.9869E+00
0.5100E+02	0.6470E+00	0.3221E+00	0.3235E+00	0.6443E+00	0.9866E+00
0.5200E+02	0.6469E+00	0.3221E+00	0.3235E+00	0.6442E+00	0.9864E+00
0.5300E+02	0.6469E+00	0.3220E+00	0.3234E+00	0.6441E+00	0.9861E+00
0.5400E+02	0.6468E+00	0.3220E+00	0.3234E+00	0.6440E+00	0.9858E+00
0.5500E+02	0.6467E+00	0.3219E+00	0.3234E+00	0.6438E+00	0.9856E+00
0.5600E+02	0.6467E+00	0.3219E+00	0.3233E+00	0.6437E+00	0.9853E+00
0.5700E+02	0.6466E+00	0.3218E+00	0.3233E+00	0.6436E+00	0.9851E+00
0.5800E+02	0.6466E+00	0.3218E+00	0.3233E+00	0.6435E+00	0.9848E+00
0.5900E+02	0.6465E+00	0.3217E+00	0.3233E+00	0.6434E+00	0.9845E+00

H/T (KOE/K)	LINE(2)	LINE(3)	LINE(4)	LINE(5)	LINE(6)
0.6000E+02	0.6465E+00	0.3216E+00	0.3232E+00	0.6433E+00	0.9843E+00
0.6100E+02	0.6464E+00	0.3216E+00	0.3232E+00	0.6432E+00	0.9840E+00
0.6200E+02	0.6463E+00	0.3215E+00	0.3232E+00	0.6431E+00	0.9838E+00
0.6300E+02	0.6463E+00	0.3215E+00	0.3231E+00	0.6430E+00	0.9835E+00
0.6400E+02	0.6462E+00	0.3214E+00	0.3231E+00	0.6428E+00	0.9832E+00
0.6500E+02	0.6462E+00	0.3214E+00	0.3231E+00	0.6427E+00	0.9830E+00
0.6600E+02	0.6461E+00	0.3213E+00	0.3230E+00	0.6426E+00	0.9827E+00
0.6700E+02	0.6460E+00	0.3213E+00	0.3230E+00	0.6425E+00	0.9825E+00
0.6800E+02	0.6460E+00	0.3212E+00	0.3230E+00	0.6424E+00	0.9822E+00
0.6900E+02	0.6459E+00	0.3211E+00	0.3230E+00	0.6423E+00	0.9819E+00

H/T (KOE/K)	LINE(2)	LINE(3)	LINE(4)	LINE(5)	LINE(6)
0.7000E+02	0.6459E+00	0.3211E+00	0.3229E+00	0.6422E+00	0.9817E+00
0.7100E+02	0.6458E+00	0.3210E+00	0.3229E+00	0.6421E+00	0.9814E+00
0.7200E+02	0.6457E+00	0.3210E+00	0.3229E+00	0.6420E+00	0.9812E+00
0.7300E+02	0.6457E+00	0.3209E+00	0.3228E+00	0.6418E+00	0.9809E+00
0.7400E+02	0.6456E+00	0.3209E+00	0.3228E+00	0.6417E+00	0.9806E+00
0.7500E+02	0.6456E+00	0.3208E+00	0.3228E+00	0.6416E+00	0.9804E+00
0.7600E+02	0.6455E+00	0.3208E+00	0.3228E+00	0.6415E+00	0.9801E+00
0.7700E+02	0.6455E+00	0.3207E+00	0.3227E+00	0.6414E+00	0.9799E+00
0.7800E+02	0.6454E+00	0.3206E+00	0.3227E+00	0.6413E+00	0.9796E+00
0.7900E+02	0.6453E+00	0.3206E+00	0.3227E+00	0.6412E+00	0.9793E+00

H/T (KOE/K)	LINE(2)	LINE(3)	LINE(4)	LINE(5)	LINE(6)
0.8000E+02	0.6453E+00	0.3205E+00	0.3226E+00	0.6411E+00	0.9791E+00
0.8100E+02	0.6452E+00	0.3205E+00	0.3226E+00	0.6410E+00	0.9788E+00
0.8200E+02	0.6452E+00	0.3204E+00	0.3226E+00	0.6408E+00	0.9786E+00
0.8300E+02	0.6451E+00	0.3204E+00	0.3225E+00	0.6407E+00	0.9783E+00
0.8400E+02	0.6450E+00	0.3203E+00	0.3225E+00	0.6406E+00	0.9780E+00
0.8500E+02	0.6450E+00	0.3203E+00	0.3225E+00	0.6405E+00	0.9778E+00
0.8600E+02	0.6449E+00	0.3202E+00	0.3225E+00	0.6404E+00	0.9775E+00
0.8700E+02	0.6449E+00	0.3201E+00	0.3224E+00	0.6403E+00	0.9773E+00
0.8800E+02	0.6448E+00	0.3201E+00	0.3224E+00	0.6402E+00	0.9770E+00
0.8900E+02	0.6447E+00	0.3200E+00	0.3224E+00	0.6401E+00	0.9768E+00

H/T (KOE/K)	LINE(2)	LINE(3)	LINE(4)	LINE(5)	LINE(6)
0.9000E+02	0.6447E+00	0.3200E+00	0.3223E+00	0.6400E+00	0.9765E+00
0.9100E+02	0.6446E+00	0.3199E+00	0.3223E+00	0.6399E+00	0.9762E+00
0.9200E+02	0.6446E+00	0.3199E+00	0.3223E+00	0.6397E+00	0.9760E+00
0.9300E+02	0.6445E+00	0.3198E+00	0.3223E+00	0.6396E+00	0.9757E+00
0.9400E+02	0.6445E+00	0.3198E+00	0.3222E+00	0.6395E+00	0.9755E+00
0.9500E+02	0.6444E+00	0.3197E+00	0.3222E+00	0.6394E+00	0.9752E+00
0.9600E+02	0.6443E+00	0.3196E+00	0.3222E+00	0.6393E+00	0.9750E+00
0.9700E+02	0.6443E+00	0.3196E+00	0.3221E+00	0.6392E+00	0.9747E+00
0.9800E+02	0.6442E+00	0.3195E+00	0.3221E+00	0.6391E+00	0.9744E+00
0.9900E+02	0.6442E+00	0.3195E+00	0.3221E+00	0.6390E+00	0.9742E+00

H/T (KOE/K)	LINE(2)	LINE(3)	LINE(4)	LINE(5)	LINE(6)
0.1000E+03	0.6441E+00	0.3194E+00	0.3220E+00	0.6389E+00	0.9739E+00
0.1100E+03	0.6435E+00	0.3189E+00	0.3218E+00	0.6378E+00	0.9714E+00
0.1200E+03	0.6429E+00	0.3183E+00	0.3215E+00	0.6367E+00	0.9688E+00
0.1300E+03	0.6423E+00	0.3178E+00	0.3212E+00	0.6356E+00	0.9662E+00
0.1400E+03	0.6418E+00	0.3172E+00	0.3209E+00	0.6345E+00	0.9637E+00
0.1500E+03	0.6412E+00	0.3167E+00	0.3206E+00	0.6334E+00	0.9611E+00
0.1600E+03	0.6406E+00	0.3161E+00	0.3203E+00	0.6323E+00	0.9586E+00
0.1700E+03	0.6400E+00	0.3156E+00	0.3200E+00	0.6312E+00	0.9561E+00
0.1800E+03	0.6394E+00	0.3150E+00	0.3197E+00	0.6301E+00	0.9535E+00
0.1900E+03	0.6388E+00	0.3145E+00	0.3194E+00	0.6290E+00	0.9510E+00

H/T (KOE/K)	LINE(2)	LINE(3)	LINE(4)	LINE(5)	LINE(6)
0.2000E+03	0.6383E+00	0.3140E+00	0.3191E+00	0.6279E+00	0.9485E+00
0.2100E+03	0.6377E+00	0.3134E+00	0.3188E+00	0.6268E+00	0.9460E+00
0.2200E+03	0.6371E+00	0.3129E+00	0.3186E+00	0.6257E+00	0.9435E+00
0.2300E+03	0.6365E+00	0.3123E+00	0.3183E+00	0.6247E+00	0.9410E+00
0.2400E+03	0.6359E+00	0.3118E+00	0.3180E+00	0.6236E+00	0.9385E+00
0.2500E+03	0.6354E+00	0.3113E+00	0.3177E+00	0.6225E+00	0.9361E+00
0.2600E+03	0.6348E+00	0.3107E+00	0.3174E+00	0.6214E+00	0.9336E+00
0.2700E+03	0.6342E+00	0.3102E+00	0.3171E+00	0.6204E+00	0.9311E+00
0.2800E+03	0.6336E+00	0.3096E+00	0.3168E+00	0.6193E+00	0.9287E+00
0.2900E+03	0.6331E+00	0.3091E+00	0.3165E+00	0.6182E+00	0.9262E+00

H/T (KOE/K)	LINE(2)	LINE(3)	LINE(4)	LINE(5)	LINE(6)
0.3000E+03	0.6325E+00	0.3086E+00	0.3162E+00	0.6172E+00	0.9238E+00
0.3100E+03	0.6319E+00	0.3080E+00	0.3160E+00	0.6161E+00	0.9213E+00
0.3200E+03	0.6313E+00	0.3075E+00	0.3157E+00	0.6150E+00	0.9189E+00
0.3300E+03	0.6308E+00	0.3070E+00	0.3154E+00	0.6140E+00	0.9165E+00
0.3400E+03	0.6302E+00	0.3065E+00	0.3151E+00	0.6129E+00	0.9141E+00
0.3500E+03	0.6296E+00	0.3059E+00	0.3148E+00	0.6119E+00	0.9117E+00
0.3600E+03	0.6290E+00	0.3054E+00	0.3145E+00	0.6108E+00	0.9093E+00
0.3700E+03	0.6285E+00	0.3049E+00	0.3142E+00	0.6098E+00	0.9069E+00
0.3800E+03	0.6279E+00	0.3044E+00	0.3140E+00	0.6087E+00	0.9045E+00
0.3900E+03	0.6273E+00	0.3038E+00	0.3137E+00	0.6077E+00	0.9021E+00

H/T (KOE/K)	LINE(2)	LINE(3)	LINE(4)	LINE(5)	LINE(6)
0.4000E+03	0.6268E+00	0.3033E+00	0.3134E+00	0.6066E+00	0.8997E+00
0.4100E+03	0.6262E+00	0.3028E+00	0.3131E+00	0.6056E+00	0.8973E+00
0.4200E+03	0.6256E+00	0.3023E+00	0.3128E+00	0.6045E+00	0.8950E+00
0.4300E+03	0.6251E+00	0.3017E+00	0.3125E+00	0.6035E+00	0.8926E+00
0.4400E+03	0.6245E+00	0.3012E+00	0.3123E+00	0.6024E+00	0.8902E+00
0.4500E+03	0.6239E+00	0.3007E+00	0.3120E+00	0.6014E+00	0.8879E+00
0.4600E+03	0.6234E+00	0.3002E+00	0.3117E+00	0.6004E+00	0.8855E+00
0.4700E+03	0.6228E+00	0.2997E+00	0.3114E+00	0.5993E+00	0.8832E+00
0.4800E+03	0.6222E+00	0.2991E+00	0.3111E+00	0.5983E+00	0.8809E+00
0.4900E+03	0.6217E+00	0.2986E+00	0.3108E+00	0.5973E+00	0.8786E+00

H/T (KOE/K)	LINE(2)	LINE(3)	LINE(4)	LINE(5)	LINE(6)
0.5000E+03	0.6211E+00	0.2981E+00	0.3106E+00	0.5962E+00	0.8762E+00
0.5100E+03	0.6206E+00	0.2976E+00	0.3103E+00	0.5952E+00	0.8739E+00
0.5200E+03	0.6200E+00	0.2971E+00	0.3100E+00	0.5942E+00	0.8716E+00
0.5300E+03	0.6194E+00	0.2966E+00	0.3097E+00	0.5932E+00	0.8693E+00
0.5400E+03	0.6189E+00	0.2961E+00	0.3094E+00	0.5921E+00	0.8670E+00
0.5500E+03	0.6183E+00	0.2956E+00	0.3092E+00	0.5911E+00	0.8647E+00
0.5600E+03	0.6178E+00	0.2951E+00	0.3089E+00	0.5901E+00	0.8625E+00
0.5700E+03	0.6172E+00	0.2945E+00	0.3086E+00	0.5891E+00	0.8602E+00
0.5800E+03	0.6166E+00	0.2940E+00	0.3083E+00	0.5881E+00	0.8579E+00
0.5900E+03	0.6161E+00	0.2935E+00	0.3080E+00	0.5871E+00	0.8556E+00

H/T (KOE/K)	LINE(2)	LINE(3)	LINE(4)	LINE(5)	LINE(6)
0.6000E+03	0.6155E+00	0.2930E+00	0.3078E+00	0.5861E+00	0.8534E+00
0.6100E+03	0.6150E+00	0.2925E+00	0.3075E+00	0.5851E+00	0.8511E+00
0.6200E+03	0.6144E+00	0.2920E+00	0.3072E+00	0.5840E+00	0.8489E+00
0.6300E+03	0.6139E+00	0.2915E+00	0.3069E+00	0.5830E+00	0.8466E+00
0.6400E+03	0.6133E+00	0.2910E+00	0.3066E+00	0.5820E+00	0.8444E+00
0.6500E+03	0.6127E+00	0.2905E+00	0.3064E+00	0.5810E+00	0.8422E+00
0.6600E+03	0.6122E+00	0.2900E+00	0.3061E+00	0.5800E+00	0.8400E+00
0.6700E+03	0.6116E+00	0.2895E+00	0.3058E+00	0.5790E+00	0.8377E+00
0.6800E+03	0.6111E+00	0.2890E+00	0.3055E+00	0.5780E+00	0.8355E+00
0.6900E+03	0.6105E+00	0.2885E+00	0.3053E+00	0.5771E+00	0.8333E+00

H/T (KOE/K)	LINE(2)	LINE(3)	LINE(4)	LINE(5)	LINE(6)
0.7000E+03	0.6100E+00	0.2880E+00	0.3050E+00	0.5761E+00	0.8311E+00
0.7100E+03	0.6094E+00	0.2875E+00	0.3047E+00	0.5751E+00	0.8289E+00
0.7200E+03	0.6089E+00	0.2870E+00	0.3044E+00	0.5741E+00	0.8268E+00
0.7300E+03	0.6083E+00	0.2865E+00	0.3042E+00	0.5731E+00	0.8246E+00
0.7400E+03	0.6078E+00	0.2861E+00	0.3039E+00	0.5721E+00	0.8224E+00
0.7500E+03	0.6072E+00	0.2856E+00	0.3036E+00	0.5711E+00	0.8202E+00
0.7600E+03	0.6067E+00	0.2851E+00	0.3033E+00	0.5701E+00	0.8181E+00
0.7700E+03	0.6061E+00	0.2846E+00	0.3031E+00	0.5692E+00	0.8159E+00
0.7800E+03	0.6056E+00	0.2841E+00	0.3028E+00	0.5682E+00	0.8138E+00
0.7900E+03	0.6051E+00	0.2836E+00	0.3025E+00	0.5672E+00	0.8116E+00

H/T (KOE/K)	LINE(2)	LINE(3)	LINE(4)	LINE(5)	LINE(6)
0.8000E+03	0.6045E+00	0.2831E+00	0.3023E+00	0.5662E+00	0.8095E+00
0.8100E+03	0.6040E+00	0.2826E+00	0.3020E+00	0.5653E+00	0.8073E+00
0.8200E+03	0.6034E+00	0.2821E+00	0.3017E+00	0.5643E+00	0.8052E+00
0.8300E+03	0.6029E+00	0.2817E+00	0.3014E+00	0.5633E+00	0.8031E+00
0.8400E+03	0.6023E+00	0.2812E+00	0.3012E+00	0.5624E+00	0.8010E+00
0.8500E+03	0.6018E+00	0.2807E+00	0.3009E+00	0.5614E+00	0.7988E+00
0.8600E+03	0.6012E+00	0.2802E+00	0.3006E+00	0.5604E+00	0.7967E+00
0.8700E+03	0.6007E+00	0.2797E+00	0.3004E+00	0.5595E+00	0.7946E+00
0.8800E+03	0.6002E+00	0.2793E+00	0.3001E+00	0.5585E+00	0.7925E+00
0.8900E+03	0.5996E+00	0.2788E+00	0.2998E+00	0.5576E+00	0.7904E+00

H/T (KOE/K)	LINE(2)	LINE(3)	LINE(4)	LINE(5)	LINE(6)
0.9000E+03	0.5991E+00	0.2783E+00	0.2995E+00	0.5566E+00	0.7884E+00
0.9100E+03	0.5985E+00	0.2778E+00	0.2993E+00	0.5556E+00	0.7863E+00
0.9200E+03	0.5980E+00	0.2773E+00	0.2990E+00	0.5547E+00	0.7842E+00
0.9300E+03	0.5975E+00	0.2769E+00	0.2987E+00	0.5537E+00	0.7821E+00
0.9400E+03	0.5969E+00	0.2764E+00	0.2985E+00	0.5528E+00	0.7801E+00
0.9500E+03	0.5964E+00	0.2759E+00	0.2982E+00	0.5518E+00	0.7780E+00
0.9600E+03	0.5959E+00	0.2754E+00	0.2979E+00	0.5509E+00	0.7760E+00
0.9700E+03	0.5953E+00	0.2750E+00	0.2977E+00	0.5499E+00	0.7739E+00
0.9800E+03	0.5948E+00	0.2745E+00	0.2974E+00	0.5490E+00	0.7719E+00
0.9900E+03	0.5943E+00	0.2740E+00	0.2971E+00	0.5481E+00	0.7698E+00

H/T (KOE/K)	LINE(2)	LINE(3)	LINE(4)	LINE(5)	LINE(6)
0.1000E+04	0.5937E+00	0.2736E+00	0.2969E+00	0.5471E+00	0.7678E+00
0.1100E+04	0.5884E+00	0.2689E+00	0.2942E+00	0.5378E+00	0.7478E+00
0.1200E+04	0.5832E+00	0.2643E+00	0.2916E+00	0.5287E+00	0.7283E+00
0.1300E+04	0.5780E+00	0.2599E+00	0.2890E+00	0.5197E+00	0.7093E+00
0.1400E+04	0.5728E+00	0.2554E+00	0.2864E+00	0.5109E+00	0.6908E+00
0.1500E+04	0.5677E+00	0.2511E+00	0.2839E+00	0.5022E+00	0.6729E+00
0.1600E+04	0.5627E+00	0.2469E+00	0.2814E+00	0.4937E+00	0.6553E+00
0.1700E+04	0.5577E+00	0.2427E+00	0.2789E+00	0.4854E+00	0.6383E+00
0.1800E+04	0.5528E+00	0.2386E+00	0.2764E+00	0.4772E+00	0.6216E+00
0.1900E+04	0.5479E+00	0.2346E+00	0.2740E+00	0.4691E+00	0.6055E+00

H/T (KOE/K)	LINE(2)	LINE(3)	LINE(4)	LINE(5)	LINE(6)
0.2000E+04	0.5431E+00	0.2306E+00	0.2715E+00	0.4612E+00	0.5897E+00
0.2100E+04	0.5383E+00	0.2267E+00	0.2692E+00	0.4535E+00	0.5743E+00
0.2200E+04	0.5336E+00	0.2229E+00	0.2668E+00	0.4458E+00	0.5594E+00
0.2300E+04	0.5289E+00	0.2192E+00	0.2645E+00	0.4383E+00	0.5448E+00
0.2400E+04	0.5243E+00	0.2155E+00	0.2621E+00	0.4310E+00	0.5307E+00
0.2500E+04	0.5197E+00	0.2119E+00	0.2599E+00	0.4237E+00	0.5169E+00
0.2600E+04	0.5152E+00	0.2083E+00	0.2576E+00	0.4166E+00	0.5034E+00
0.2700E+04	0.5107E+00	0.2048E+00	0.2553E+00	0.4097E+00	0.4904E+00
0.2800E+04	0.5063E+00	0.2014E+00	0.2531E+00	0.4028E+00	0.4776E+00
0.2900E+04	0.5019E+00	0.1980E+00	0.2509E+00	0.3961E+00	0.4652E+00

H/T (KOE/K)	LINE(2)	LINE(3)	LINE(4)	LINE(5)	LINE(6)
0.3000E+04	0.4975E+00	0.1947E+00	0.2488E+00	0.3895E+00	0.4531E+00
0.3100E+04	0.4932E+00	0.1915E+00	0.2466E+00	0.3830E+00	0.4414E+00
0.3200E+04	0.4890E+00	0.1883E+00	0.2445E+00	0.3766E+00	0.4299E+00
0.3300E+04	0.4848E+00	0.1852E+00	0.2424E+00	0.3703E+00	0.4188E+00
0.3400E+04	0.4806E+00	0.1821E+00	0.2403E+00	0.3642E+00	0.4079E+00
0.3500E+04	0.4765E+00	0.1791E+00	0.2382E+00	0.3581E+00	0.3973E+00
0.3600E+04	0.4724E+00	0.1761E+00	0.2362E+00	0.3522E+00	0.3870E+00
0.3700E+04	0.4683E+00	0.1732E+00	0.2342E+00	0.3463E+00	0.3770E+00
0.3800E+04	0.4643E+00	0.1703E+00	0.2322E+00	0.3406E+00	0.3672E+00
0.3900E+04	0.4604E+00	0.1675E+00	0.2302E+00	0.3350E+00	0.3577E+00

H/T (KOE/K)	LINE(2)	LINE(3)	LINE(4)	LINE(5)	LINE(6)
0.4000E+04	0.4565E+00	0.1647E+00	0.2282E+00	0.3294E+00	0.3485E+00
0.4100E+04	0.4526E+00	0.1620E+00	0.2263E+00	0.3240E+00	0.3395E+00
0.4200E+04	0.4488E+00	0.1593E+00	0.2244E+00	0.3187E+00	0.3307E+00
0.4300E+04	0.4450E+00	0.1567E+00	0.2225E+00	0.3134E+00	0.3221E+00
0.4400E+04	0.4412E+00	0.1541E+00	0.2206E+00	0.3083E+00	0.3138E+00
0.4500E+04	0.4375E+00	0.1516E+00	0.2188E+00	0.3032E+00	0.3057E+00
0.4600E+04	0.4338E+00	0.1491E+00	0.2169E+00	0.2982E+00	0.2978E+00
0.4700E+04	0.4302E+00	0.1467E+00	0.2151E+00	0.2934E+00	0.2901E+00
0.4800E+04	0.4266E+00	0.1443E+00	0.2133E+00	0.2886E+00	0.2826E+00
0.4900E+04	0.4230E+00	0.1419E+00	0.2115E+00	0.2838E+00	0.2754E+00

H/T (KOE/K)	LINE(2)	LINE(3)	LINE(4)	LINE(5)	LINE(6)
0.5000E+04	0.4195E+00	0.1396E+00	0.2097E+00	0.2792E+00	0.2683E+00
0.5100E+04	0.4160E+00	0.1373E+00	0.2080E+00	0.2747E+00	0.2614E+00
0.5200E+04	0.4125E+00	0.1351E+00	0.2063E+00	0.2702E+00	0.2546E+00
0.5300E+04	0.4091E+00	0.1329E+00	0.2046E+00	0.2658E+00	0.2481E+00
0.5400E+04	0.4057E+00	0.1307E+00	0.2029E+00	0.2615E+00	0.2417E+00
0.5500E+04	0.4024E+00	0.1286E+00	0.2012E+00	0.2572E+00	0.2355E+00
0.5600E+04	0.3990E+00	0.1265E+00	0.1995E+00	0.2531E+00	0.2294E+00
0.5700E+04	0.3958E+00	0.1245E+00	0.1979E+00	0.2490E+00	0.2235E+00
0.5800E+04	0.3925E+00	0.1225E+00	0.1963E+00	0.2450E+00	0.2178E+00
0.5900E+04	0.3893E+00	0.1205E+00	0.1946E+00	0.2410E+00	0.2122E+00

H/T (KOE/K)	LINE(2)	LINE(3)	LINE(4)	LINE(5)	LINE(6)
0.6000E+04	0.3861E+00	0.1186E+00	0.1930E+00	0.2371E+00	0.2068E+00
0.6100E+04	0.3829E+00	0.1166E+00	0.1915E+00	0.2333E+00	0.2015E+00
0.6200E+04	0.3798E+00	0.1148E+00	0.1899E+00	0.2295E+00	0.1963E+00
0.6300E+04	0.3767E+00	0.1129E+00	0.1884E+00	0.2259E+00	0.1913E+00
0.6400E+04	0.3737E+00	0.1111E+00	0.1868E+00	0.2222E+00	0.1864E+00
0.6500E+04	0.3706E+00	0.1093E+00	0.1853E+00	0.2187E+00	0.1817E+00
0.6600E+04	0.3676E+00	0.1076E+00	0.1838E+00	0.2152E+00	0.1770E+00
0.6700E+04	0.3647E+00	0.1059E+00	0.1823E+00	0.2117E+00	0.1725E+00
0.6800E+04	0.3617E+00	0.1042E+00	0.1809E+00	0.2084E+00	0.1681E+00
0.6900E+04	0.3588E+00	0.1025E+00	0.1794E+00	0.2050E+00	0.1638E+00

H/T (KOE/K)	LINE(2)	LINE(3)	LINE(4)	LINE(5)	LINE(6)
0.7000E+04	0.3559E+00	0.1009E+00	0.1780E+00	0.2018E+00	0,1596E+00
0.7100E+04	0.3531E+00	0.9928E-01	0.1765E+00	0.1986E+00	0.1556E+00
0.7200E+04	0.3503E+00	0.9771E-01	0.1751E+00	0.1954E+00	0.1516E+00
0.7300E+04	0.3475E+00	0.9616E-01	0.1737E+00	0.1923E+00	0.1478E+00
0.7400E+04	0.3447E+00	0.9463E-01	0.1723E+00	0.1893E+00	0.1440E+00
0.7500E+04	0.3420E+00	0.9314E-01	0.1710E+00	0.1863E+00	0.1404E+00
0.7600E+04	0.3392E+00	0.9167E-01	0.1696E+00	0.1833E+00	0.1368E+00
0.7700E+04	0.3366E+00	0.9022E-01	0.1683E+00	0.1804E+00	0.1333E+00
0.7800E+04	0.3339E+00	0.8880E-01	0.1669E+00	0.1776E+00	0.1300E+00
0.7900E+04	0.3313E+00	0.8740E-01	0.1656E+00	0.1748E+00	0.1267E+00

H/T (KOE/K)	LINE(2)	LINE(3)	LINE(4)	LINE(5)	LINE(6)
0.8000E+04	0.3287E+00	0.8603E-01	0.1643E+00	0.1721E+00	0.1235E+00
0.8100E+04	0.3261E+00	0.8468E-01	0.1630E+00	0.1694E+00	0.1204E+00
0.8200E+04	0.3235E+00	0.8336E-01	0.1618E+00	0.1667E+00	0.1173E+00
0.8300E+04	0.3210E+00	0.8205E-01	0.1605E+00	0.1641E+00	0.1144E+00
0.8400E+04	0.3185E+00	0.8077E-01	0.1592E+00	0.1615E+00	0.1115E+00
0.8500E+04	0.3160E+00	0.7951E-01	0.1580E+00	0.1590E+00	0.1087E+00
0.8600E+04	0.3135E+00	0.7827E-01	0.1568E+00	0.1565E+00	0.1059E+00
0.8700E+04	0.3111E+00	0.7705E-01	0.1556E+00	0.1541E+00	0.1033E+00
0.8800E+04	0.3087E+00	0.7586E-01	0.1543E+00	0.1517E+00	0.1007E+00
0.8900E+04	0.3063E+00	0.7468E-01	0.1532E+00	0.1494E+00	0.9815E-01

H/T (KOE/K)	LINE(2)	LINE(3)	LINE(4)	LINE(5)	LINE(6)
0.9000E+04	0.3039E+00	0.7352E-01	0.1520E+00	0.1470E+00	0.9569E-01
0.9100E+04	0.3016E+00	0.7239E-01	0.1508E+00	0.1448E+00	0.9329E-01
0.9200E+04	0.2993E+00	0.7127E-01	0.1496E+00	0.1425E+00	0.9095E-01
0.9300E+04	0.2970E+00	0.7017E-01	0.1485E+00	0.1403E+00	0.8868E-01
0.9400E+04	0.2947E+00	0.6909E-01	0.1474E+00	0.1382E+00	0.8646E-01
0.9500E+04	0.2925E+00	0.6802E-01	0.1462E+00	0.1360E+00	0.8430E-01
0.9600E+04	0.2902E+00	0.6698E-01	0.1451E+00	0.1340E+00	0.8220E-01
0.9700E+04	0.2880E+00	0.6595E-01	0.1440E+00	0.1319E+00	0.8015E-01
0.9800E+04	0.2858E+00	0.6494E-01	0.1429E+00	0.1299E+00	0.7816E-01
0.9900E+04	0.2837E+00	0.6395E-01	0.1418E+00	0.1279E+00	0.7621E-01

H/T (KOE/K)	LINE(2)	LINE(3)	LINE(4)	LINE(5)	LINE(6)
0.1000E+05	0.2815E+00	0.6297E-01	0.1408E+00	0.1259E+00	0.7432E-01
0.1010E+05	0.2794E+00	0.6201E-01	0.1397E+00	0.1240E+00	0.7247E-01
0.1020E+05	0.2773E+00	0.6107E-01	0.1386E+00	0.1221E+00	0.7068E-01
0.1030E+05	0.2752E+00	0.6014E-01	0.1376E+00	0.1203E+00	0.6893E-01
0.1040E+05	0.2731E+00	0.5922E-01	0.1366E+00	0.1184E+00	0.6722E-01
0.1050E+05	0.2711E+00	0.5832E-01	0.1355E+00	0.1166E+00	0.6556E-01
0.1060E+05	0.2691E+00	0.5744E-01	0.1345E+00	0.1149E+00	0.6394E-01
0.1070E+05	0.2671E+00	0.5657E-01	0.1335E+00	0.1131E+00	0.6236E-01
0.1080E+05	0.2651E+00	0.5572E-01	0.1325E+00	0.1114E+00	0.6082E-01
0.1090E+05	0.2631E+00	0.5488E-01	0.1316E+00	0.1098E+00	0.5933E-01

H/T (KOE/K)	LINE(2)	LINE(3)	LINE(4)	LINE(5)	LINE(6)
0.1100E+05	0.2612E+00	0.5405E-01	0.1306E+00	0.1081E+00	0.5787E-01
0.1110E+05	0.2592E+00	0.5324E-01	0.1296E+00	0.1065E+00	0.5644E-01
0.1120E+05	0.2573E+00	0.5244E-01	0.1287E+00	0.1049E+00	0.5506E-01
0.1130E+05	0.2554E+00	0.5165E-01	0.1277E+00	0.1033E+00	0.5371E-01
0.1140E+05	0.2535E+00	0.5088E-01	0.1268E+00	0.1018E+00	0.5239E-01
0.1150E+05	0.2517E+00	0.5012E-01	0.1258E+00	0.1002E+00	0.5111E-01
0.1160E+05	0.2498E+00	0.4937E-01	0.1249E+00	0.9874E-01	0.4986E-01
0.1170E+05	0.2480E+00	0.4863E-01	0.1240E+00	0.9727E-01	0.4864E-01
0.1180E+05	0.2462E+00	0.4791E-01	0.1231E+00	0.9582E-01	0.4746E-01
0.1190E+05	0.2444E+00	0.4720E-01	0.1222E+00	0.9439E-01	0.4630E-01

H/T (KOE/K)	LINE(2)	LINE(3)	LINE(4)	LINE(5)	LINE(6)
0.1200E+05	0.2426E+00	0.4650E-01	0.1213E+00	0.9299E-01	0.4517E-01
0.1210E+05	0.2409E+00	0.4581E-01	0.1204E+00	0.9161E-01	0.4408E-01
0.1220E+05	0.2391E+00	0.4513E-01	0.1196E+00	0.9026E-01	0.4301E-01
0.1230E+05	0.2374E+00	0.4446E-01	0.1187E+00	0.8892E-01	0.4196E-01
0.1240E+05	0.2357E+00	0.4381E-01	0.1178E+00	0.8761E-01	0.4095E-01
0.1250E+05	0.2340E+00	0.4316E-01	0.1170E+00	0.8632E-01	0.3996E-01
0.1260E+05	0.2323E+00	0.4252E-01	0.1161E+00	0.8505E-01	0.3899E-01
0.1270E+05	0.2306E+00	0.4190E-01	0.1153E+00	0.8380E-01	0.3805E-01
0.1280E+05	0.2290E+00	0.4128E-01	0.1145E+00	0.8257E-01	0.3713E-01
0.1290E+05	0.2273E+00	0.4068E-01	0.1137E+00	0.8136E-01	0.3624E-01

CHAPTER IV

THE MAGNETIC HYPERFINE FIELD AT Co^{57} IN ANTIFERROMAGNETIC CoO

The mono-oxides of transition group ions are known to be antiferromagnetic substances. This CoO is specially interesting since its Co ions have large residual orbital moments. The Mössbauer measurements on Co^{57} doped CoO has been done at various temperatures down to 0.08 K, using a He^3-He^4 dilution refrigerator and the magnetic hyperfine field at Co^{57} in CoO has been estimated.

$ 4.1 Introduction

In the preceding chapter, it was stated that, from the Mössbauer emission spectrum on Fe^{57} at very low temperatures, the hyperfine field at Co^{57} of the parent nucleus embeded in a substance can be known. This new method to estimate the hyperfine fields is especially useful in anyiferromagnetic substance, because the application of NMR is techniqually difficult.

In this chapter, the Mössbauer measurements on Co^{57} embeded in an antiferromagnetic material, CoO, down to 0.08 K which was obtained with a He^3-He^4 dilution refrigerator are described and the estimation of the hyperfine field at Co^{57} is attempted.

The magnetic scattering from CoO has been studied by Shull et al. [65] who established the presence of the antiferromagnetic transition. CoO has a NaCl structure above the Néel temperature and lattice undergoes a large tetragonal contraction. The antiferromagnetic structure is skeched in figure 4.1, but the precise direction of the magnetic spin is not fixed and still in controversy.[66] Although CoO seems to be one of the simplest materials, many interesting and unresolved problem exist in its magnetic

properties and gathered the attentions of many scientists in the fields of neutron diffraction and also Mössbauer spectroscopy. For a futher study on CoO, microscopic information by NMR experiment will be very important. The estimation of the hyperfine field done in the present work will be helpful to find the NMR signals. Although the search for NMR signal has not yet been successful, a theoretical prediction was carried out by Motizuki about ten years ago.[67] The hyperfine field at 0 K was estimated to be +490 kOe.

The anormalous charge state observed in Mössbauer emission and absorber spectra have brought about a number of discussions.[68] CoO is the most extensively studied material from this point of view and many Mössbauer studies have published in the past ten years. Wertheim [69] has first measured the Mössbauer source spectrum of Fe^{57} in CoO and found a condiderable amount of Fe^{3+} coexisting with Fe^{2+} Wertheim suggest that the observed $Fe^{3+}$is a metastable state resulting from the Auger after effect.[70] Because the content of Co^{3+} in CoO is very small, the observed Fe^{3+} ions are supposed to be produced very rapidly after the nuclear transition from Co^{57} to Fe^{57}. However, it was also found that the relative amount of Fe^{3+} drastically

depends on the method of sample preparation and the measuring temperature.[71,72] On the other hand, a delayed coincidence measurement was applied by Trifthauser and Craig,[73] but the observed ratio of Fe^{3+}/Fe^{2+} showed no time dependence within the availavle time intervals. This result has been regarded as a negative evidence for the interpretation with Auger effect. At the present stage, however, no explanation is completely satisfactory for those experimental facts on CoO.

$ 4.2 Crystalogrophic and Magnetic Structure of Antiferromagnetic CoO

$ 4.2.a Crystalographic structure

CoO is an antiferromagnetic substance with its Neel temperature (T_N) at about 290 K. The precise value of the Néel temperature obtained from different experiment[52-60] varies slightly. Table 4.1 compares the Neel temperature of CoO obtained different methods.

Below the Néel temperature, the lattice undergoes a large tetragonal contraction along the cube-edge. Nagamiya et al.[61] reported that the tetragonal contraction is 1.2×10^{-2} and additional rhombohedral elongation occurs with $e_{xy}=e_{yz}=e_{zx}$ of magnitude 5×10^{-4}.

Saito et al. reported that CoO has two types of magnetic domains, named t-domain and r-domain, in the antiferromagnetic state by a X-ray diffraction.[62] The t-domain is in connection with tetragonal deformation and r-domain in connection with rhombohedral deformation. CoO has the lattice parameter of 4.24 A at 300 K.

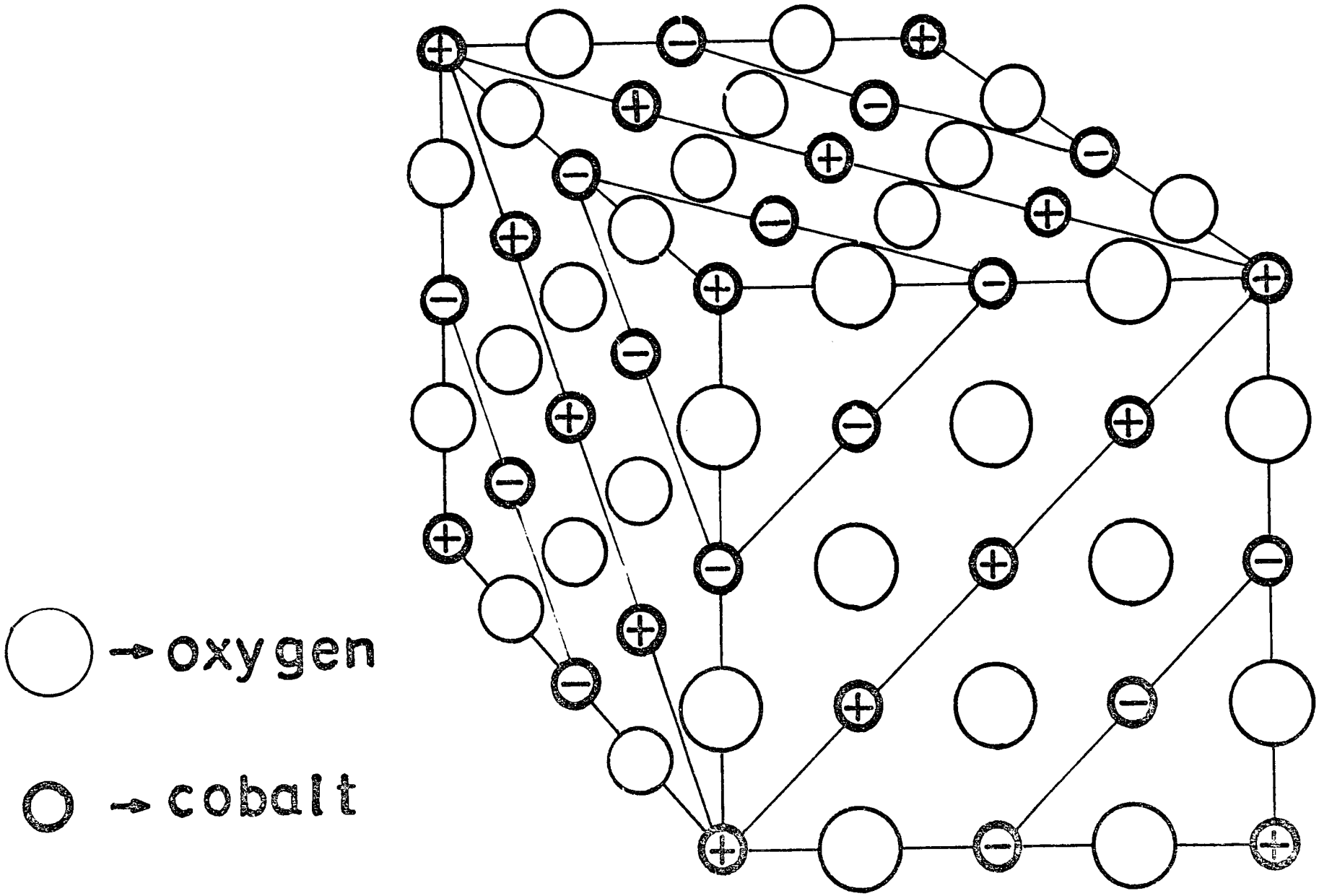

Figure 4.1 Antiferromagnetic structure of CoO

Table.4.1 Comparison of the Néel temperature of CoO obtained by different methods

Author	Method	Transition temperature (K)	Ref.
La Blanchatais	Succeptibility	292.2	(53)
Foex	Dilation	292.2	(54)
Street and Lewis	Young's modulus	289.2	(55)
Fine	Young's modulus	271.0	(56)
Trombe	Succeptibility	292.0	(57)
Greenwald	X-rays	278-284	(58)
Bizette and Assayag	Specific heat	289.7	(59)
Khan and Erickson	Neutron	295.±1	(60)

$ 4.2.b Magnetic structure

Jasnom and Wortis[63] have hypothesized that the behavior of a magnetic system near its critical point has one-to-one correspondence to the system. If so, CoO should become like an Ising antiferromagnetic near T_N. Salamon[64] by specific heat measurement and Rechtin and Aberbach[96] by the neutron intensity study reported that CoO shows the behavior of the 3-dimentional Ising like antiferromagnet, which has the critical indecies of $\alpha'=0.05\pm0,02$ $\alpha=0.29\pm 0.25$ and $\beta=0.29\pm0,25$ ($\alpha'=0.05$, $\alpha=0,12$, and $\beta=0,315$ by the prediction of the 3-dimentional Ising model.

The spin arrangement firstly determined by a neutron diffraction study by Shull, Strauser and Wollen in 1951.[65] Figure 4.1 shows the spin structure of CoO which believed by many investigators, such that the spin are parallel on each (111) planes but antiparalle to those on neighbering (111) planes. However, the spin assingment in CoO in the antiferromagnetic state has been in a controversal stage. Li proposed two models, model A and Model B, based on the assumption of a single magnetic axis in figure 4.2. From powder diffraction data, Shull et al.[65] as well as Roth[76] accepted model A. Roth assigned the spin direction paralle to [117], which makes an angle $11^{o}30'$ with respect

Table 4.2 Spin Arrangement in CoO

investigators	model	angle
Nagamiya, motizuki[77]	collinear	10°
Shull et al.[65]	Li-A	
Roth[78]	..	11°30'
Uchida et al.[81]	..	11°30'
Saito et al[82]	..	10°
Ok , Mullen[72]	..	10°
Rechtin Averbach[84]	..	7°50'
Y.Y.Li[85]	Li-A and B	
van Laar[74]	Li-A	27°4'
Greiner et al.[80]	..	27°4'
van Laar[74]	multispin	
Roth[78]	multispin	

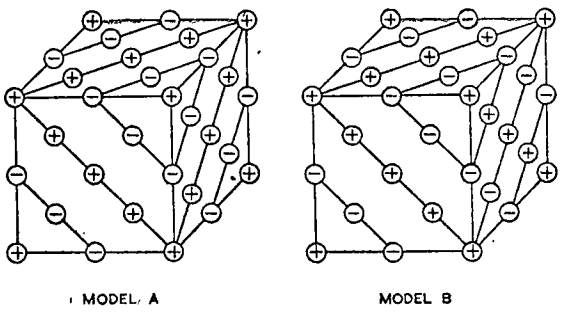

FIG. 1. Li's models A and B. Circles with + sign represent Co^{++} ion with spin-up. Circles with − sign represent that with spin-down.

Figure 4.2 Schematic of spin structure models in CoO

to [001]. Nagamiya and Motuzuki[77] theoretically arrived at a similar result (angle of deviation 10^{o}). Roth, later introduced a number of multispin axis structures(I,K, R,T,U) with tetragonal symmetry in keeping with the tetragonal distortion.[78] Later on, van Laar et al.[79] repeated Roth's experiment with a high-resolution diffractmeter and rejected the Roth s multi-spin. He could explain these data with a collinear model A with an angle of deviation 27.4^{o} (α=-0.325,β=-0.325,γ=+0.888) or equally well with a multispin axis structure described in Table 1 in ref 85. On the other hand. Uchida et al.[80] interpreted their recent magnetic anisotropy measurements in terms of Roth's single axis model A with spin along [117] (11.30^{o}). Greiner, Berkowitz and Weinborner studied the torque courves of single crystal CoO. They ruled out the multispin model by van Laar and decide in favor of the collinear model with the spin making an angle of 27.4^{o}. Again, Saito et al. found that their low temperature X-ray diffraction data could best be explained by Roth s collinear model(10^{o}).[81] Recently Ok and Mullen[82] concluded from the analysis of Mössbauer experiment that the spin arrangement agree with the van Laar model. Rechtin and Averbach[83] reported a collinear structure with the moments tipped out the [111] planes $7^{o}50'$ toward the c-axis.

For the determination of the spin arrangement, microscopic information by NMR experiment will be important. The search for NMR signal has not yet been succesful. In table 4,2 the results of spin arrangement obtained by meny investigators is summalized.

§ 4.3 Mössbauer investigations on CoO

In 1961, Wertheim[69] has first measured the Mössbauer source spectrum in CoO doped with Co^{57} and found a considerable amount of Fe^{3+} coexisting with Fe^{2+}. Because the content of Co^{3+} in CoO is very small, the observed Fe^{3+} ions are supposed to be produced very rapidly after the nuclear transition from Co^{57} to Fe^{57}. Wertheim suggested that the observed Fe^{3+} is a metastable state resulting from the Auger after effect[70].

A. Auger effect

If radioactive Co^{57} is embeded in a lattice which contains Co or Fe, the Co^{57} goes into Co or Fe substitutional position. By K or L electron capture the Co^{57} is transformed into Fe^{57} This can be in different states of ionization, due to Auger cascades, which is metastable states. Resonance absorption of 14.4 keV Fe^{57} gamma-ray detects usually one kind of ions which have the valency of the substituted ion. This means that the electroncapture time of highly ionized atoms is very short compared to the lifetime of Fe^{57} isomeric state. Pollk has reported the theoretical studies on the Auger cascade and Mössbauer effect in 1962. The experimental data concerning the electron capture of Co^{57} is the K/L

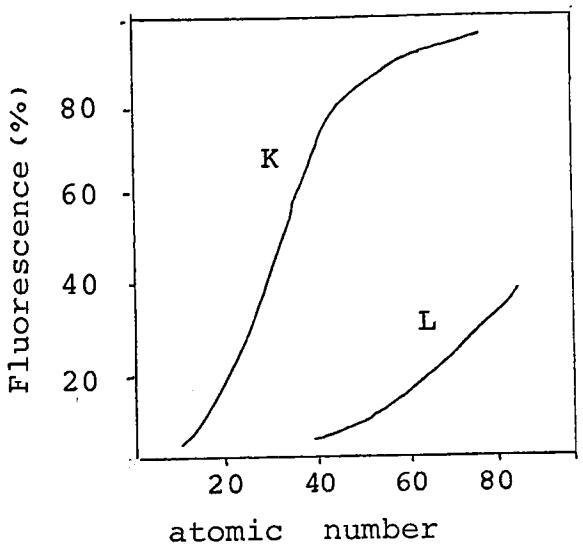

Figure 4.3.a K and L fluorescence

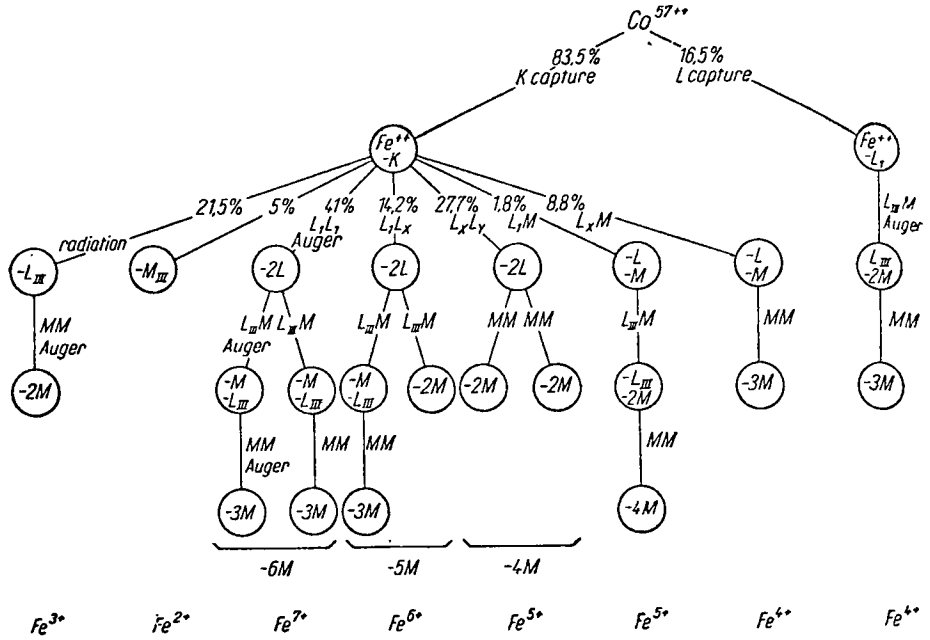

Figure 4.3.b The Auger cascade scheme of Co^{57}

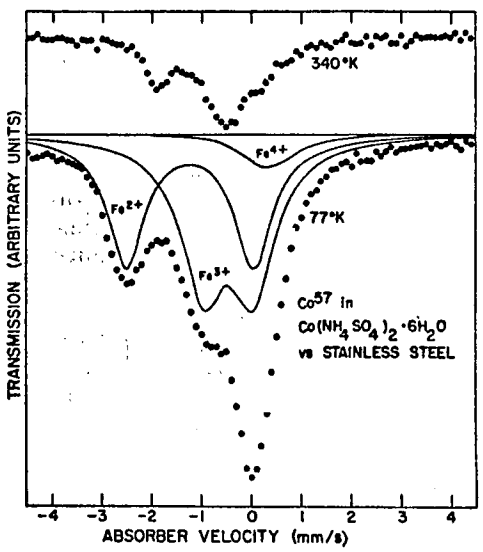

Figure 4.3.c The Mössbauer spectrum of Co^{57} in $Co(NH_4SO_4)_2 \cdot 6H_2O$ as an example of Auger after effect

capture ratio; 83.5% K-capture and 16.5% L-capture, and the K=fluorescence yields

$$0.32 \pm 0.05 = \frac{R_K}{R_K + A_K} , \qquad (5.1)$$

where R_K is a radioactive transition probability and A_K is total Auger transition probability. Figure 4.3.a shows the K-fluorescence (L) vs atomic number. Pollak built up the Auger cascade scheme of Co^{57} , figure 4.3.b shows the scheme and figure 4.3.c is the Mössbauer spectrum of Co^{57} in $Co(NH_4SO_4)_2.6H_2O$ as typical example of Auger after effect.[74)]

At time t=0 one has the following situation; Fe^{++}=5% and Fe^{+++}=95% from this theory. After the decay, Wertheim detected by Mössbauer effect two states of ionization for the ion; Fe^{++}= 53% and Fe^{+++}=47% at the time $t=10^{-7}$sec. Herefrom, Pollak deduced the time of atomic electron capture by Fe^{+++}in CoO to be $(1.4\pm0.2)\times10^{-7}$sec.

Later on, it was also found that the relative amount of Fe^{+++} drastically depends of the method of sample prepalation and measuring temperature [71)]. The amount of Fe^{+++} definitly increase with crystal imperfections. In 1966 Trifthauser and Craig succeeded to develope the delayed-coincident Mössbauer technique which permits measurements

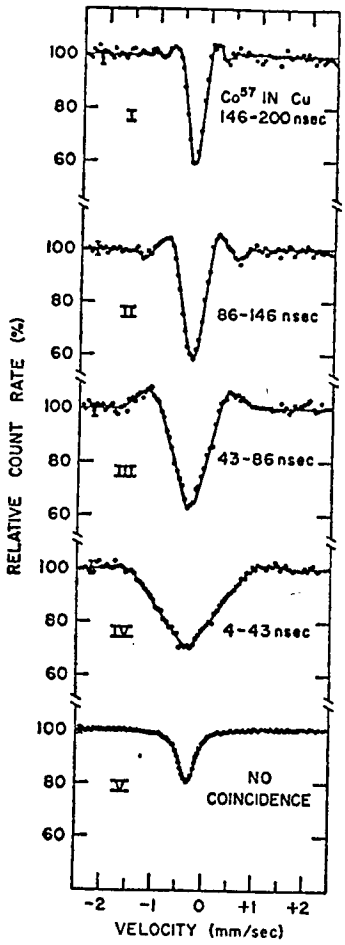

FIG. 2. Delayed coincidence Mössbauer studies using a source of Co^{57} in Cu and an absorber of potassium ferrocyanide. The "time filtering" effects displayed with this unsplit source were used to permit resolving more complex spectra in systems displaying multiple charge states. Note the "negative absorption" which is particularly strong in curves II and III. The last curve (taken without coincidence) is shown for comparison.

(A)

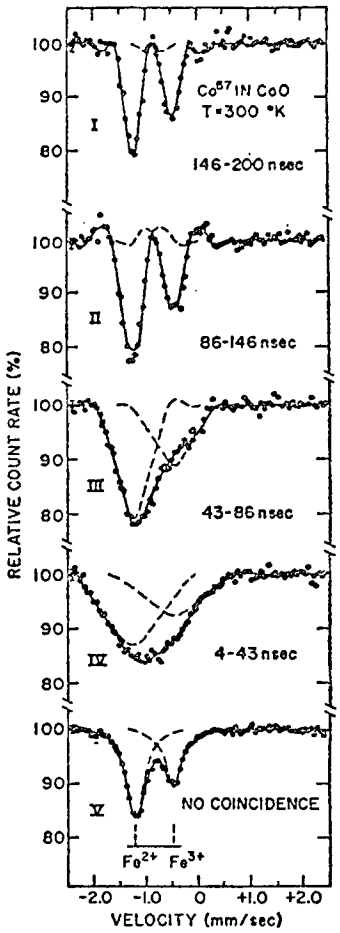

FIG. 3. Delayed coincidence ME spectra for Co^{57} in CoO at 300°K. No evidence for metastable charge states is found. In all measurements, an unsplit absorber of potassium ferrocyanide was used.

(B)

Figure 4.4 Delayed coincidence Mössbauer spectra.

(A) is the spectra for Co^{57} in Cu metal.

(B) is the spectra for Co^{57} in CoO. No evidence for metastable states is found.

of the time evolution of the Mössbauer resonance following the resonant nuclear level. Such delayed coincident measurement was applied on Co^{57} of CoO, but the observed ratio of Fe^{+++}/Fe^{++} showed no time dependence within the available time interavals; 10^{-8}-10^{-9} sec. Figure 4.4(B) shows the delayed-coincident Mössbauer spectra for Co^{57} in CoO at 300 K. This result has been regarded as a negative evidence for the interpretation with Auger effect.

At the present stage, however, no explanation is completely satisfactory for those experimental facts in CoO. For the possible mechanisms of Fe^{+++} formation in CoO, four reasons are to be considered(see Table 4.3).

Table 4.3 The possible mechanism of Fe^{+++} formation
(1) Due to the after effect of the nuclear decay, metastable Fe^{+++} or more higher charged states produced. The Fe^{+++} state observed in CoO is such a long-lived metastable state(10^{-7}sec). Ref. 69,92
(2) There are two crystallographic forms for CoO; CoO(I) has a complete NaCl structure and CoO(II) has a NaCl structure with half of its positive ion sites and half of its negative sites vacant. Only the Fe^{+++}state can be observed in the spectrum for CoO(II) and usually obtained samples are the mixtures of this two forms. Ref. 86,83
(3) In the vicinity of defects, the cations will have a finite probability to be in +3 charge state.

Since the ionization potential is much smaller for Fe^{++} than Co^{++}, pairs of Fe^{+++} ion and vacacy should be stabilized relative to paires containing Co^{+++}. Blomquist et al. have suggested a large mobility of vacancies in order to account for the experimental results that the Fe^{+++}/Fe^{++} ratio is very large even if the vacancy concentration is rather low.

Ref. 87, 73

(4) The semiconducting properties of CoO is important. The ratio of Fe^{+++}/Fe^{++} observed in Mössbauer pattern is a function of the p-type dopant and n-type dopant density.

Ref. 88

$ 4.4 Experimental

Two samples of CoO including Co^{57} were prepared. Small platinum plate were used as sample holders. Cobaltous chlaride was thinly spread on the plate and the carrier-free Co^{57} solution was dropped. Sample-I was heated for 24 hours at 1000° C in the atmosphere of CO_2 and Sample-II was heated in air for 24 hours at 1200° C. The samples were rapidly cooled after the heat treatments. The source strength at room temperature was 0.3 mCi. The Mössbauer source spectra at room temperature and liquid He^4 temperature were in good agreement with the formerly reported ones (e.g. figure 11 in ref 83). The characteristics of the spectra could confirm the samples were single phase CoO.

All mearsurements were made with moving a standard absorber, which was unenriched stainless steel foil, whose thickness was enough to obtain an ideal powder pattern. The analysis of the spectra was made with a computer, Facom 270/30, at the Data Processing Center, Kyoto University, with the combination of the graphic display or digital X-Y plotter. The least square method was applied for fitting the theoretical curve with the observed spectrum.

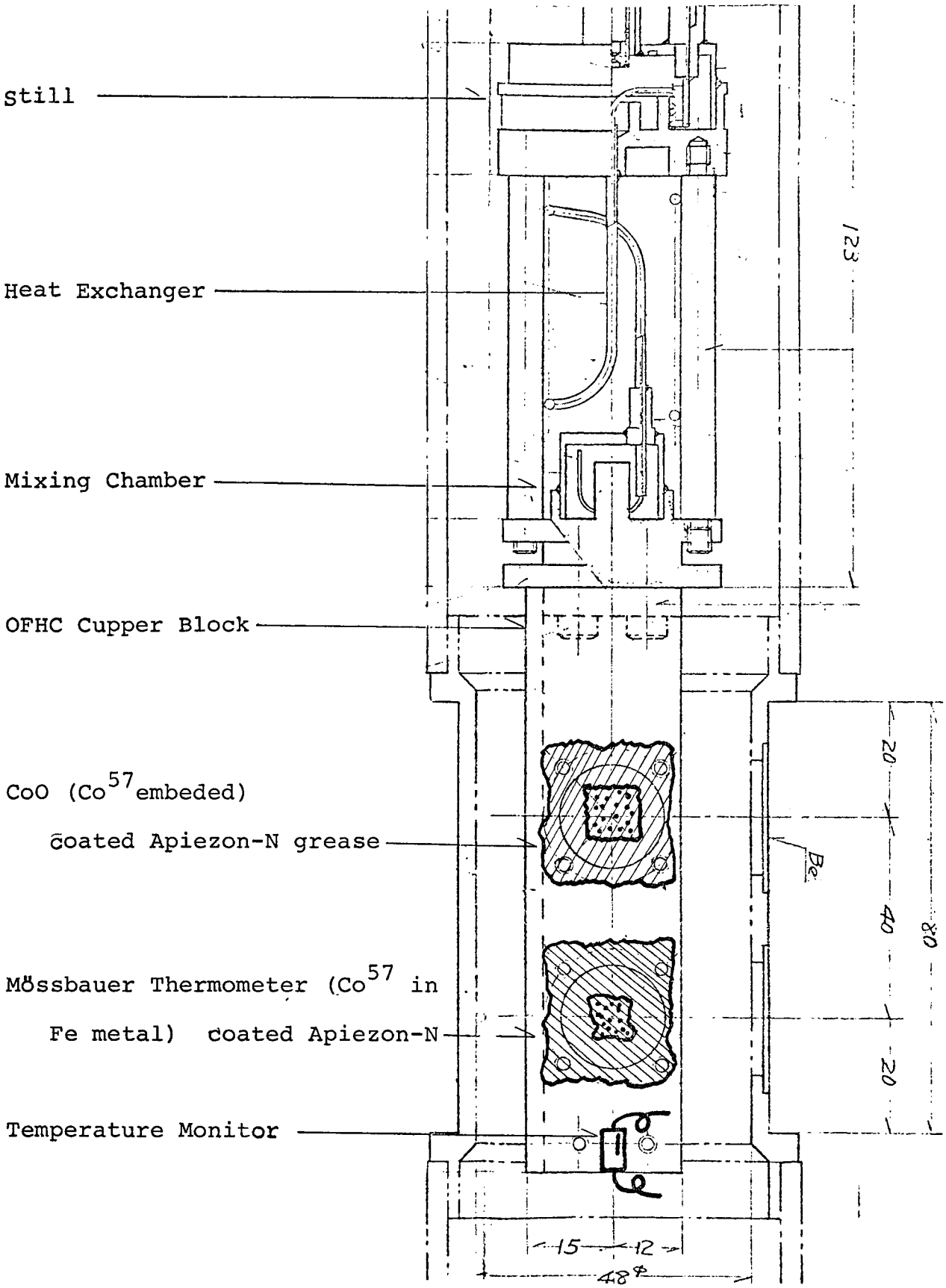

Figure 4.5 Schematic of the sample attachment

The He^3-He^4 dilution refrigerator was described in Chapter II.[93] The sample was attached to the copper block by Apiezon-N grease to ensure the thermal conduction.

Carbon resistres, Speer 100 Ω 1/2 w, were used for the temperature monitors at the still, the mixing chamber and the sample place. The time length for each measurement was about 10 hours and the temperature fluctuation was less than 0.01 K. The absolute temperature was determined by the Mössbauer thermometery. A standard source, Co^{57} in a thin Fe foil was attached to the same block, whose activity was about 2 mCi. The mössbauer spectra of the standard source at the lowest temperature of 0.08 K and at room temperature are sown in figure 3.2. The asymmetry caused by the nuclear polarization of Co^{57} nuclei is obviously seen in the spectrum at 0.08 K. The absolute temperature was determined from the intensity ratio of the outermost peaks.

The self heating effect for the radioactive sources seems to be unimportant above 0.05 K (see p.240 in Ref. 6), as far as the activity is not very high.

§ 4 5 Experimental Re lts

The Mössbauer source [illegible] various temperatures are sc[illegible] figure 4.6. A[illegible] each temperature, the coex[illegible]e of the two k[illegible] state, Fe^{2+} [illegible] was ob[illegible]. The re[illegible] Sample-I was very similar to [illegible]r Sample-[illegible]ept that the relative content of Fe[illegible] Sample-II was a little less than that in Sample-I. [illegible]he spectra above 4.2 K were almost identical to thos[illegible]tained by Ok and Mull[illegible] and their line assignment se[illegible] to be reliable.

Although the position [illegible]ach line was no more varied below 1.17 K, the relative intensities of the lines showed a remarkable temperature variation. This change was resulted from the polarization of the parent nucleus, Co^{57} The degree of the polarization can be calculated from the intensity difference of the two outermost peaks.

In order to estimate the intensity ratio, Fe^{2+} and Fe^{3+} spectrs must be separated. Because the three of the six lines for Fe^{3+} state are seen as independent peaks, the position and intensities of the other three, superposing with the Fe^{2+} spectrum, can be unambiguously determined.

The thre[illegible]eaks also a[illegible]ffe[illegible]nuclear polariz[illegible]on and the effects are ta[illegible]tion. In figure 4.1[illegible], the re[illegible] amo[illegible] of Fe^{3+}/Fe^{2+} for the case of Sample-II ar[illegible]hown as a [illegible]tion of temperature.

Figure 4.6 The Mössbauer spectra of Fe^{57} in antiferromagnetic CoO (Sample-II) at various temperatures.

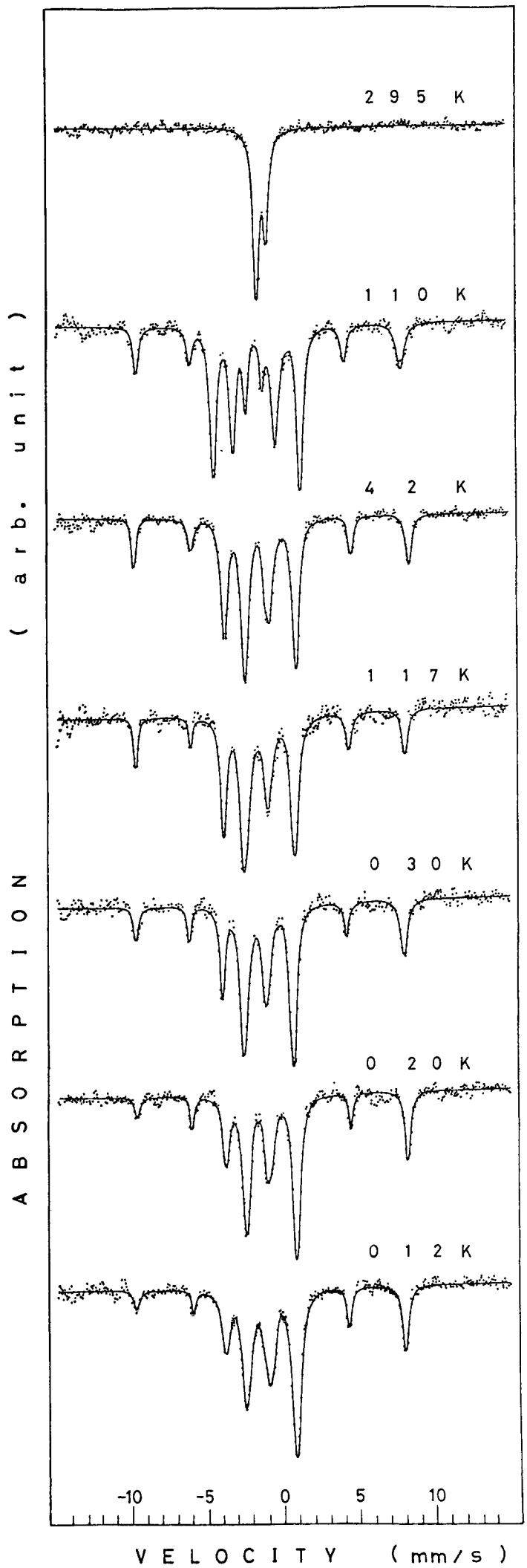
295 K
110 K
42 K
117 K
030 K
020 K
012 K
ABSORPTION (arb. unit)
-10
-5
0
5
10
VELOCITY (mm/s)

$ 4.6 Analysis and Discussion

$ 4.6.a The Fe^{2+} spectrum

In order to obtaine the intensity ratio of lines for Fe^{2+} state only, the subtraction of the six lines for Fe^{3+} state from the observed Mössbauer spectrum was made. Figure 4.7 shows such spectra for Fe^{2+} state only.

In the case of Fe^{2+} state, a quadrupole interaction is comparable with a magnetic hyperfine interaction and as result, eight kinds of Mössbauer transition are possible. Below 4.2 K, the observed Mössbauer spectrum for Fe^{2+} state consisted from four lines since the two middle lines were respectively composed of three transitions. Fortunately, each of the two outer peaks correspondings to one kind of transition and the nuclear polarization of parent Co^{57} nuclei can be caluculated the intensity ratio of the outer lines. In figure 4.8, the relative intensity ratio of temperature.

Figure 4.7 The Mössbauer spectra for Fe^{2+} state in antiferromagnetic CoO at various temperatures.

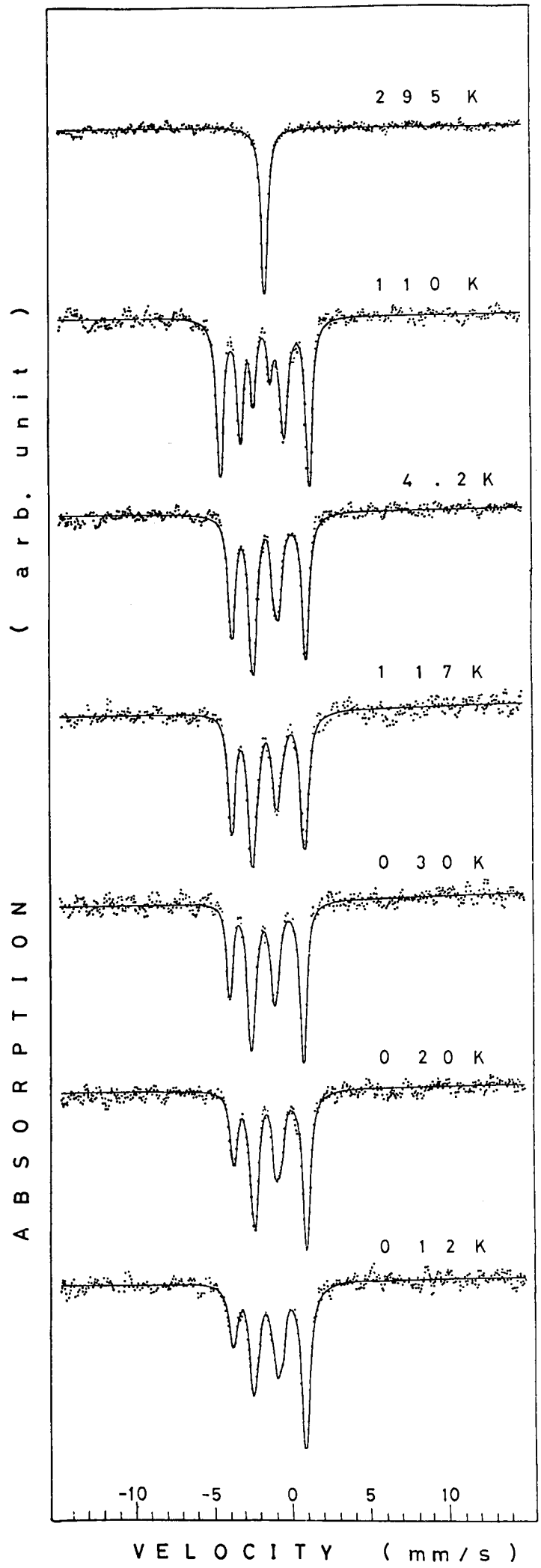
2 9 5 K
1 1 0 K
4 . 2 K
1 1 7 K
0 3 0 K
0 2 0 K
0 1 2 K
(a r b. u n i t)
A B S O R P T I O N
-10
-5
0
5
10
V E L O C I T Y (m m / s)

Figure 4.8 Intensity ratio of the outer peaks of the Mössbauer spectra for Fe^{2+} state in antiferromagnetic CoO as a function of temperature.

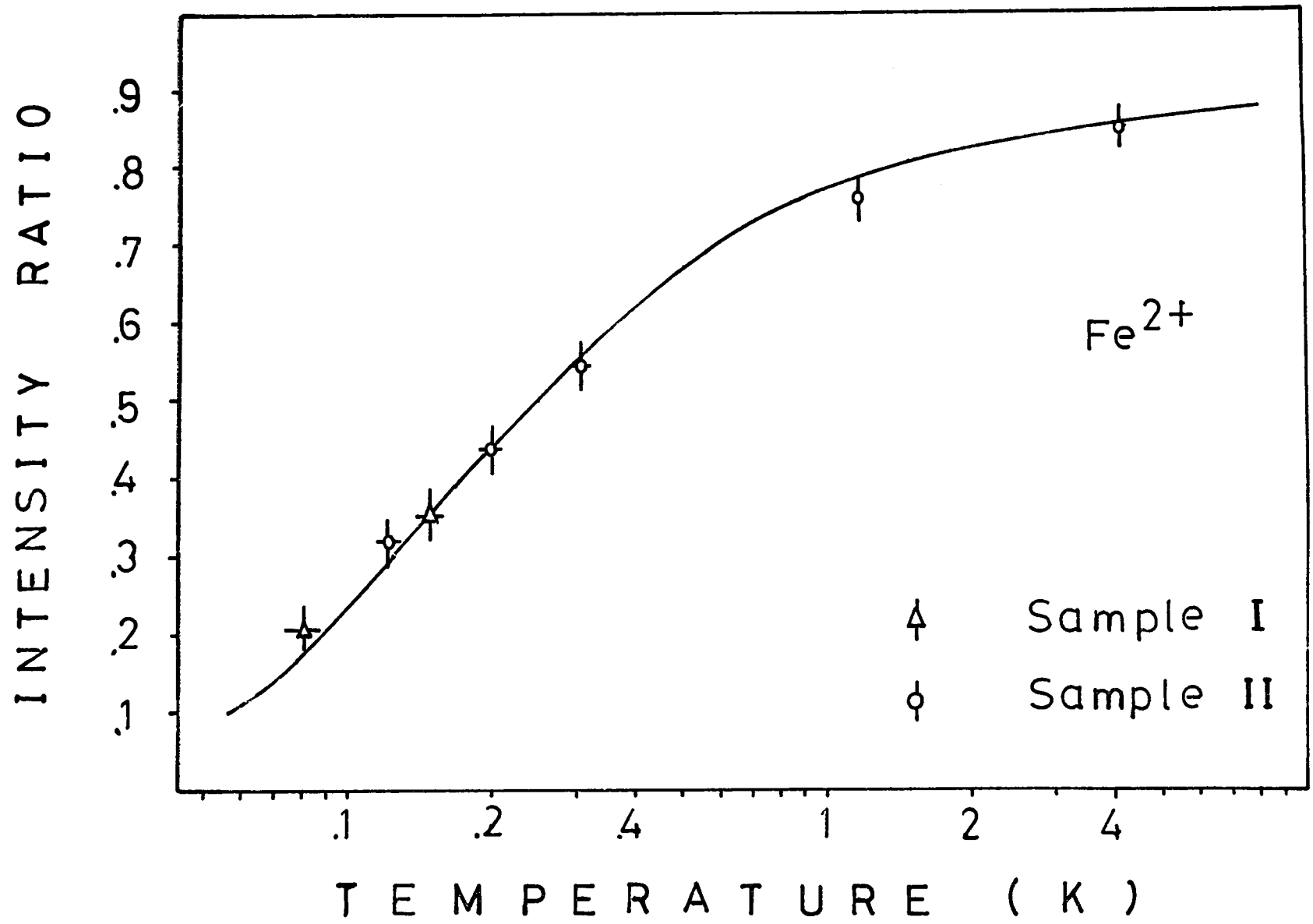
INTENSITY RATIO
.9
.8
.7
.6
.5
.4
.3
.2
.1
.1
.2
.4
1
2
4
TEMPERATURE (K)
Fe2+
Sample I
Sample II

The theoretical principles for the calculation are described in section 3.4. Since a quadrupole interaction is comparable to the magnetic interaction, the mixing effect of the wave functions of Fe^{57} nucleus must be taken into consideration. The wave functions of Fe^{57} nucleus obtained by Ok and Mullen[83] were used for this calculation. Namely, the quadrupole interaction and the magnetic interaction for Fe^{57} nucleus in CoO are

$$H = 150 \text{ kOe}, \tag{5.1}$$

$$eqQ/2 = -1.01 \text{ mm/sec}, \tag{5.2}$$

$$\Theta = 39.5^{\circ} \tag{5.3}$$

$$P \equiv eqQ/6g_e\mu_N H = -0,33 \tag{5.4}$$

where H is the hyperfine field at Fe^{57} nucleus, eqQ/2 is the quadrupole interaction and Θ is the angle between the direction of H and the principle axis of EFG tensor.[83] The wave functions of Fe^{57} first excited state can be calculated with these values of the hyperfine parameters for Fe^{57} nucleus. And the hyperfine field at Co^{57} nucleus was estimated with that wavw functions of Fe^{57} nucleus. Table 4.4 gives the observed

ratio of the two outer most peaks at various temperatures. The last column of the table shows the magnetic hyperfine field at Co^{57}nucleus caluculated at the respective temperature. The average valus of the hyperfine field is 590 kOe and the possible error ahould be smaller than 40 kOe. The solid curve in figure 4.8 shows the temperature dependence of the intensity ratio, when the hyperfine field iS 590 kOe.

It is to be noted that the asymmetry caused by the nyclear polarization is seen in the oppsite direction to the case of Co^{57} in Fe metal shown in figure 3.2. The hyperfine fields at Co and Fe nuclei in Fe metal are known to be negative and from the temperature dependence of the hyperfine field, the sign of the field at Fe^{57} in CoO was also determined to be negative. Therefore, the sign of that at Co^{57} is concluded to be positive. It is a merit of the present method that the sign of the hyperfine field can be estimated without applying an external field even for antiferromagnetic materials.

The hyperfine field at Co^{57} in antiferromagnetic CoO was thus determined to be $+590 \pm 40$ kOe, when is a little larger than the theoretically predicted value, +490 kOe by Motizuki[93]. If we consider the possible

error in the estimation of the intensity ratio and also consider the ambiguities in the calculation of the hyperfine field, such as the hyperfine constant and the ground state wave function, the agreement between the experimental and theoretical values seems to be fairly good.

Table 4.4 The magnetic hyperfine field at the site of Co^{57} nucleus in CoO (from the Mossbauer spectrum of the Fe^{2+} ion)

Temperature(mK)	Intensity ratio of outer lines	Hyperfine field(kOe)
Sample I		
80 ± 10	0.20 ± 0.03	545 ± 30
150 ± 10	0.35 ± 0.03	608 ± 30
Sample II		
120 ± 10	0.32 ± 0.03	556 ± 30
200 ± 10	0.44 ± 0.03	610 ± 30
300 ± 10	0.54 ± 0.03	630 ± 30
1.17 (K)	0.76 ± 0.03	
4.20 (K)	0.86 ± 0.03	
	weighted average	590 ± 40

$ 4.6.b Analysis and Discussion about Fe^{3+} spectrum

The spectrum for Fe^{3+} also shows a remarkable asymmetry due to the nuclear polarization. Figure 4.9 shows the Mössbauer spectra for Fe^{3+} state only at various temperatures. With the same treatment as the case of Fe^{2+} spectrum, the fyperfine field at Co^{57} could be deduced as $+603\pm80$ kOe. The intensity ratio of the outermost ines is plotted in figure 4.10, with the calculated curve in which the hyperfine field was assumed to be 603 kOe. Since the statistics of Fe^{3+} spectra were rather poor, the possible error was somewhat larger.

Figure 4.11 shows the ratio of Fe^{3+}/Fe^{2+} observed in the spectra. The relative intensity of the Fe^{3+} spectrum decreased remarkably with a decrease of temperature. This result is in accordance with the previous observation (e.g. Fig.11 in ref.83). Such a large temperature dependence cannot be explained with the difference of the Debye temperatures for the two ionic states. Therefore, the atomic ratio of Fe^{3+}/Fe^{2+} should vary with temperature. On the other hand, at low temperatures, between 4.2 K and 0.1 K, the ratio was practically constant and about 21% of the total iron remained as the Fe^{3+} state.

Figure 4.9; Mössbauer spectra for Fe^{3+} state in antiferromagnetic CoO (Sample-II) at various temperatures.

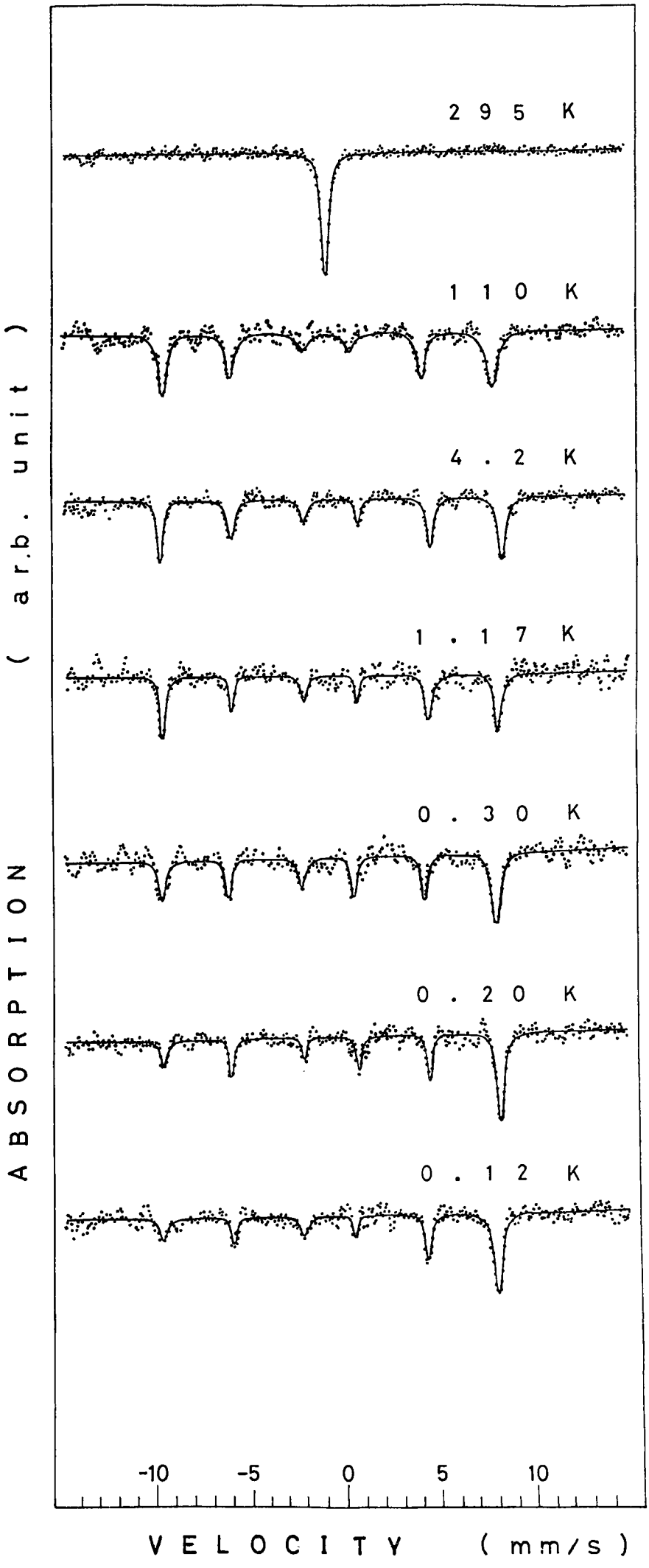
2 9 5 K
1 1 0 K
4 . 2 K
1 . 1 7 K
0 . 3 0 K
0 . 2 0 K
0 . 1 2 K
ABSORPTION (ar.b. unit)
-10
-5
0
5
10
VELOCITY (mm/s)

Figure 4.10. Intensity ratio of the outermost lines of the Mössbauer spectra for Fe^{3+} state in antiferromagnetic CoO as a function of temperature.

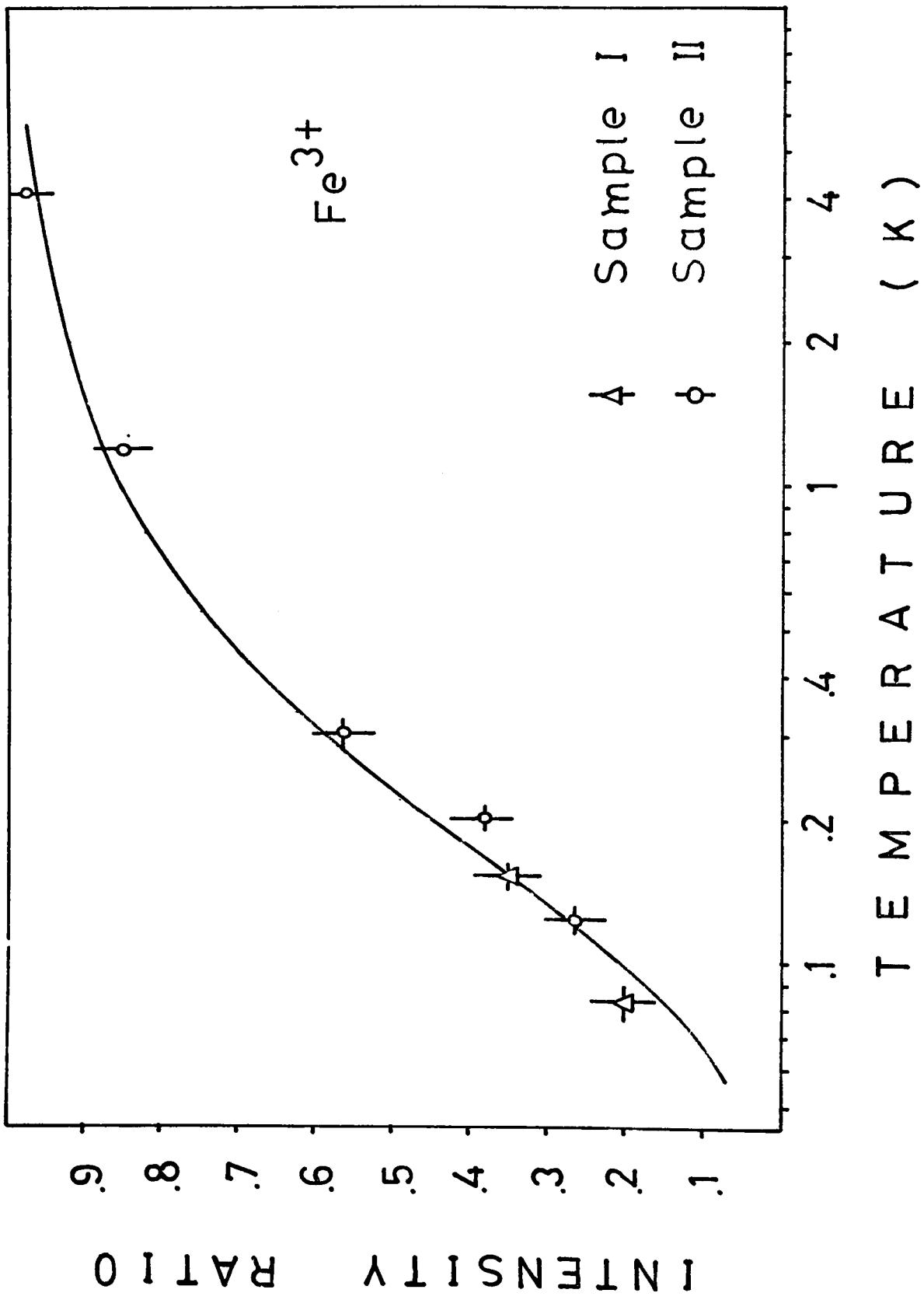
INTENSITY RATIO
9.
8.
7.
6.
5.
4.
3.
2.
1.
TEMPERATURE (K)
.1
.2
.4
1
2
4
Fe3+
Sample I
Sample II

Table The magnetic hyperfine field at the site of Co^{57} nucleus in CoO (from the Mossbauer spectrum of the Fe^{3+} ion)

Temperature(mK)	Intensity ratio of outermost lines	Hyperfine field(kOe)
Sample I		
80 ± 10	0.20 ± 0.05	530 ± 60
150 ± 10	0.35 ± 0.05	605 ± 60
Sample II		
120 ± 10	0.26 ± 0.05	610 ± 60
200 ± 10	0.38 ± 0.05	640 ± 60
300 ± 10	0.56 ± 0.05	630 ± 60
1.17 (K)	0.85 ± 0.05	
4.20 (K)	0.98 ± 0.05	
	weighted average	603 + 80

Figure 4.11 Atomic ratio of Fe^{3+}/Fe^{2+} versus temperature

RATIO (Fe3+ / Fe2+)
0
.1
.2
.3
.4
.5
.6
.7
TEMPERATURE (K)
1
10
100

For Sample-I, the amount of Fe^{3+} below 4.2 K was about 31%.

Concerning the state of Fe^{3+} state produced from Co^{57} atoms in CoO, we have obtained the following two experimental results.

(1) The hyperfine field at the parent nucleus estimated from the Fe^{3+} spectrum is nearly as the same as that from the Fe^{2+} spectrum. In other words, all the cobalt ions are crystallographically equivalent.

(2) The atomic ratio of Fe^{3+}/Fe^{2+} has no temperature dependence between 4.2 K and 0.1 K.

According to the result (1), it is very doubtful to assume that the cobalt ion to be transformed into Fe^{3+} is crystallographically different from that into Fe^{2+}. Ok and Mullen[89] had assumed that CoO has two crystal phases. According to their speculation, the parent cobalt ion of Fe^{3+} has definitely a different surrounding. In contrast to the parant ion of Fe^{2+} having six oxygens as the nearest neighbors, that of Fe^{3+} has only three oxygens. If it

is the case, the hyperfine field at the parent cobalt ion of Fe^{3+} should not be the same as that of Fe^{2+}.

At the higher temperature range, the temperature dependence of the Fe^{3+}/Fe^{2+} ratio seems to correspond to the thermal equilibrium at each temperature. Since the mobility of vacancy should be very small at low temperature, below 4.2 K, Fe^{3+} ions cannot be stabilized except in the vicinity of a defect. The concentration of cobalt ions in a surface layer or neighboring a crystal defect(possibly much less than 0.1%) is surely too small to explain the observed number of Fe^{3+} ions.

At the low temperature, the mobility of electron should also very small. Therefore, the semiconducting property of CoO is not important below 4.2 K.

Therefore much of the Fe^{3+} ions observed below 4.2 K are thought to be a metastable state produced after the nuclear decay.

A complete interpretation is not yet possible but the present result are helpful to consider the mechanism of the formation of Fe^{3+} state.

CHAPTER V

NMR STUDY OF Co^{59} NUCLEUS IN ANTIFERROMAGNETIC CoO

With the help of the information on the hyperfine field at Co^{57} nucleus obtained by Mössbauer experiments at very low temperatures, the spectrum of Co^{59} NMR in CoO single crystal was observed in antiferromagnetic state. The observed absolute value of the hyperfine field at Co^{59} nucleus was found to be 495.5 ± 0.5 kOe at 4.2 K in zero external magnetic field, which was smaller than the value of 590 kOe estimated by the Mössbauer experiments at very low temperatures. This error on the estimation in Mössbauer studies is considered to be caused to an over estimation of the absolute temperatire of sample due to heating of the source thermometer itself, which, if the thermal contact is not complete, the hyperfine field at Co^{57} nucleus will be estimated to be larger than the real value. The detail analysis of Co^{59} NMR in CoO will be given in this section.

$ 5.1 Introduction to Co^{59} NMR

Nuclear magnetic resonance experiments, with particular use of the transient NMR technique, provide detailed information conserning the static and dynamic properties of the ordered spin system. Since each Co^{59} nuclear spin is coupled to the Co^{2+} electronic spin via intra-atomic hyperfine interaction, the Co^{59} NMR signals in CoO are expected to reflect the microscopic nature of the respective sublattices. The hyperfine interaction between the nucleus and electrons in ion can be written as

$$\mathcal{H} = \mathcal{H}_F + \mathcal{H}_l + \mathcal{H}_d + \mathcal{H}_Q , \tag{5.1}$$

where

$$\mathcal{H}_F = 2\beta g_N \beta_N \sum_k \frac{8}{3} \pi \delta(r_k)\ \bar{s}_k . \bar{I}, \tag{5.2}$$

$$\mathcal{H}_l = 2\beta g_N \beta_N \sum_k \frac{1}{r_k^3}\ \bar{l}_k . \bar{I}\ , \tag{5.3}$$

$$\mathcal{H}_d = 2\beta g_N \beta_N \sum_k \left[\frac{\bar{s}_k . \bar{I}}{r_k^3} + \frac{3(\bar{r}_k . \bar{s}_k)(\bar{r}_k . \bar{I})}{r_k^5}\right] \tag{5.4}$$

and

$$\mathcal{H}_Q = \frac{e^2 Q}{2I(2I-1)} \sum_k \left[\frac{I(I-1)}{r_k^3} - \frac{3(\bar{r}_k . \bar{I})}{r_k^5}\right] \tag{5.5}$$

Here l_k and s_k stand for the orbital and spin angular momentum of the k-th e;ectron, respectively, r_k the distance of the k-th

electron from the nucleus, β the Bohr magneton, β_N the nuclear magneton, g_N the nuclear gyromagnetic factor in units of e/2Mc, and $\bar{I}$ the nuclear spin angular momentum of magnitude I. The sum $\sum_k$ extends over all the electrons in the ion and outside the ion. The latter inter-atomic interaction is considerably smaller than the former intra-atomic interaction. The effective Hamiltonian for the nucleus is obtained by averaging the above Hamiltonian with respective to the electronic wave function of the ground state of the ion. The most simple way to do it is to use the effective hyperfine Hamiltonian in the ground term of the ion

The ground states of the 3d-transition metal ions in the weak-field coupling scheme are as follows;

1) the orbital singlet state ion

A_1; Mn^{2+}, Fe^{3+}, Cu^{+} ets,

A_2; C_r^{3+}, Mn^{4+}, Ni^{2+}(Oc); Co^{2+}(Td) etc,

2) the orbital doublet state ion

E ; Mn^{3+} (Oc) etc,

3) the orbital triplet ion

T_1; Cr^{4+}, V^{3+}, Co^{2+} (Oc) etc,

T_2; Fe^{2+} (Oc) etc.

Here Oc and Td indicate octahedral and tetrahedral sites. Most of NMR signals have been observed associated with the ions in the orbital siglet states A_1 and A_2 and orbital doublet E, and

the origins of the hyperfine fields in such cases are well understood by now,[96] while observation of signals associated with the ions in the orbital triplet T_1 and T_2 have been very rare.[97-101] So that it is very interesting to observe such as Co^{59} NMR in CoO where Co^{2+} ions located at octahedral site and clarify the origin of the hyperfine field and why it was difficult to observe the signals.

$ 5.2 Experimental Methods

The crystal of CoO used was a commercial single crystal grown by a flame fusion method by Nakazumi Crystal Co. The specimen with rectangular flat (001) surfaces was cleaved out of as-grown crystal and had about 8X7X15 mm in the size. The crystal axis was determined by using an X-ray photograph, which showed a Braff diffraction pattern characteristic of NaCl type structure. In order to get a single domain sample below T_N, the sample was cooled through the Néel temperature with a temperature gradient imposed along one of the cubic principal axes very slowly. There coexist two types of domain, t-domain and r-domain, in antiferromagnetic state which was first found by Saito, et al.[102] Since the r-domain remain after this stress-cooling, the NMR spectrum could not been obtained from a complete single domain sample.

The Co^{59} NMR in antiferromagnetic CoO was performed by a standard pulse technique. The single crystal was mounted in a re-entrant type coaxial cavity in Fig.5.1. A high power pulsed rf-oscillator (Nihon Koshuha Model PMN 1000) was used to produce a large transverse rf-field of about 100 Oe at the sample position. The integrated amplitude of the spin echo signals was stored in a boxcar integrator (PAR Model 160) and recorded as a function of the direction of the external

magnetic field. The precise frequency of echo signals was determined by looking beats between echo signals and the output of a standard signal generator whose frequency was read by a digital counter.

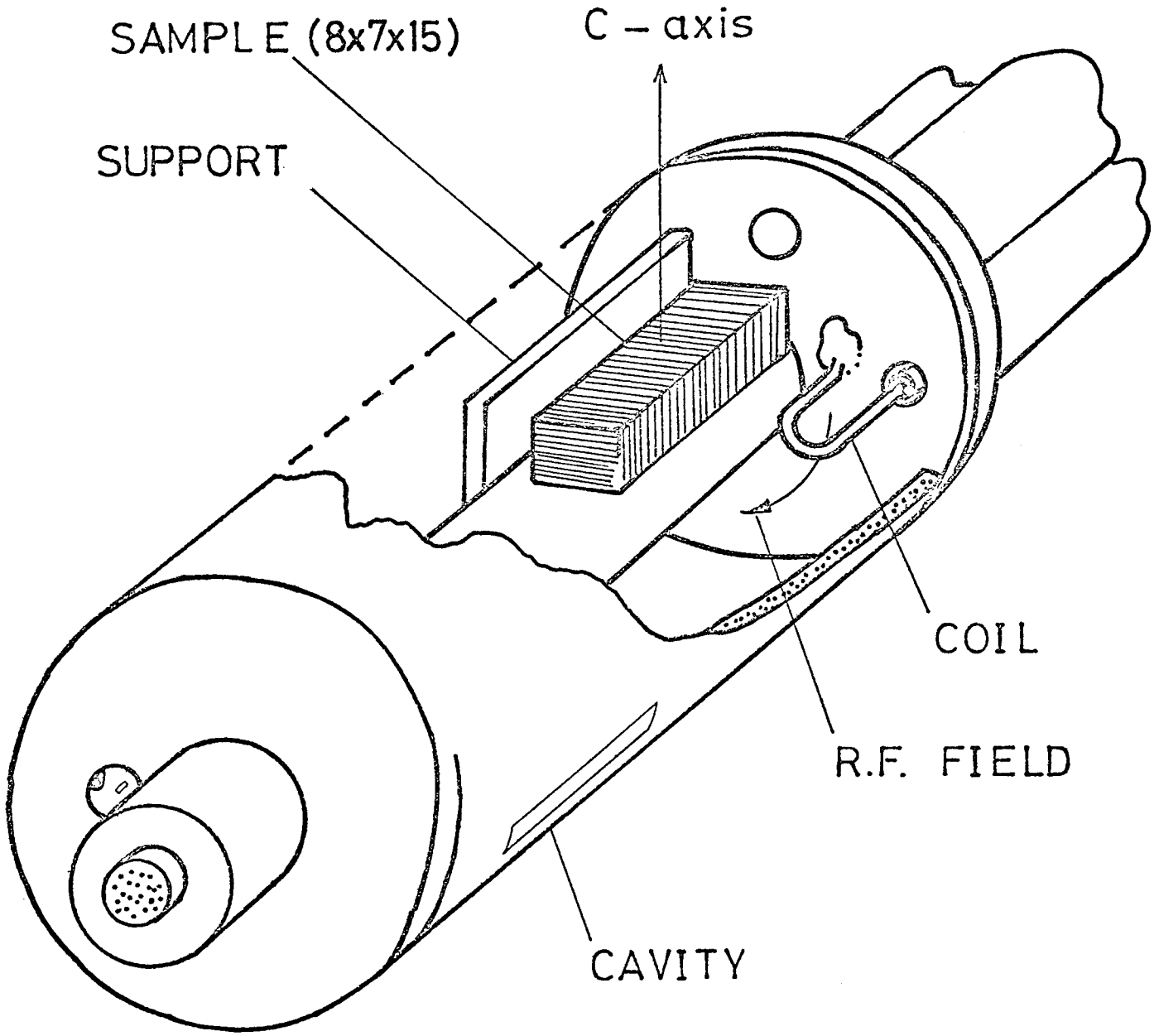
SAMPLE (8x7x15)
C – axis
SUPPORT
COIL
R.F. FIELD
CAVITY

$ 5.3 Experimental Results in Zero External Magnetic Field

A single line spectrum of Co^{59} NMR in CoO single crystal was observed at zero external magnetic field. The obtained spin echo intensities were normalized when at $\tau=0$, taking into account the variation of the echo decay constants associated with the measured frequency. Figure 5.2 shows such spectrum obtained 4.2 K and 77 K. The center resonance frequencies (and the corresponding hyperfine fields at Co^{59} nucleus) were 498.2±0.5 MHz (495.5±0.5 kOe) and 493.3±0.5 MHz (490.6±0.5 kOe) , respectively. The ratio of a square of 2-nd moment and a 4-th moment in connect with both observed spectrum was about 0.7, where the integral from 488 to 508 MHz, was made in this moment calculation. When the spectrum is of Lorentzian, the ratio becomes 2.6 and when of Gaussian, the ratio becomes 0.33. Therefore, the observed spectra of Co^{59} NMR in CoO are almost of Gaussian and both half width of each spectrum are estimated to be 2.5 MHz. On the other hand, the spin echo decay time had the temperature variation and its decay behavior was single expornential with time constants (T_2) of 21±5 μ sec at 77 K and 75±5 μ sec at 4.2 K, respectively, at each center frequency in Fig.5.3. Assuming the homogeneous line shape to be of Lorentian , those decay constants corresponding to half-line width of about 8 kOe and 2 kOe, respectively. Since these width is narrower

than the observed half width of about 2.5 MHz, the width of the obtained spectrum is considered to be caused by an inhomogeneous broadening with splitting due to the electric quadrupole interaction, although no such clear splitting were observed. The splitting is estimated to be less than about 0.8 MHz.

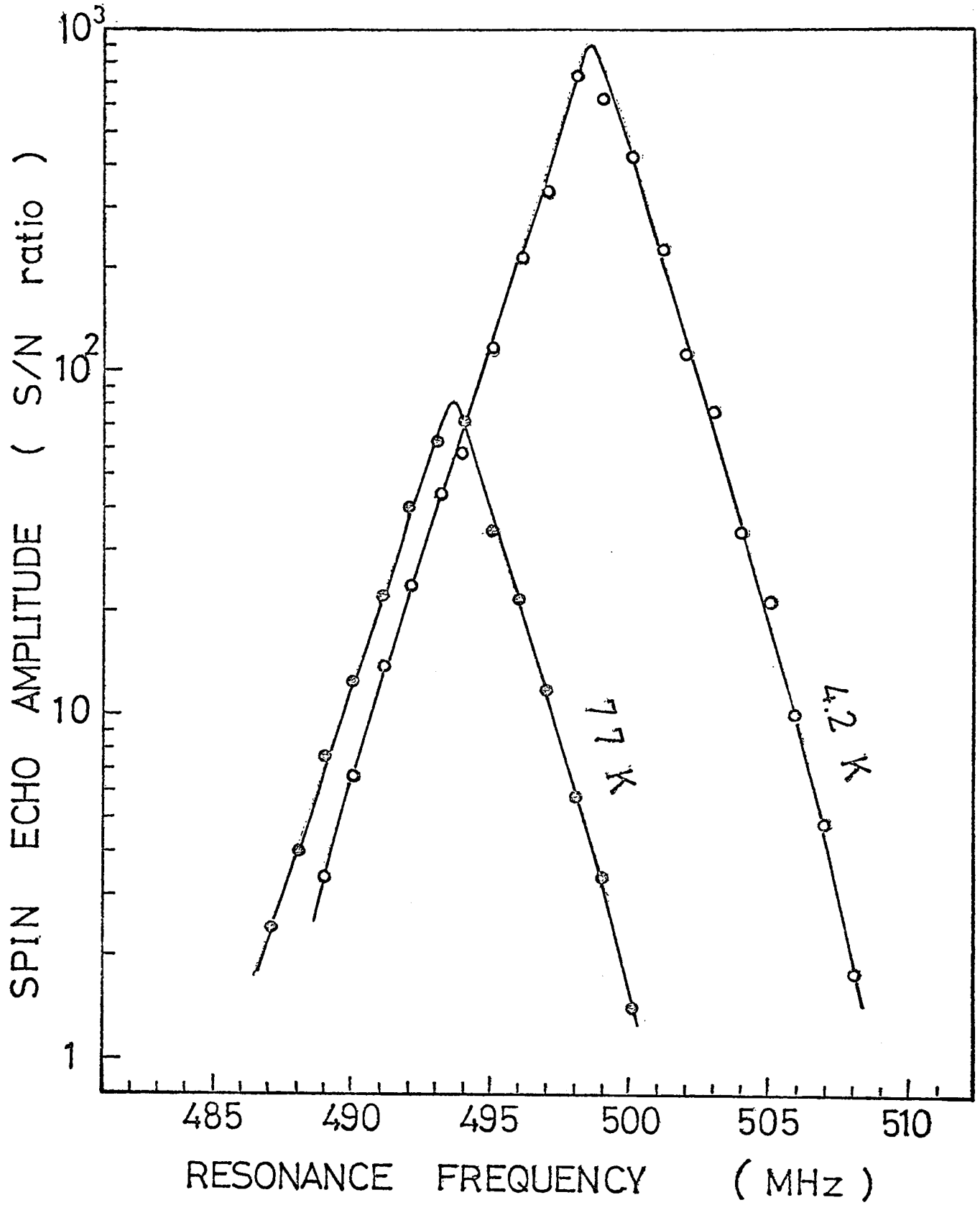
SPIN ECHO AMPLITUDE (S/N ratio)
10³
10²
10
1
485
490
495
500
505
510
RESONANCE FREQUENCY (MHz)
77 K
4.2 K

Fig 5.2

Fig 5 3

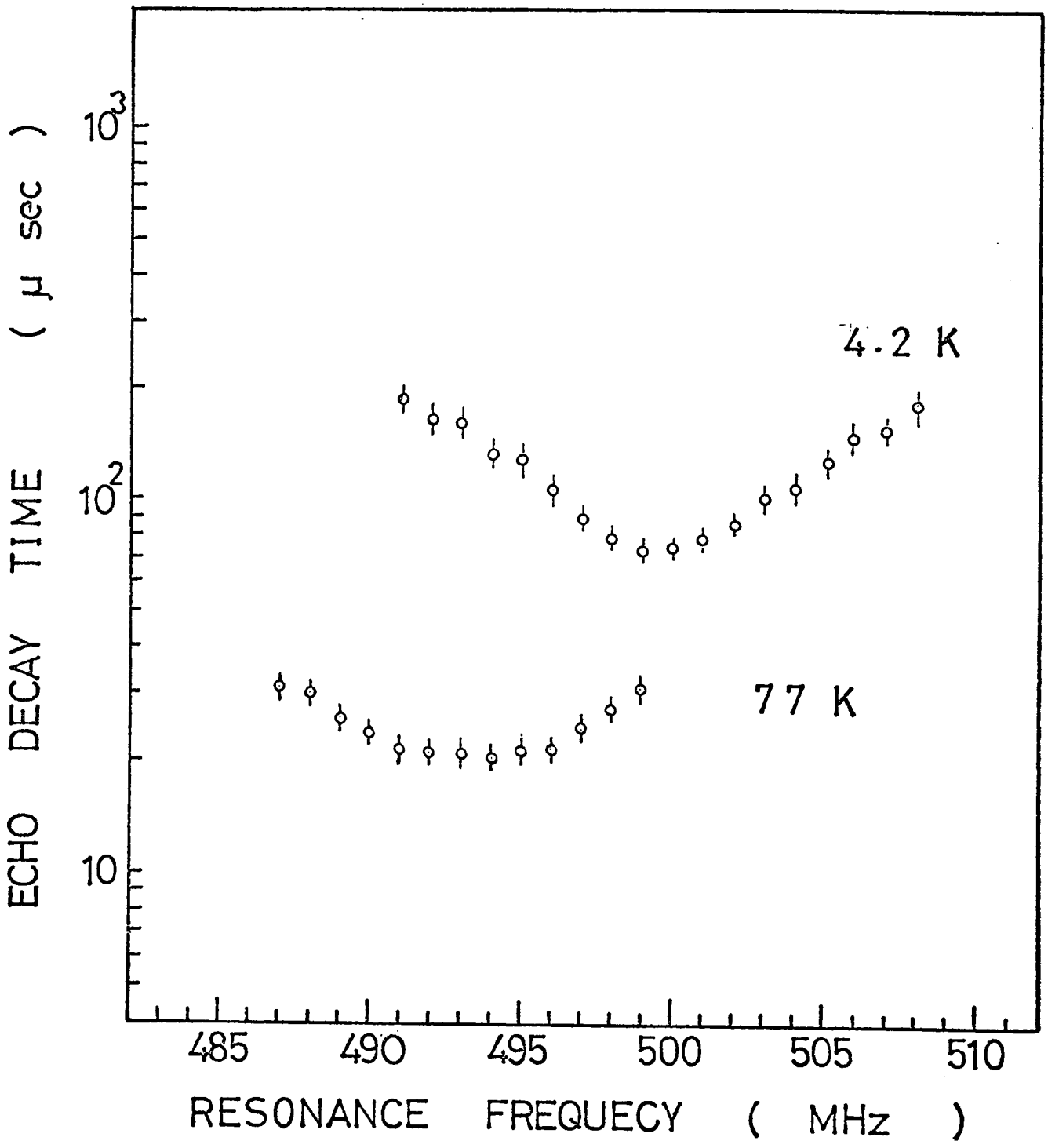
ECHO DECAY TIME (μ sec)
10³
10²
10
4.2 K
77 K
485
490
495
500
505
510
RESONANCE FREQUECY (MHz)

$ 5.4 Analysis and Discussions about Zero Field Spectrum

The NMR constants (hyperfine field, quadrupole splitting and line width etc.) of Co^{59} in CoO were calculated theoretically by Motizuki.[93] In the calculation, however, the old values of the hyperfine constants of Co^{2+} ion were used. Here the author will recalculate them by using the equations associated with the NMR constants derived by Motizuki and the latest values of the hyperfine constants.

In order to obtain the effective Hamiltonian for Co^{59} nucleus , the interaction (5.1-5)has to be averaged with respective to the electronic wave function of the ground state of the Co^{2+} ion as following;

$$\langle \Psi_g | \mathcal{H}_N | \Psi_g \rangle = \langle \Psi_g | \mathcal{H}_F + \mathcal{H}_l + \mathcal{H}_d | \Psi_g \rangle$$

$$= -g_N \beta_N \bar{I} \cdot (\bar{H}_F + \bar{H}_l + \bar{H}_d) \qquad (5.6)$$

and

$$\langle \Psi_g | \mathcal{H}_Q | \Psi_g \rangle = \frac{e^2 q Q}{4I(2I-1)} [3I_Z^2 - I^2 + \eta (I_X^2 - I_Y^2)] \qquad 5.7)$$

where H_F, H_l and H_d are the contact, the orbital and the dipole hyperfine fields resulting from the interaction, $\mathcal{H}_F$, $\mathcal{H}_l$, $\mathcal{H}_d$, respectively. the X- Y-and Z- axis denote three principal axes of the electric field gradient tensor, and η is an asymmetric parameter defined by $(V_{XX}-V_{YY})/V_{ZZ}$.

The electronic state of the free Co^{2+} ion is $(3d^7)\,^4F$. In the cubic crystalline field of CoO, the orbital degeneracy of this state is partially lifted leaving the ground state triply degenerate. This ground state can be described in terms of the angular momentum operator $\bar{l}$ of magnitude one , the total angular momentum operator $\bar{L}$ being replaced by $-(3/2)\bar{l}$. This small $\bar{l}$ is coupled to the spin angular momentum, $\bar{S}$, through the spin-orbit coupling and they form the total angular momentum $\bar{l}+\bar{S}$. The eigen states of the ion are characterized by the eigen values of $(\bar{l}+\bar{S})^2 = j(j+1)$, with $j=1/2,3/2,5/2$. However there exists exchange interaction among the ions, and when this is taken into account the Weiss molecular field, those states which have been different j but l_z+S_z couple each other, where z is the direction of the Weiss field. With this idea, Kanamori[94,95] calculated the wave function on the ground state of Co^{2+} ion at absolute zero, taking into account the effect of small tetragonal deformation of the crystal. In this calculation the direction of spins was simply assumed to be along [001], i.e. the direction of the contraction. The Hamiltonian used is

$$\mathcal{H} = 2J_1 z_1 \langle S \rangle S_z + \lambda' \bar{l}.\bar{S} - c l_z^2. \qquad (5.8)$$

and the ground state wave function was determined self-consistency as the lowest eigen state of this Hamiltonian. In this expression, $J_1(>0)$ is the exchange interaction constant between next nearest neighboring ions, z_1 the number of next nearst neighbores ($z_1=6$)

and $\lambda'=(-3/2)\lambda$, being the usual spin-orbit coupling constant. The ground state wave function thus determined was of the form

$$\psi_g = k_1|3/2,-1\rangle + k_2|1/2,0\rangle + k_3|-1/2,1\rangle \tag{5.9}$$

where the first and second suffices of represent the values of S_z and l_z, respectively, and k_1 k_2 and k_3 are numerical factors which depend on the magnitude of J_1, λ' and the deformation of coefficient c. Using the values of $2J_1z_1$= 180 cm^{-1}, λ'=270 cm^{-1} and c=140 cm^{-1}, the k_1,$k_2$and k_3 were calculated to be

$$k_1=0.909, \quad k_2=0.385, \quad k_3=0.162 \tag{5.10}$$

Averaging the interaction (5.1-5) with this wave function (5.9), the intra-atomic hyperfine field at 0 K in zero external fields are

$$H_F = -A\langle S\rangle/g_N\beta_N \tag{5.11}$$

$$H_l = 2\beta g_N\beta_N\langle r^{-3}\rangle \tfrac{1}{2}(k_k^2-k_3^2)(3-5\gamma^2) \tag{5.12}$$

$$H_d = 2\beta g_N\beta_N\langle r^{-3}\rangle \tfrac{1}{7}[\tfrac{1}{5}(2-9\gamma^2+12\gamma\sqrt{1-\gamma^2})(k_1^2-2k_2^2-k_3^2/3)$$

$$+\tfrac{\sqrt{2}}{10}(1+13\gamma^2+16\gamma\sqrt{1-\gamma^2})(\sqrt{3}k_1-2k_3)k_2\ ] \tag{5.13}$$

where γ represents that amplitude of the ^4P wave function which is mixed by configuration interaction to the ground orbital triplet

arising from ^4F (γ=0.185 according to Kanamori).

Motizuki assumed the hyperfine constant of the Fermi contact term, $-A/g_N\beta_N = 5.3\times10^{-3}$ cm^{-1} and the expectation value of inverse cube distance $\langle r^{-3}\rangle$ = 5.2 a.u.,and calculated these hyperfine fields. These constants were obtained by Abragam, Horowits and Pryce[103], analysing the paramagnetic resonance experiments for Co^{2+} ions, which was made for

$CoSO_4(NH_4)_2SO_4.6H_2O$, $CoSiF_6.6H_2O$ (Bleaney & Ingram 1951)[104]

and $3Co(NO_3)_2.2Bi(NO_3)_3.24H_2O$ (Trenam 1953)[105]

By using these hyperfine constants, Motizuki calculated the hyperfine fields to be

$$H_F = -2.69\times10^5 \text{ Oe} \qquad (5.14)$$

$$H_l = 7.32\times10^5 \text{ Oe} \qquad (5.15)$$

$$H_d = 0.282\times10^{-5} \text{ Oe} \qquad (5.16)$$

And the total field acting on the Co^{59} nucleus was

$$H_N^{total} = H_F + H_l + H_d = +490 \text{ kOe} \qquad (5.17)$$

which was good accord with the experimental value of +495.5 kOe,

However, Fry and Llewellyn made the electron double resonance experiments, refer to as ENDOR, of Co^{2}+ ions in MgO in 1961.[106] and determined the hyperfine constant , A=290.55±0.06 MHz. It is considered that this value of A has to use for the calculation of the hyperfine field at Co^{59} nucleus in CoO. By using this constant A=290.55±0.06 MHz, and the calculated value of $\langle r^{-3} \rangle$= 6.035 a.u.[106], the hyperfine fields were recalculated as following,

$$H_F = -369 \text{ kOe} \tag{5.18}$$

$$H_l = 849 \text{ kOe} \tag{5.19}$$

$$H_d = 32.7 \text{ kOe} \tag{5.20}$$

And the total field acting on the Co^{59} nucleus was

$$H_N^{total} = H_F + H_l + H_d = +511 \text{ kOe} \tag{5.21}$$

which is also good accord with the experimental value of 495.5 kOe. In spite of no taking into account of the effect of the spin inclination on the ground state wave function of Kanamori, the error between the theory and the experimental datum was only about 3 %. Such smallness of the effect was showed by Motizuki theoretically by using the perturbed ground state wave function. The dominance of the orbital hyperfine field seems to be the prominent feature of the residual orbital ions.

By using the hyperfine constants obtained by ENDOR experiments, the electric field gradient, q_{3d}, due to ($3d^7$) electrons was also calculated as following,

$$q_{3d} = e\langle\frac{1}{r^3}\rangle \frac{1}{35}(2-9\gamma^2+12\gamma\sqrt{1-\gamma^2})(k_1^2-2k_2^2+k_3^2)$$

$$= 12.0 \times 10^{14} \quad \frac{e.s.u.}{cm^3} \tag{5.22}$$

which yields the quadrupole splittings, δ, to be

$$\delta = 2\,\frac{3eQ}{4I(2I-1)}\,q_{3d}$$

$$= 2.5 \times 10^6 \quad Hz. \tag{5.23}$$

where the latest value of Q used was 0.4 barn.[107] This theoretical quadrupole splitting was 3.2 times larger than the observed one, 0.8 MHz. On the other hand, the field gradient , $q_{lattice}$, due to the structure outside of the ion has been calculated by taking into account only the nearest neighbour octahedron consisting of six ions and by taking the point charge model as following,

$$q_{lattice} = 1.7 \times 10^{12} \quad \frac{e.s.u.}{cm^3} \tag{5.24}$$

which is three orders of magnitude smaller than (5.23). In general, an electric field gradient can be expressed

$$q = q_{3d}(1-R) + q_{lattice}(1-\gamma_\infty) \qquad (5.25)$$

where R and γ_∞ are a shielding and antishielding coefficients which are effected by inner core electrons. Usually, the R is plus several tenth and γ_∞ is minus of the order of several tens but those are very difficult to estimate.[108] Since the R and γ_∞ have not been taken into account here, the discrepancy between (5.23) and the experimental calue should not be taken too seriously. This is because, if R is 0.7, the theoretical value of the quadrupole splitting will be the same as the experimental value. Such value is not unreasonable.

The homogeneous line width due to the indirect nuclear spin-spin coupling was estimated to be 57.6Oe theoretically by Motizuki, which was considerably larger than the experimental value,2.3 Oe,at 4.2 K. The cause of this discrepancy is not easy to understand. The problem of the homogeneous line width is closely related to the dynamical properties of the electronic spin system of CoO and will be investigated further in future.

From these analysis of the zero field spectrum, it is concluded that the calculated NMR constants were reasonable in spite of no taking into consideration about the effect of the spin inclination in CoO.

$ 5.5 Experimental Results about Spin Echo Pattern in an External Magnetic Field

Figure 5.4 shows the typical spin echo intensity as a function of an angle between an external field and c-axis, where the strength of the external field was 15.0 kOe. The larger peaks correspond to the center of the resonance when the external field was rotated in the a-c plane of CoO single crystal. The weak peaks correspond to the center of the resonance when the external field rotated in the a-b plane. Since this sample had multi-domains, the problem associated with the magnetic structure of CoO, a collinear or multi-spin ,could not be settled from this experiments. The resonance pattern of Co^{59} NMR in CoO is shown in Fig.5.5. The solid lines in this Fig.5.5 are the best fit curves of the experimental data in corresponding to the application of the external field in the a-c plane in CoO. The broken lines are the predicted curves in corresponding to the application in the a-b plane.

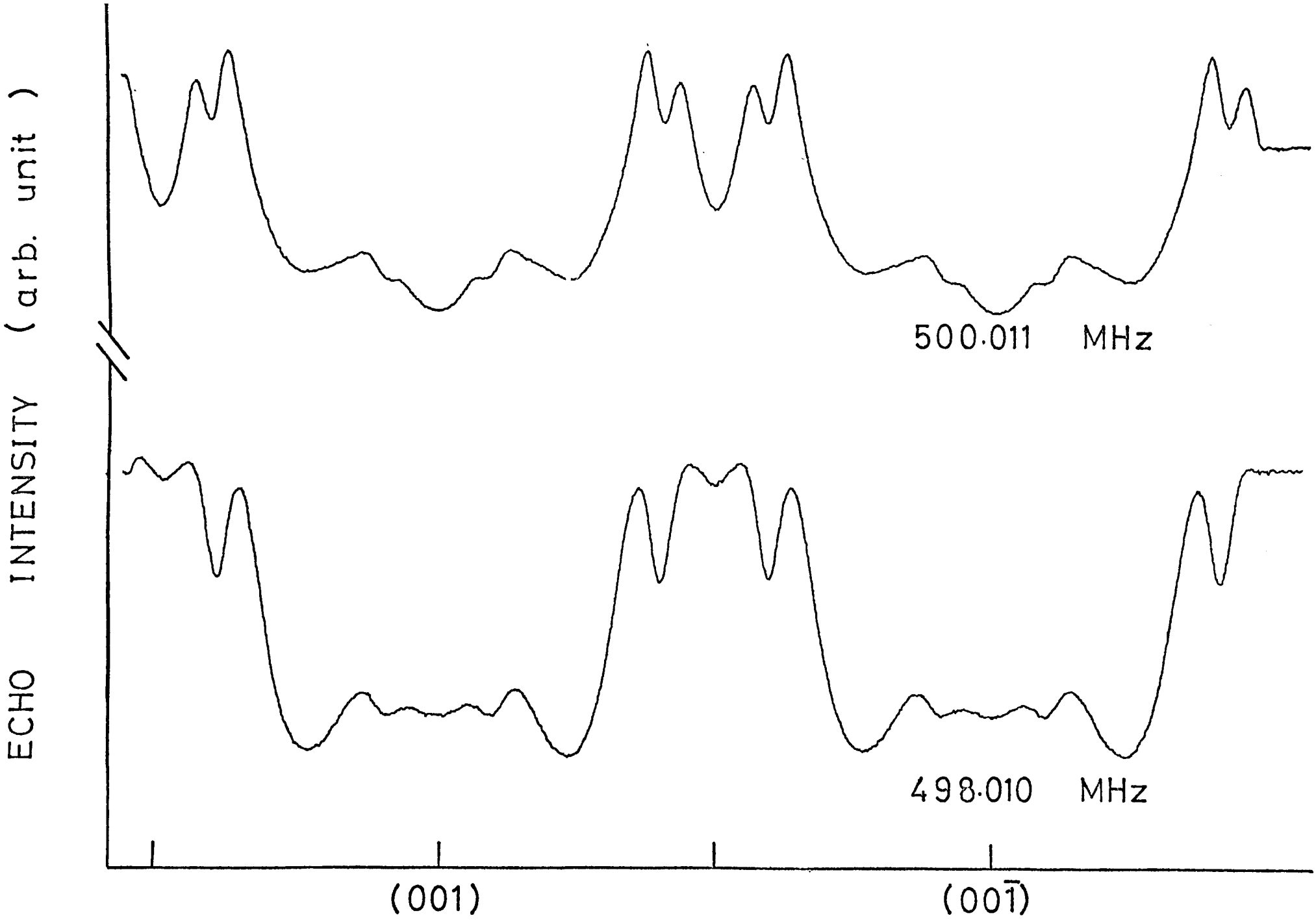
ECHO INTENSITY (arb. unit)
500.011 MHz
498.010 MHz
(001)
(00$\bar{1}$)
DIRECTION OF EXTERNAL MAGNETIC FIELD

Fig. 5.4

Fig. 5.5.

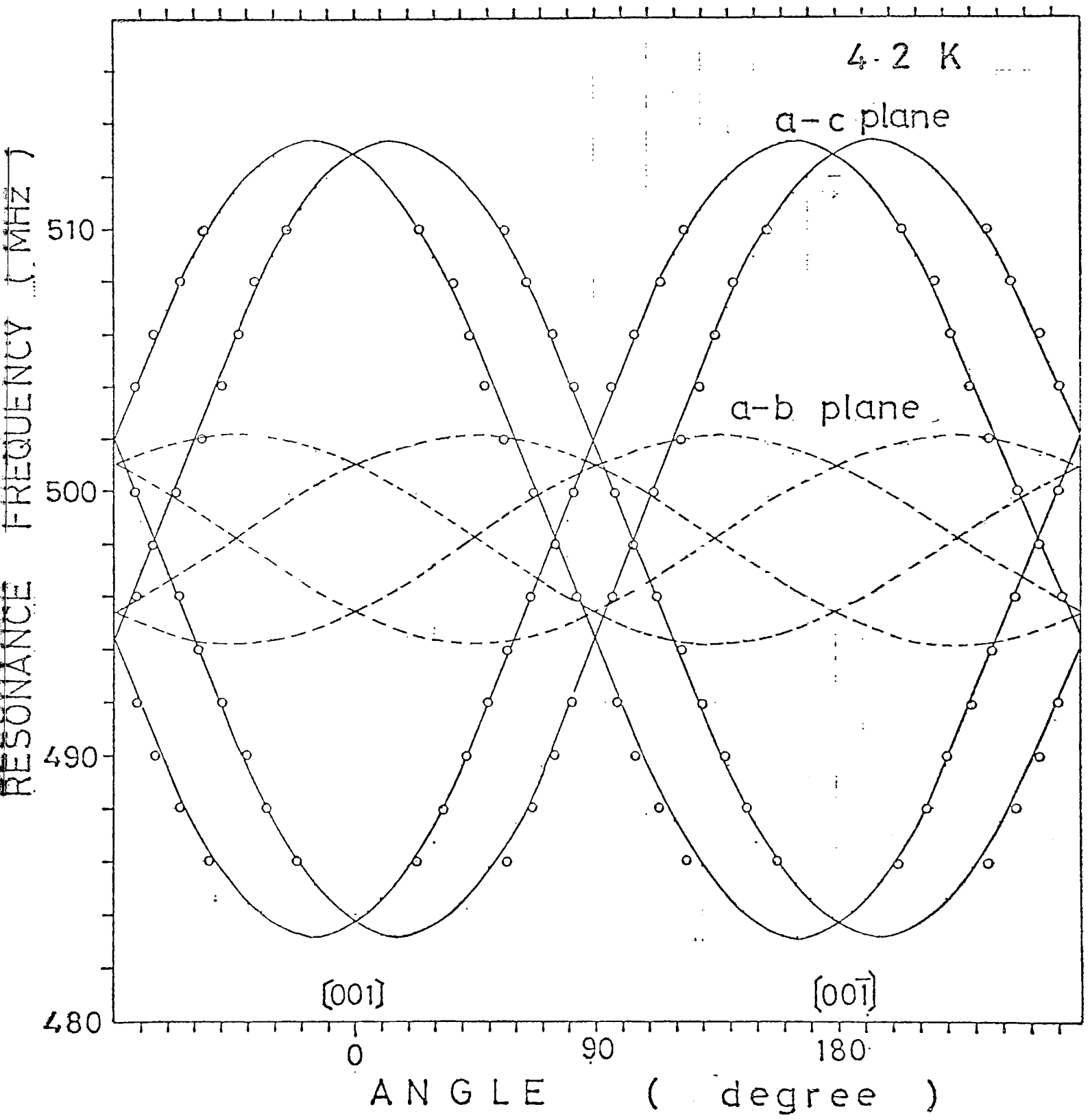
4.2 K
a-c plane
a-b plane
RESONANCE FREQUENCY (MHz)
510
500
490
480
[001]
[00$\bar{1}$]
0
90
180
ANGLE (degree)

$ 5.6 Analysis and Discussions about Spin Echo Pattern

Since the spin of Co^{2+} ion in CoO is known to lie in the [110] plane in neutron diffraction data,[72-87] the direction of the hyperfine field at Co^{59} nucleus also lies in the [110] plane. In order to avoid an error due to the effect of the field induced momentum, the analysis was made at another external field strength, 8 kOe. As the same results for the error were obtained, the effect of the field induced momentum was not serious. This was also shown by Motizuki theoretically, that is, the frequency shift of the central line is no more than -0.0655 MHz for H_{ext}= 10 kOe.

As shown in Fig.5.6, the effective field acting on Co^{59}nucleus can be written as

$$H_x = \pm H_N \sin(\phi)/\sqrt{2} + H_{ext}\sin(\theta) \tag{5.26}$$

$$H_y = \pm H_N \sin(\phi)/\sqrt{2} \tag{5.27}$$

$$H_z = \pm H_N \cos(\phi) + H_{ext}\cos(\theta) \tag{5.28}$$

where x, y, and z stand for the a, b and c-axis in CoO single crystal, and H_{ext} the external field, H_N the hyperfine field at Co^{59} nucleus. And ϕ is the angle between the hyperfine field and c-axis, and θ is the angle between the external field and

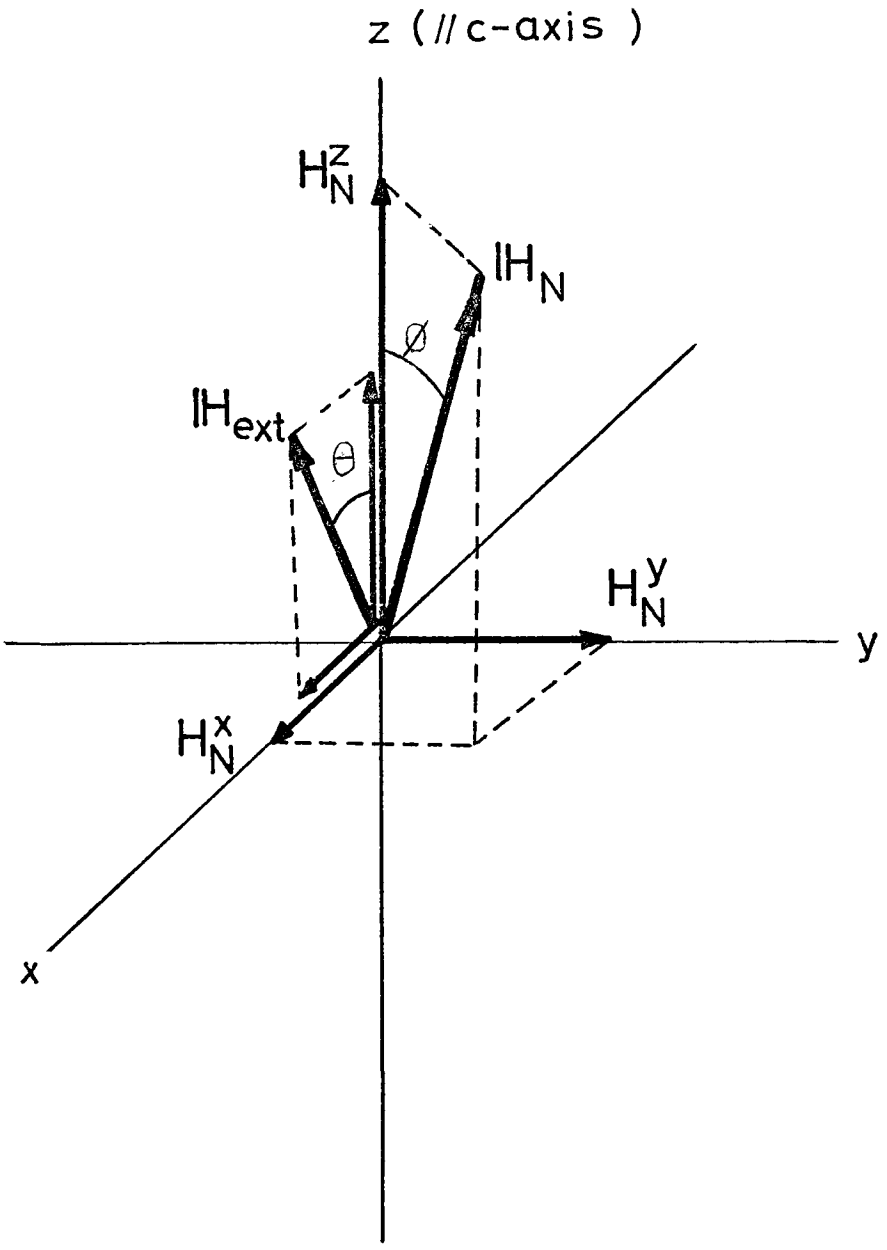

Fig. 5 6

c-axis. The 8 kinds of the combination associated with the sign of H_N are possible because of the multi domain structure of the sample. When the external field is applied in the Θ direction in the a-c plane, the center resonance frequency, f, is written as following,

$$f(\Theta) = \left(\frac{g_N\beta_N}{h}\right)\sqrt{H_x^2+H_y^2+H_z^2}$$

$$= \left(\frac{g_N\beta_N}{h}\right)\sqrt{\left[\pm H_N\sin(\phi)/\sqrt{2}+H_{ext}\sin(\Theta)\right]^2}$$

$$\overline{+H_N^2\sin^2(\phi)/2+\left[\pm H_N\cos(\phi)\pm H_{ext}\cos(\Theta)\right]^2}$$

$$= \left(\frac{g_N\beta_N}{h}\right)\sqrt{H_N^2+H_{ext}^2\pm 2H_NH_{ext}\left[\cos(\Theta)\cos(\phi)\pm\sin(\Theta)\sin(\phi)/\sqrt{2}\right]}$$

$$\cong f_o \pm f_{ext}\cos(\Theta\pm\phi') \qquad (5.29)$$

where $$f_o = \left(\frac{g_N\beta_N}{h}\right)H_N \qquad (5.30)$$

$$f_{ext} = \left(\frac{g_N\beta_N}{h}\right)H_{ext}\sqrt{1-\frac{\sin^2(\phi)}{2}} \qquad (5.31)$$

and

$$\tan(\phi') = \tan(\phi)/\sqrt{2} \qquad (5.32)$$

The solid lines in Fig.5.6 are the best fit curves of the experimental data as written the following functions,

$$f(\Theta) = 498.2 \pm 15.1\cos[\Theta\pm(14.9\pm0.5)^\circ] \qquad (5.33)$$

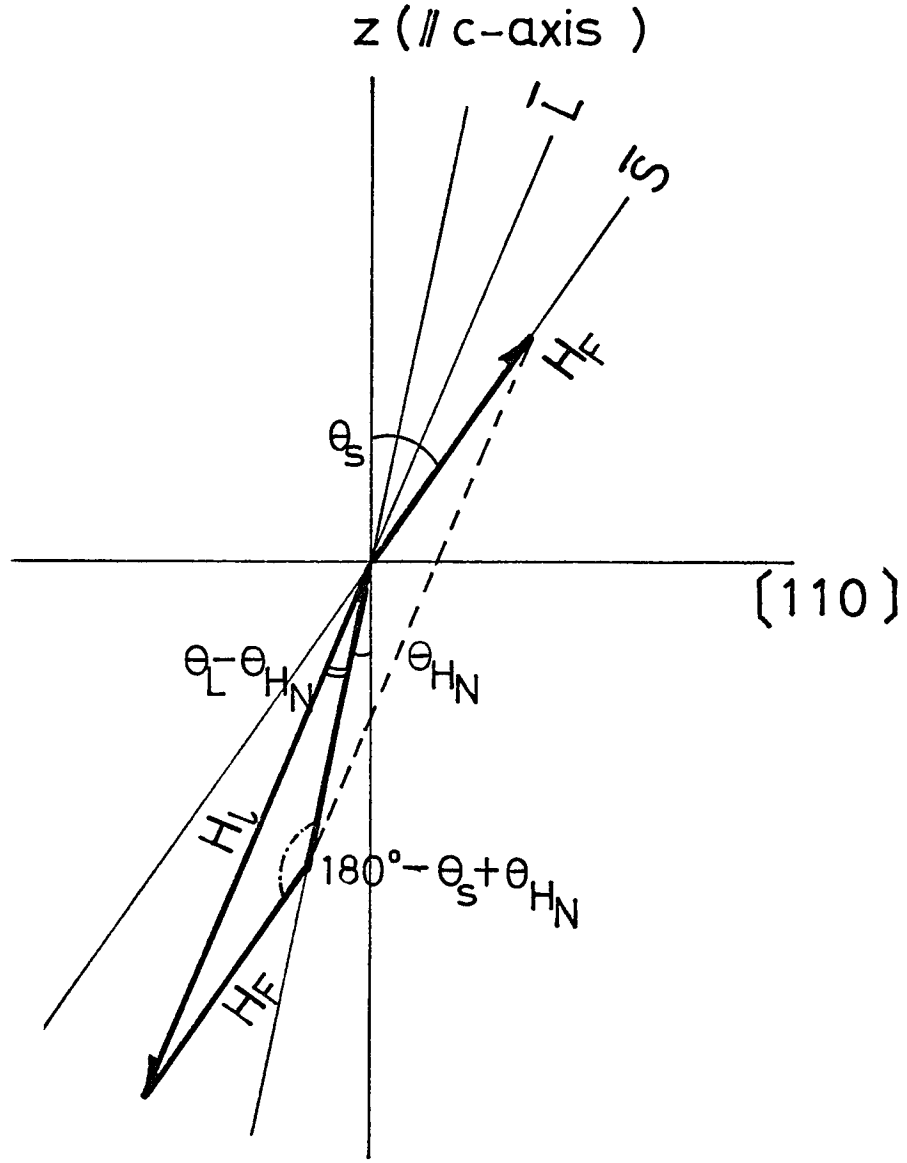
z (// c-axis)
'L
'S
H_F
θ_S
〔110〕
$\theta_L - \theta_{H_N}$
θ_{H_N}
H_L
$180° - \theta_S + \theta_{H_N}$
H_F

Fig. 5.7

By using the (5.32) and (5.33), the angle between the hyperfine field and c-axis was determined to be 20.6 ± 0.5^{o}. That is, the direction of the hyperfine field was found to be not parallel to the spin, which is considered that the orbital momentum of Co^{2+} ion is not parallel to the spin. In order to estimate the direction of the orbital momentum, the author used the contact and the orbital hyperfine field calculated theoretically ,(5.18) and (5.19), and the angle between the spin of Co^{2+} ions and c-axis. As shown in Fig.5.7, the following equation is concluded,

$$H_F/\ \sin(\Theta_L-\Theta_{H_N}) = H_L/\sin(180^{o}-\Theta_S+\Theta_{H_N}) \qquad (5.34)$$

By using the ratio of the contact and the orbital hyperfine field from eq.(5.34), the angle between the orbital momentum of Co^{2+} ion and c-axis, Θ_L, is written as

$$\Theta_L = \Theta_{H_N}+\sin^{-1}[\frac{H_F}{H_L}\sin\ (\Theta_S-\Theta_{H_N})\ ] \qquad (5.35)$$

where Θ_{H_N} and Θ_S are the angle of the observed hyperfine field and the reported spin associated with c-axis, respectively. Figure 5.8 shows the schematic. Assuming the ratio of H_F/H_L to have ten percents accuracy and taking into account the experimental error, Θ_L may be written to be

$$\Theta_L = 23.2\ \pm 1.0^{o} \qquad (5.36)$$

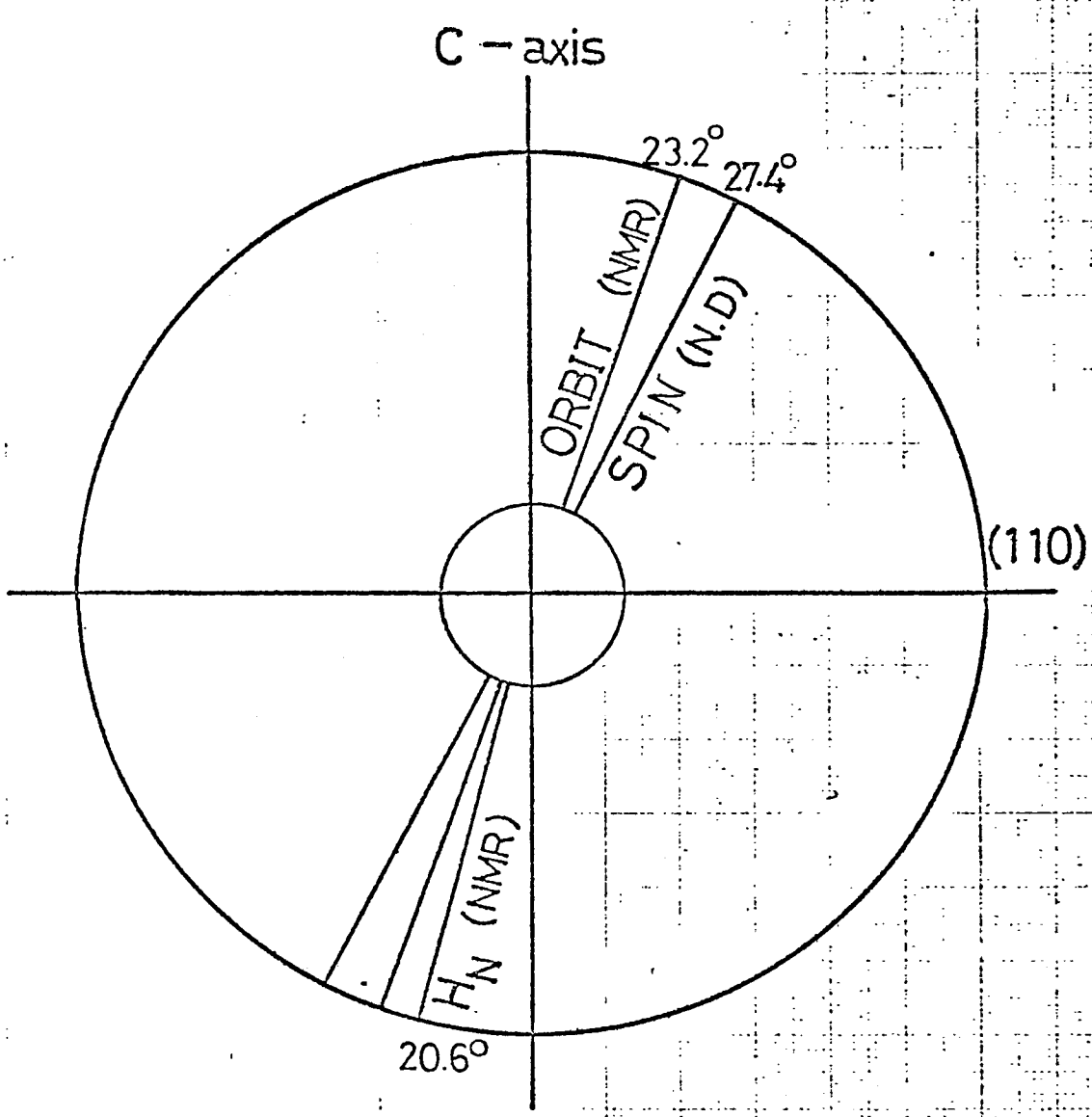
C – axis
23.2°
27.4°
ORBIT (NMR)
SPIN (N.D)
(110)
H_N (NMR)
20.6°

It is plaussible that the angle of the orbital momentum is smaller than the spin angle, 27.4°. This is because the orbital momentum tends towards the c-axis for the tetragonal crystal field term in a Hamiltonian for 3d electrons. It was revealed by Motizuki group[14] that the estimation of this angle is very difficult to make by taking into account the effect of the spin inclination with a simple perturbation theory. If neutron diffraction peaks contributed mainly by the orbital angular momentum are studied, this estimated value, 23.2° will be checked.

The experiments were also performed at the temperature of 20 K and 77 K. The results obtained were that the angle between the hyperfine field and c-axis increased when the temperature was increased. These results are smmed up in Table 5.1. This temperature variation of the angle of the hyperfine field at Co^{59} nucleus associated with c-axis cannot be explain easily. This is because, so far, a theory for the cause of the spin inclination has not been formulated with success.[109,110] If such theory is formulated in future, these results obtained here will be used to test the theory.

Table 5.1 The obtained results from this Co^{59} NMR experiment. θ_{H_N} is the angle between the c-axis and the hyperfine field at Co^{59} nucleus in CoO. f_c is the center resonance frequency of Co^{59} NMR. T_2 is the echo decay time constant.

θ_{H_N}	20.6 ± 0.5^{o}	at 4.2 K
	21.3	at 20 K
	23.9	at 77 K
f_c	498.2±0.5 MHz	at 4.2 K
	498	at 20 K
	493.3	at 77 K
T_2	72±5 u sec	at 4.2 K
	21	at 77 K

REFERENCES

1) J.G.Dash, R.D.Taylor, P.P.Craig, D,R.Cochran and W.E. Keller; Phy. Rev. Letters 5(1960) 152.

2) J.G.Dash, R.D.Taylor, D.E.Nagle, P.O.Craig and W.M. Visscher; Phy. Rev. 122 (1961) 1116.

3) R.D.Taylor; The Mössbauer Effect(Proc. Second International Conference on the Mössbauer Effect), D.M.Compton and Sons, New York,(1962)p203.

4) M.Shinohara, A.Ito, T.Fujita, A.Ishigaki and K.Ono; Japan J. Appl. Phys. 6 (1967) 982.

5) M.Shinohara, A.Ito, T.Fujita, A.Ishigaki and K.Ono; Japan J. Appl. Phys. 7 (1968) 170.

6) G.M.Kalvius, T.E.Katila and O.V.Lounasmaa; "Mössbauer Effect Methodology, Vol.5", ed. I.J.Gruverman (Plenum Press, New York, 1966) 231.

7) G.J.Ehnholm, T.E.Katila, O.V.Lounasmaa, and P.Reivari ; Cryogenics June (1965) 136.

8) O.E.Vilches and J.C.Wheatley, Physics letters 24A (1967) 440 and 25A (1967) 344.

9) J.C.Wheatley, O.E.Vilches, and W.R.Abal; Physics 4 (1968) 1.

10) G.A.Bykov and Phan Zuy Hien; Soviet Phys.-JETP 16 (1963) 646.

11) G.M.Kalvius, G.J.Ehnholm, T.E.Katila, O.V.Lounasmma

and P.Reivari; Bull. Am. Phy. Soc. 13 (1968) 1469.

12) H.London; Proc. Int. Conf. Low Temperature Physics, Oxford (1951) 157.

13) L.D.Landau and I.Pomenranchuk; Dokl. Akad. Nauk SSSR 59 (1948) 157.

14) T.P.Das, R.DE Bruyu Ouboter and K.W.Taconis; Proc. 9th Int. Conf. Low temperature Physics, Columnbus, Ohio, eds. J.G.Daunt, D.O.Edwards, F.J.Milford and M.Yaqub, Part B. p.1253. Plenum Press, New York (1965)

15) W.M.Fairbank and G.K.Walters, in Proceedings of the Symposium on Solid and Liquid Helium Three (Ohio State Research Foundation, Columbus, Ohio, 1957) p.220.

16) H.London, G.R.Clarke and E.Mendoza; Phys. Rev. 128 (1962) 1992.

17) H.E.Hall,P.J.Ford and K.Thompson; Cryogenics 6 (1966) 80.

18) B.S.Neganov, N.Borisov, and K.Thompson; Soviet Phys. Jetp 23 (1966) 959.

19) Prigogine, Bingen and Bellemans; Phys. 20 (1964) 633.

20) G.V.Chester; Proceedings of the Paris Conference on the Physics of Low Temperatures 1955 (Centre National de la Recherche Scientifique and UNESCO, Paris) p.385.

21) Cohen , E.G.D. and Van Leewen, J.M.J; Physica 26 (1960)385.

22) D.O.Edwards, D.F.Brewer, P.Selignan, M.Skertic, and Yaqub; Phys. Rev. Letters 15 (1965) 15

23) R.deBreyn Ouboter, K.W.Taconis, C.Le.Pair and J.J.M.

Beenakker; Physics 26 (1960) 853.

24) I.Pomenrunchuk; Zh Eksperium. i. Theor Fitz 19 (1949) 42.

25) A.C.Anderson, W.R.Roach, R.E.Sarwinski and J.C.Wheatley; Phs. Rev. Letters 16 (1966) 262.

26) A.C.Anderson, W.R.Roach, R.E.Sarwinski and J.C.Wheatley; Phy. Rev. Letters L7 (1966) 367.

27) " Teion Kougaku " 3 (1968) 227 (in Japanese).

28) D.F.Brewer, J.G.Daunt and A.K.Screekhar; Phy.Rev.115 (1959) 836.

29) W. Abel, A.C.Anderson, W.C.Black and J.C.Wheatley; Physics 1 (1965) 337

30) K.W.Taconis, N.H.Pennings, P.Das and R.De Bryun Ouboter; Physica 56 (1971) 108.

31) B.M.Abraham, Y.Eckstein, J.B.Ketterson and J.H.Vignos; Phys.Rev. Letters 17 (1960) 1254.

32) G.Bayn and C.Ebner; Phys. Rev. 164 (1967) 235.

33) W.R.Roach; Ph.D thesis, University of Illinous 1966 (unpublished).

34) J.Bardeen, G.Baym, D.Pines; Phys. Rev. 156 (1967) 207.

35) W.R.Abel, R.T.Johnson, J.C.Wheatley and W.Zimmerman, Jr; Phys. Rev. Letters 18 (1967) 737.

36) A.C.Anderson; Rev. Sci. Ins. 41 (1970) 1446.

37) A.C.Anserson, J.I.Connolly, and J.C.Wheatley. Phys. Rev. 135 (1964) A910.

38) S.C.Whitmore, J.M.Sanders and S.R.Ryan; Proceedings of the 11-th International Conference of Low temperature Physics, St. Andrews (1968).

39) W.J.HUikamp and O.V.Lounasmaa; Rev. Prog. Phys. 36 (1973) 424.

40) G.M.Kalvius, T.E.Katila and O.V.Lounasmaa: "Mössbauer Effect Meyhodology, vol.5", ed.I.J.Gruverman (Plenum Press, New York, 1966) p.231.

41) H.Frauenfelder; "Mössbauer Effect" (W.A.Benjamin,1962)

42) G.Wertheim; "Mössbauer Effect, Principles and Applications" (Academic Press).

43) V.I.Goldanskii, R.H.Herber; "Chemical Application of Mössbauer Spectroscopy",(Academic Press,1968)

44) "An Introduction to Mössbauer Spectroscopy" ed. L. May (Plenum Press, 1971).

45) A.H.Muir,Jr., K.J.Ando, and H.M.Coogan; "Mössbauer Effect Data Index 1958-1965" (Intersxience,1966).

46) W.M.Visscher; Ann.Phys.(NY) 9 (1960)194.

47) Y.Koi, A.Tsujimira, T.Hihara and T.Kashida; J. Phys. Soc. Japan 16(1961) 1040.

48) W.A.Steiyert and R.D.Taylor; "Mössbauer Effect Methodology vol.4" ed. I.J.Gruverman (Plenum Press, New York, 1965)

49) P.Reivari; Phys Res.Letters 22 (1969) 167.

50) T.Ericsson, M.T.Hirvonen, T.E.Katila and V.K.Typpi;

51) R.Geller, F.Wagner, W.Wiedemann, and P.Kienle; private comminucation (1968).

52) G.M.Katvius, G.J.Ehnholm, T.E.Katila, O.V.Lounasmaa and P.Relvari; Bul. Ann. Phy. Soc. 13 (1968) 1469.

53) C.H.Lablanchtais; J.Phys. Radium, Paris 12 (1951) 1036.

54) M.Foex; c.r. bebd séanc. Acad. Sci. Paris 227 (1948) 193.

55) R.Steet and B.Levis; Nature 168 (1951) 1036.

56) M.E.Fine; Phys.Rev. (1952) 1143.

57 M.F.Trombe; J. Phys. 12 (1951) 170.

58) S.Greenwald; Acta Crystallogr. 6 (1953) 396.

59) G.Assayag and M.H.Bizettee; Cr. bebd séanc Acad. Sci. Paris 239 (1954) 238.

60) J.S.Smart; Phys. Rev. 86 (1952) 968.

61) T.Nagamiya, S.Saito, Y.Shinimura and E.Uchida; J. Phys. Soc. Japan 20 (1965) 1285.

62) S.Saito, K.Nakahigashi, and Y.Shimomura; J. Phys. Soc. Japan 21 (1966) 850.

63) D.Jasnow and M.Wortis; Phys. Rev 176 (1965) 195.

64) M.B.Salamon; Phys. Rev. B,2 (1970) 210.

65) C.G.Shull, W.A.Strauser and E.O.Wollen; Phys. Rev. 83 (1951) 333.

66) D.C.Khan and R.A.Erickson; Phys. Rev. 1 (1970) 2243.

67) K.Motizuki; J. Phys. Soc. Japan 15 (1960) 5

68) W.R.Helms and J.G.Mullen; Phys. Rev. B 4 (1971) 751.

69) G.K.Wertheim; Phys. Rev. 124 (1961) 764.

70) H.Polak; Phys. Satus Solidi 2 (1961) 764.

71) J.Blomquist, S.Grapenqiesser and R.Soderquist; Phys. Status Solidi(a) (1971) 435.

72) J.G.Mullen and H.N.Ok; Phys. Rev. Letters 8 (1966) 287.

73) W.Trifthaüser and P.P.Craig; Phys. Rev. 162 (1967) 274.

74) B.van Laar; Phys. Rev. 19 (1965) 584.

75) B.van Laar; J. Phys. Soc. Japan 20 (1965) 1282.

76) W.L.Roth; Phys. Rev. 110 (1958) 1333.

77) T.Nagamiya and K.Motizuki; Rev. Mod. Phys. 30 (1958) 89 .

78) W.L.Roth; Phys. Rev. 111(1958) 772.

80) B.van Laar, J.Schweizer and R.Lemaire;Phys. Rev 141 (1966) 538.

81) E.Uchida,N.Fukuoka, H.Kondoh, T.Takeda, Y.Nakazumi and T.Nagamiya;J. Phys. Soc. Japan 19(1964) 2088

82) S.Saito, K.Nakahigashi and Y.Shimomura; J.Phys.Soc. Japan 21(1966)850

83) H.N.Ok and J.G.Mullen; Phys. Rev. 168 (1968) 563.

84) R.D.Rechtin and B.L.Averbach; Phys. Rev 100 (1972)4294.

85) Y.Y.Li; Phys. Rev 100 (1955) 627.

86) H.N.Ok and J.G.Mullen; Phys. Rev. 21 (1968) 823.

87) J.Blomquist, S.Grapenglesser and R.Söderquist;Phys. Stat. Sol. (a) 4 (1971) 435.

88) W.R.Helms and J.K.Mullen; Phys. Rev. B 4 (1971) 749.

89) H.N.Ok, W.R.Helms and J.K.Mullen; Phys. Rev. 187 (1968) 1242.

90) H.N.Ok and J.G.Mullen; Phys. Rev. Letters 27 (1968) 1242.

91) D.Schroeer and W.Trifthäuser; Phys. Rev. 147 (1966) 306.

92) W.G.Bhide and G.K.Shenoy; Phys. Rev. 147 (1966) 306.

93) K.Motizuki; J.Phys. Soc. Japan 15 (1960) 888.

94) J.Kanamori; J.Phys. Soc. Japan 17 (1957) 177.

95) J.Kanamori; J.Phys. Soc. Japan 17 (1957) 197.

96) T. Kubo, A. Hirai and H. Abe; J. Phys. Soc. Japan 26 (1969) 1094.

97) V. Jaccarino; Phy. Rev. Letters 2 (1959) 163.

98) H. Nishihara, H. Yasuoka and A. Hirai; J. Phys. Soc. Japan 32 (1972) 1135.

99) K. Okada and H. Yasuoka; J. Phys. Soc. Japan 32 (1974) 1711.

100) T. Tsuda, K. Okada and H. Yasuoka; J. Phys. Soc. Japan 37 (1974) 1713.

101) H. Yasuoka; Private communication.

102) S. Saito, K. Nakahigashi and Y. Shimomura; J. Phys. Soc. Japan 21 (1966) 850.

103) A. Abragam, J. Horowitz and M. H. L. Pryce; Proc. Roy. Soc. A 230 (1955) 169.

104) B. Bleaney and D. J. E. Ingram; Proc. phys. Soc. A63 (1950) 408. R. S. Trenam; Proc. Phys. Soc. A66 (1953) 118.

106) D. J. I. Fry and P. M. Llewellyn; Proc. Roy. Soc. A266 (1962) 84.

107) Nuclear Moments Compiled by G. H. Fuller and V. W. Cohen, Appendex 1 to Nuclear Data Sheets, issued with Vol.6 Set 5.

108) A. J. Freeman and R. E. Watson; "Magnetism", ed. G. T. Rado and H. Suhl (Academic Press, New York, 1965) Vol.II A,p.273.

109) T. Yamada and O. Nakahigashi; J. Phys. Soc. Japan 36 (1974) 1304.

110) O. Nakahigashi and T. Yamada; J. Phys. Soc. Japan 36 (1974) 136.